Failure Analysis Associates

ENGINEERING AND METALLURGICAL CONSULTANTS
2225 EAST BAYSHORE ROAD P.O. BOX 51470
PALO ALTO CALIFORNIA 94303 (415) 856-9400 TELEX 704216

FaAA-84-2-14
7396/PAO:R03341A

INVESTIGATION OF TYPES AF AND AE PISTON SKIRTS

Prepared by
Failure Analysis Associates

Prepared for
TDI Diesel Generator Owners Group

May 23, 1984

STATEMENT OF APPLICABILITY

This report addresses the structural adequacy of the Transamerica Delaval Inc. types AE and AF piston skirts supplied for use in R-4 Series diesel engines. The modified Type AF skirt was originally installed in the engines at Shoreham Nuclear Power Station, Grand Gulf Nuclear Station and San Onofre Nuclear Generating Station. These skirts have been replaced at Shoreham and Grand Gulf by Type AE skirts. Type AE skirts have also been installed at Comanche Peak Steam Electric Station. Evaluation of the type AF skirts at San Onofre will be reported separately.

EXECUTIVE SUMMARY

PISTON REPORT

This report addresses the structural integrity of the Transamerica Delaval Inc. (TDI) types AF and AE piston skirts. This report was prepared on behalf of the TDI Diesel Generator Owners Group as one of a series of reports on generic components of those diesel engines in nuclear installations -- the generically termed Phase I components.

All of the AF type piston skirts installed in the DSR-48 diesel engines at Shoreham were found to exhibit linear indications during dye penetrant inspection in one or more of the crown-to-skirt stud attachment bosses. Upon destructive examination the indications were found to be fatigue cracks. The cracks were determined not to result from material or fabrication defects.

The AF piston skirts had been factory modified by TDI to replace the original spherical washer sets used in the stud attachments by two stacks of Belleville washers. These skirts were replaced by a later version, denoted as the AE, which incorporated increased stud attachment thickness and eliminates one of the Belleville washer stacks.

The AE skirts have now been operated for over 300 hours in one of the Shoreham engines, including 100 hours at full power operation. Other AE skirts have accumulated over 6,000 hours in a stationary generating plant and over 600 hours in an advanced development engine. Inspection of these skirts (one after 6,000 hours, two after 600 hours, and four after 300 hours) with high-resolution, eddy-current procedures disclosed no cracking.

Comparative isothermal experimental and finite element stress analyses were performed on the AE and AF skirts. These analyses showed that the stresses are substantially lower in the AE skirt than in the AF. Fatigue and fracture mechanics analyses were performed on both types of skirts. Cracks were predicted to initiate in the AF, and to propagate under certain conditions to a depth of less than 0.15 inch. Crack arrest was predicted to occur in all cases. Cracks were predicted not to initiate in the AE under stress

levels experimentally observed. Under stress levels calculated by finite element analysis, cracks might initiate in the AE under certain conditions, but if initiated, cracks were predicted never to grow.

It was concluded that, based on isothermal analysis, testing and field experience, the crown to skirt stud attachment area of the AE skirt will not fail in fatigue. It was further concluded that the modified AF skirts are satisfactory for service provided inspections of the stud boss attachment area are carried out or under conditions of operation below full rated load.

TABLE OF CONTENTS

Section		Page
STATEMENT OF APPLICABILITY		i
EXECUTIVE SUMMARY		ii
1.0	INTRODUCTION	1-1
1.1	Section 1 References	1-2
2.0	LABORATORY EVALUATION OF CRACKED (MODIFIED AF) PISTON SKIRTS	2-1
2.1	Nondestructive Examination	2-1
2.2	Destructive Examination	2-2
2.3	Electron Microscopy	2-3
2.4	Optical Metallography	2-4
2.5	Chemical Composition	2-5
2.6	Hardness	2-5
2.7	Tensile Properties	2-6
2.8	Residual Stress Measurements	2-6
2.9	Section 2 References	2-6
3.0	EXPERIMENTAL STRAIN MEASUREMENTS	3-1
3.1	Comparative Description of Piston Skirt	3-1
3.2	Test Set-Up	3-2
3.3	Stress Coat Test	3-4
3.4	Strain Gage Test	3-5
3.4.1	AE Piston Skirt	3-5
3.4.2	AF Piston Skirt	3-9
3.5	Section 3 References	3-14
4.0	FINITE ELEMENT STRESS ANALYSIS	4-1
4.1	Load Considerations	4-1
4.2	Stress Analysis	4-3
4.2.1	AE Piston Skirt Analysis	4-4
4.2.2	AF Piston Skirt Analysis	4-5
4.3	Crown/Skirt Interactions	4-6
4.4	Section 4 References	4-7
5.0	COMPARISON OF FINITE ELEMENT AND EXPERIMENTAL RESULTS	5-1
5.1	Stress Magnitudes	5-1
5.2	Gap Closure Pressures	5-2

TABLE OF CONTENTS
(continued)

Section		Page
6.0	FATIGUE AND FRACTURE ANALYSIS	6-1
6.1	Material Properties	6-1
6.1.1	Fatigue	6-1
6.1.2	Fracture Mechanics Properties	6-2
6.2	Cyclic Stress Levels	6-4
6.3	Fatigue Crack Initiation Analysis	6-5
6.4	Fatigue Crack Growth Analysis	6-6
6.5	Section 6 References	6-9
7.0	AE PISTON SKIRT INSPECTIONS	7-1
8.0	CONCLUSIONS	8-1

1.0 INTRODUCTION

This report supercedes an earlier version issued in February 1984 under the same report number and title. The current version of this report incorporates more realistic boundary conditions on the finite element models than were employed earlier. Experimental results for the modified AF skirt are also added.

Inspection of 24 piston skirts from the Transamerica Delaval Inc. (TDI) DSR-48 engines at the Shoreham Nuclear Power Station disclosed linear indications in one or more of the skirt-to-crown stud attachment bosses in each of 23 of the skirts. The one exception proved to be a later version of the skirt, designated by TDI as AN-type. With this one exception, the piston skirts were the AF-type, factory modified according to a service information memo issued by TDI [1-1]. This modification, performed by TDI late in 1981, consisted of spot-facing each of the four bosses through which studs extend to secure the piston crown and replacing the originally supplied spherical washer set with two stacks of Belleville washers. The spot-facing reduced the height of the stud attachment bosses from 2 inches to approximately 0.25 inch.

The AF piston skirts are no longer in use at Shoreham. LILCO has replaced all 24 piston skirts with the latest TDI production type, designated AE. (The AE design has also been installed at Grand Gulf Nuclear Station and Comanche Peak Steam Electric Power Station.) The AE design restores half the original height of the attachment boss and incorporates one stack of Belleville washers per stud instead of two. In addition, the boss is wider and is blended more smoothly to the skirt wall. These changes provide additional material for support of the loads on the top of the skirt. This addition of material provides improved stiffness and strength in the AE-skirt. The major differences in dimensions are illustrated in Figure 3-1. Thus, qualitative review of the AE design indicates that it has improved strength and crack resistance over the AF design.

In order to provide a quantitative comparison of the two designs, Failure Analysis Associates (FaAA) undertook a comparative stress analysis of the two skirt configurations. This consisted of isothermal finite element and

experimental stress analyses of the AE and AF skirts with attached crown. The finite element stress results are presented in Section 4, and the experimental results in Section 3. The maximum cyclic stresses determined by the finite element calculations are combined with the fatigue and fracture properties of the material in Section 6 to provide analysis of the possibility of crack initiation, growth and arrest of fatigue cracks in the two skirt designs.

1.1 Section 1 References

1-1 Transamerica Delaval Inc. Service Information Memo, "Modifications of the Two-Piece Piston Four Valve R and RV Engines Prior To and Including SN/75079," November 10, 1980.

2.0 LABORATORY EVALUATION OF CRACKED (MODIFIED AF) PISTON SKIRTS

Metallurgical evaluation of three of the 23 type-AF piston skirts from the Shoreham Nuclear Power Station (SNPS) emergency diesel generators disclosed fatigue cracks in all but one of the twelve crown-to-stud attachment bosses. None of the cracks had grown to failure. The chemistry and microstructures appeared consistent with typical ductile iron properties. TDI reported that all SNPS piston skirts were manufactured to ASTM specification A536-65 for ductile cast iron. Skirt Brinell hardness values were within the specifications attributed to the manufacturer.

According to TDI, the AF skirts were normalized and tempered. They were reportedly austenitized at 1700°F - 1750°F for 3 hours, then cooled in ambient air. They were reported to have been subsequently tempered at 1050°F for 3 hours, then cooled in ambient air. AE skirts were processed similarly, except they were cooled in fan circulated air after normalizing at 1700°F to 1750°F [2-1].

Three of the skirts identified as having potential cracks were shipped to Failure Analysis Associates (FaAA) for confirmation and analysis of the cause of these cracks. These skirts have been designated Nos. 1, 2, and 3. The No. 1 skirt was removed from the No. 4 cylinder of EDG #101. The No. 2 piston skirt was from the No. 6 cylinder of EDG #102. The No. 3 skirt was from the No. 7 cylinder of EDG #103. The No. 3 piston skirt was previously rejected because of prior scuffing damage.

In addition, an unused AE skirt was supplied by LILCO for evaluating residual stress and, metallurgical and mechanical properties.

2.1 Nondestructive Examination

Figure 2-1 is a photograph of one of the modified AF-type piston skirts after disassembly from the crown. The interior of a piston skirt is shown in Figure 2-2. The white color is from the dye-penetrant test. The spot-faced bosses are shown in Figures 2-3 and 2-4. A linear indication of red dye from the dye penetrant test is seeping out of a suspected crack as shown in Figure

2-4. All of the cracks found were similarly located and oriented on a spot-faced boss.

2.2 Destructive Examination

Three AF-type piston skirts were examined by eddy current to confirm the presence of cracks; eleven of the twelve bosses contained one or two cracks. The cracks appeared on the inside of the skirt in the vertical ridges remaining after spot-facing of the bosses. A total of four linear indications, revealed by dye penetrant testing, were subsequently saw-cut and fractured out of the three skirts. These indications were opened by fracturing and proved to be cracks. All the cracks were located at the base of the vertical ridges approximately 0.1 inch above the spot-faced surface. The crack size varied from 0.3-inch deep by 0.9-inch long to 0.2-inch deep by 0.3-inch long. Location of these cracks is shown in Figures 2-3 and 2-4. Macrophotographs of the four opened cracks are given in Figures 2-5 to 2-9.

These cracks appeared to be fatigue cracks. Some of them had faint beach marks. In addition, no evidence of ductile dimples or cleavage was observed in the flat fatigue crack region. The exart origin was impossible to locate for three of the cracks. However, one crack appeared to have its origin at the tip of the ridge that remained after the bosses had been spot-faced. The overloaded portions of the fractures produced in opening the cracks were rougher than the smooth, pre-existing cracks. A notable feature, visible using a lower power stereomicroscope, was the large number of graphite nodules intersected by the fracture surface. These nodules were smoothly fractured in the fatigue cracked areas but were more disturbed in the overloaded regions of the fractures. Several of the pre-existing cracks had faintly visible beach marks. The distinctly different appearance of the pre-existing fracture surfaces identified them as fatigue cracks.

On several of the fractures, black included material was apparent near as-cast surfaces. Instances of the included material are noted and outlined in Figures 2-5 and 2-6. This material appeared to have been organic binder that had been incorporated from the core. The included material did not

appear to significantly affect the initiation or growth of the four cracks which were broken open.

2.3 Electron Microscopy

Cracks from each piston skirt were examined in a scanning electron microscope (SEM). The character of fractographic features varied with location on the fatigue crack surfaces. Locations adjacent to the tip of the ridge, near the suspected origins, were more rubbed and damaged than regions closer to the crack front. Near the crack front on two fractures, i.e., in the fatigue region most recently formed, areas containing fatigue striations were observed. Although these striations were not observed on each specimen or in other areas on the crack surfaces, features were observed that were similar but without distinct fatigue striations. Worn or abraded features, such as those observed here, are typical of high-cycle fatigue crack surfaces that result from cycling between tension and compression.

Since the crack that was removed from EDG #101 is typical of all the observed cracks, its fractographic features are discussed. A low-magnification SEM montage of the EDG #101 crack is shown in Figure 2-10. As one moves away from the suspected origin (Area A) toward the crack front (Area C), the fracture surface shows evidence of less rubbing and abrasion. High-magnification SEM photographs of Areas A, B, and C are given in Figures 2-11 through 2-14. In region C, near the most recently formed crack surface, fatigue striations can be seen. Fatigue striation spacings, i.e., the amount the crack extended with each fatigue cycle, can be seen in Figures 2-14 and 2-15. The spacing of the striations is approximately 1.2×10^{-5} inch/cycle.

These cracks in the piston skirt ridges were clearly the result of fatigue. First, striations or rubbed fatigue areas were present over the entire crack surface. Second, no evidence of ductile dimples was observed between the graphite nodules. This strongly suggests that the maximum cyclic stress was below the ultimate tensile strength. In addition, it also suggests that major ove loads were not responsible for crack extension. For comparison, an uncracked piece of this piston skirt was fractured under a bending load in the laboratory. In a very narrow region near the tensile surface,

ductile dimples mixed with some cleavage were observed. Such a region is shown at various magnifications in Figures 2-16 through 2-18. No such features were found on the fatigue crack surfaces.

Finally, no cleavage was observed on the pre-existing crack surfaces. Evidence of cleavage was found only in regions where the fracture was fresh, i.e., caused by overload when the specimen was broken open in the laboratory. Cleavage features, such as those shown from the exemplar failure in Figures 2-19 through 2-21, were not observed on the fatigue crack surface. In addition, the graphite nodules were more disturbed in both the cleavage and ductile dimple region than the nodules on the fatigue crack surface. This again supports the evidence that these pre-existing flaws were the result of high cycle fatigue and were not caused by ductile or cleavage fracture processes.

2.4 Optical Metallography

The ductile cast iron was examined metallographically. Small specimens, removed from an area near the fatigue-cracked bosses, were mounted, polished, and etched to reveal the microstructure. The AF microstructure consisted of about 10-volume-percent graphite particles in a matrix of pearlite and ferrite. The graphite nodules were somewhat less regular than ideal; however, this would have had no influence on the fatigue strength of the material. The matrix was about 75% pearlite and 25% ferrite; the ferrite appeared around the graphite particles, as expected. Figure 2-22 shows a polished and etched photomicrograph of a sample of ductile cast iron removed from the No. 2 skirt of the piston from the EDG #102 engine. This microstructure is consistent with the heat treatment reportedly used by TDI.

The microstructure of the AE piston skirt is similar to that observed for the AF piston skirt. The amount of ferrite is approximately one-half that in the AF skirt; this reduction in the volume fraction of ferrite is consistent with the increased cooling rate imposed after normalizing the AE skirt.

2.5 Chemical Composition

A sample of the No. 2 AF piston skirt was removed and analyzed by Metallurgical Testing Incorporated using various chemical analysis techniques. The resultant chemical analysis is shown in Table 2-1. This chemistry is typical for ductile cast iron.

2.6 Hardness

Brinell hardness was measured on several pieces removed from the cracked piston skirts. The measured hardness values varied from 235 to 255 BHN; the average hardness was 241 BHN. These hardness readings fall within the Brinell hardness range of 217 BHN to 269 BHN typical of ASTM A536 grade 100-70-03. This notation implies minimum tensile properties of 100 ksi ultimate strength, 70 ksi yield strength, and 3% elongation. This grade of A536-67 has a pearlite matrix that is consistent with the microstructure observed in the examined AF piston skirts. This is the grade specified for Shoreham's AF piston skirt. The piston skirt hardness values suggest that the ultimate tensile strength would be between 110 ksi and 120 ksi. This ultimate strength would be consistent with ASTM A536 grade 100-70-03. It should be noted that ASTM A536 does not specify hardness requirements.

Brinell hardness measurements were made in the same locations on an AE piston skirt as on the AF piston skirts. Hardnesses measured on the inner skirt web were between 262 and 285 BHN; the average hardness was 277 BHN. Hardnesses taken on the boss face ranged between 229 and 241 BHN; the average value was 235 BHN. This is similar to the hardness values, 255 and 261 BHN, measured near the wrist pin by FaAA and TDI.

The slightly higher hardnesses measured on the AE piston skirt than on the AF piston skirts are consistent with forced air cooling after normalizing. These values appear proper for 100-70-03 grade ASTM A536 ductile cast iron. These measured hardnesses are within the typical range of hardnesses for 100-70-03 grade nodular iron.

2.7 Tension Tests

Mechanical property test samples were machined from two of the three fatigue-cracked AF piston skirts and from an unused AE piston skirt. The tension test samples were cut from the piston skirts from a location as near as possible to the fatigue cracked ridges adjacent to the spot-faced bosses. The specimens conformed to the ASTM specification E8-80; they were 1/4 inch in diameter. The specimen deformation was measured with a snap-on extensometer with a one-inch gage length. This method of chosing a specimen size and its location in the piston skirt did not comply rigorously with ASTM A536-65. This specification recommends that the properties of the cast ductile iron be measured using specimens machined from separately cast and heat-treated Y blocks or keel blocks rather than with 1/4 inch diameter specimens removed from an actual cast part. The tension test results are reported in Table 2-2. It is apparent that none of the tension tests complied totally with the mechanical test requirements for grade 100-70-03 ductile iron castings.

If larger tension test specimens had been machined and tested from separately cast and heat-treated test blocks, the results might have been in compliance with ASTM A536-65 for grade 100-70-03 ductile iron.

2.8 Residual Stress Measurements

Residual stress measurements were made on the piston skirt removed from the No. 6 cylinder of EDG #102 and on the unused AE piston skirt. A dissection technique was used to determine the principal residual stresses near the ridges and boss region. The maximum residual stress measured was 11.4 ksi tension on the spot-faced region of the AF skirt. The residual stresses in this region measured on the AE skirt were much smaller, being typically about 1 ksi.

2.9 Section 2 References

2-1 Private communication between Al Fleischer of TDI and Cliff Wells of FaAA, November 1983.

Table 2-1

CHEMISTRY OF NO. 2 AF PISTON SKIRT

Element	Weight Percent
C	3.46
Si	2.43
Mn	0.53
Cr	0.11
Ni	0.76
Mo	0.038
Mg	0.072
S	0.005
P	0.027

Table 2-2

TENSION TESTS OF SPECIMENS TAKEN FROM PISTONS

Specimen Number	Yield Strength (ksi)	Ultimate Strength (ksi)	Percent Elongation at Fracture *
AF Pistons			
1-101	64.5	94.2	5.2
2-101	63.3	97.5	4.8
3-102	53.6	100.0	6.4
4-102	61.6	98.6	5.4
AE Pistons			
AE-1-1	68.0	90.21	2.3**
AE-1-2	70.5	85.36	1.6
AE-2-1	63.5	93.4	2.8
AE-2-2	65.9	91.5	2.4**

* Determined from extensometer output.
** Fractured outside of gage length.

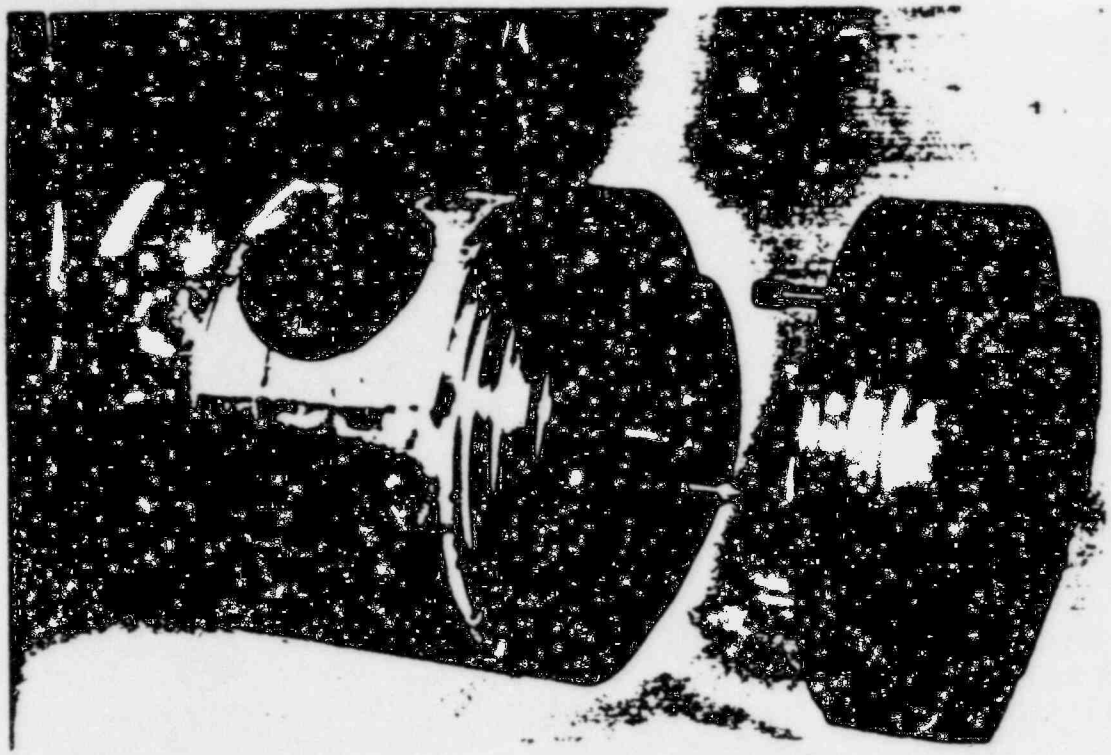

Figure 2-1. Photograph of an AF-type piston from the Shoreham Nuclear Power Station emergency diesel generator piston skirt (left) and crown (right).

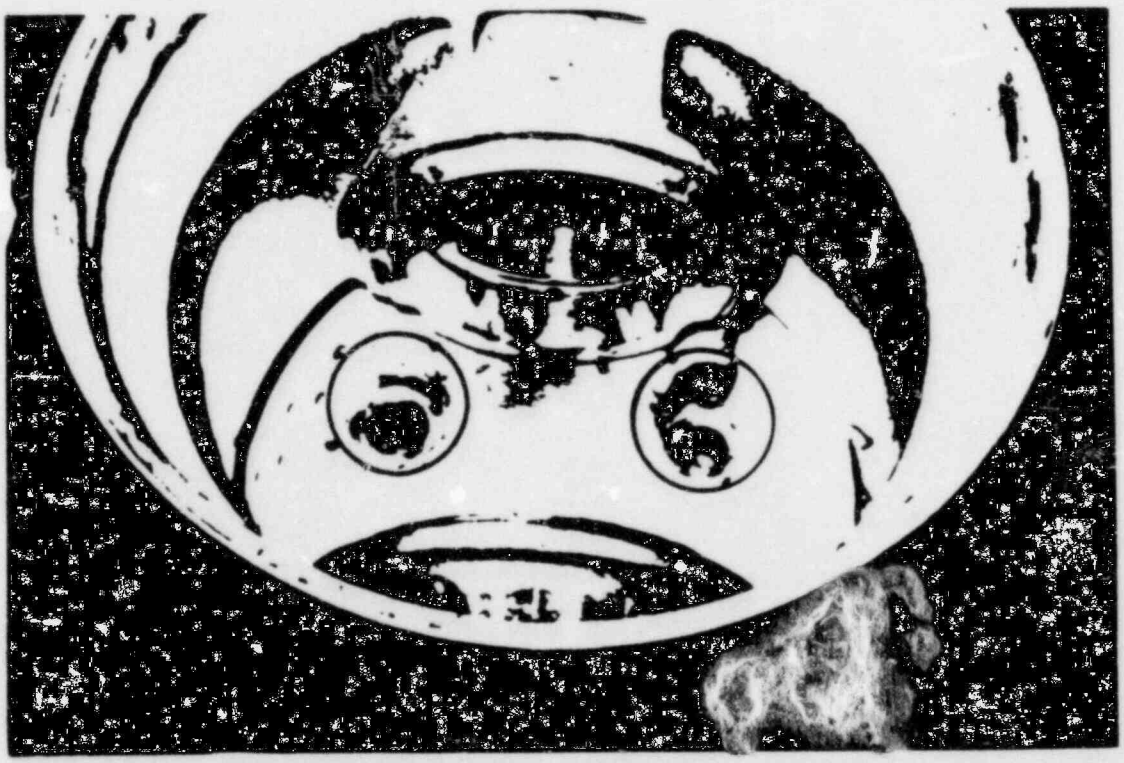

Figure 2-2. Interior of an AF-type piston skirt. The white coating and red dye are from the dye penetrant examination. Through holes for the crown studs and spot-faced boss are circled.

Figure 2-3. A crown-to-skirt attachment boss inside a piston skirt removed from EDG #101. The boss has been machined by spot-facing from 2 inches high down to the observed $^{1}/_{4}$ inch. The removed segment of ridge was subsequently broken open and is shown in Figures 8 and 9.

Figure 2-4. A crown-to-skirt attachment boss from EDG #102. The piston skirt has been tested with dye penetrant and white developer. A red linear indication is visible at the base of the vertical ridge that remained after spot-facing.

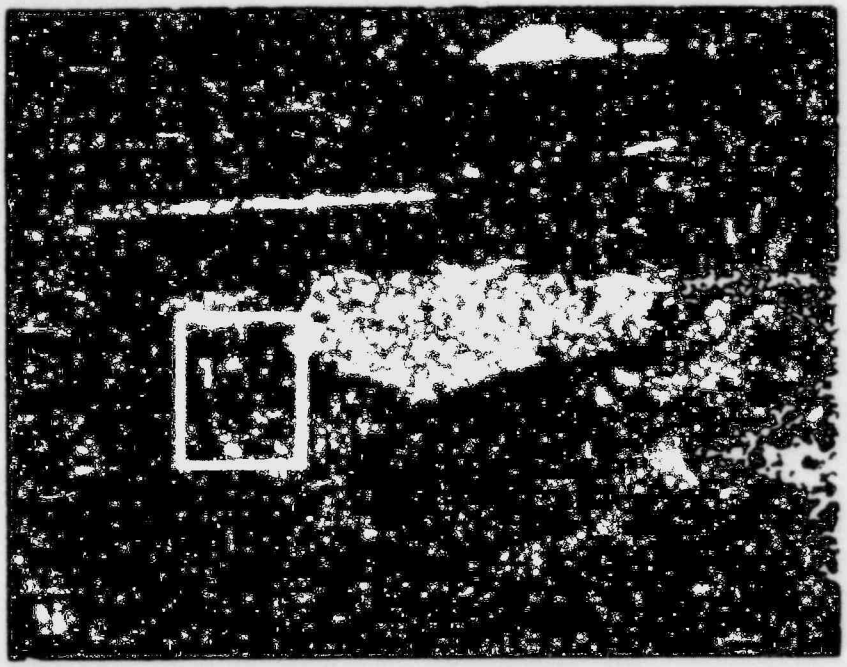

Figure 2-5. Macrophotograph of a pre-existing crack cut out of the piston skirt from EDG #101, No. 4 cylinder.

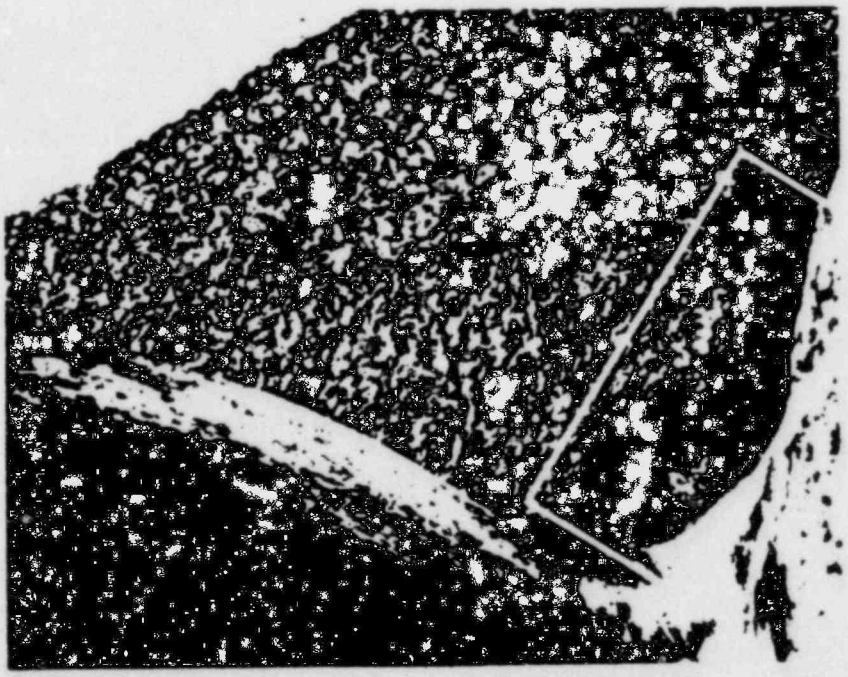

Figure 2-6. Macrophotograph of a pre-existing crack cut out of the piston skirt from EDG #102, No. 6 cylinder.

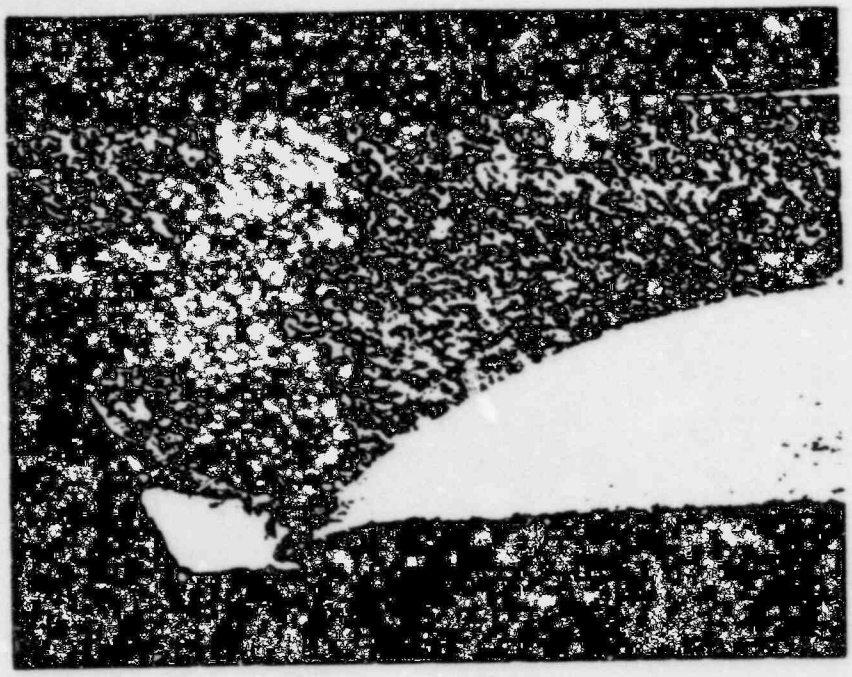

Figure 2-7. Macrophotograph of another pre-existing crack cut out of the piston skirt removed from EDG #102 and fractured open.

Figure 2-8. Macrophotograph of a pre-existing crack cut out of EDG #103, No. 7 cylinder piston skirt and fractured open. This low magnification photograph shows both of the mating fracture surfaces after the ridge segment was opened.

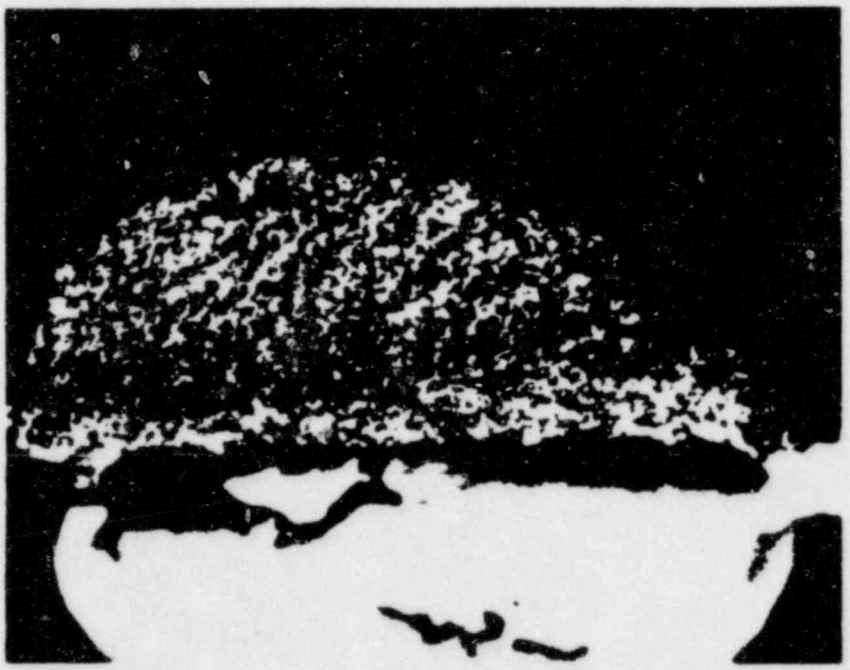

Figure 2-9. Macrograph of the fracture surface from the piston skirt removed from EDG #103.

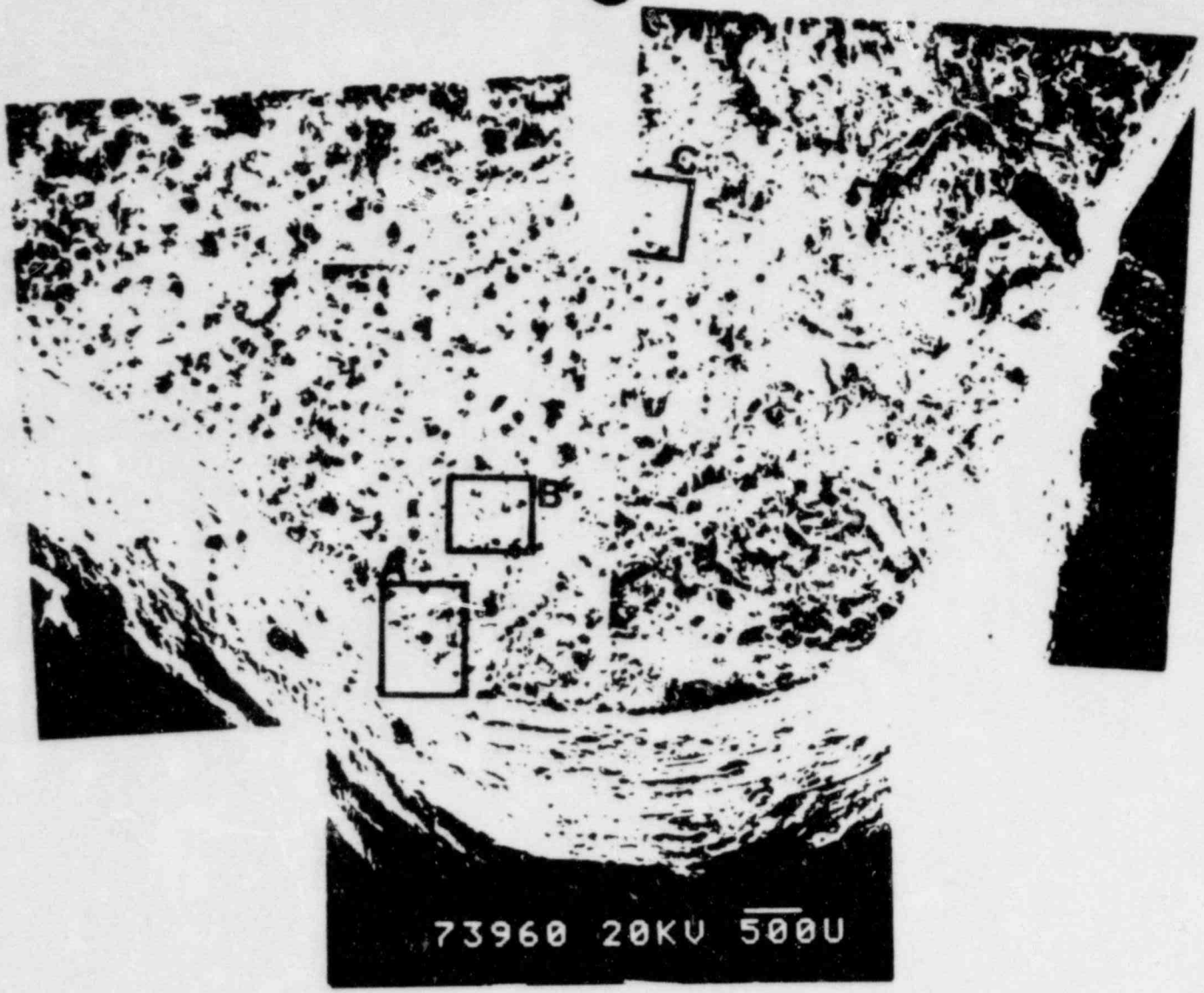

Figure 2-10. A composite SEM photograph of the pre-existing crack found in the piston skirt removed from No. 4 cylinder from EDG #101. This photo was taken of the mating fracture surface of the sample shown in Figure 2-5. Areas A, B, and C are shown at higher magnifications in Figures 2-11 to 2-13. 13X

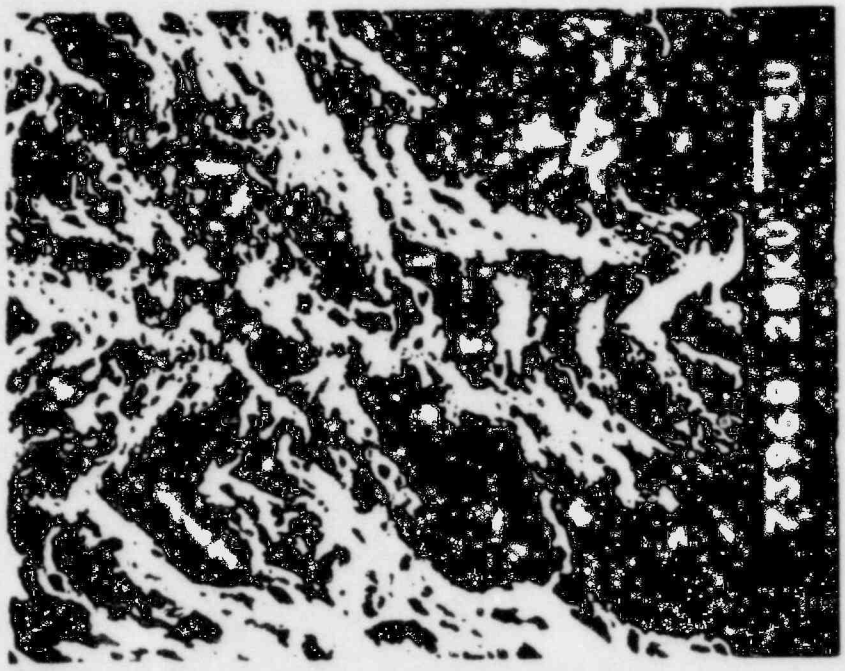

Figure 2-11. Area A of Figure 2-10. This SEM photograph shows how the fractographic details of the fracture have been rubbed and abraded. 2KX

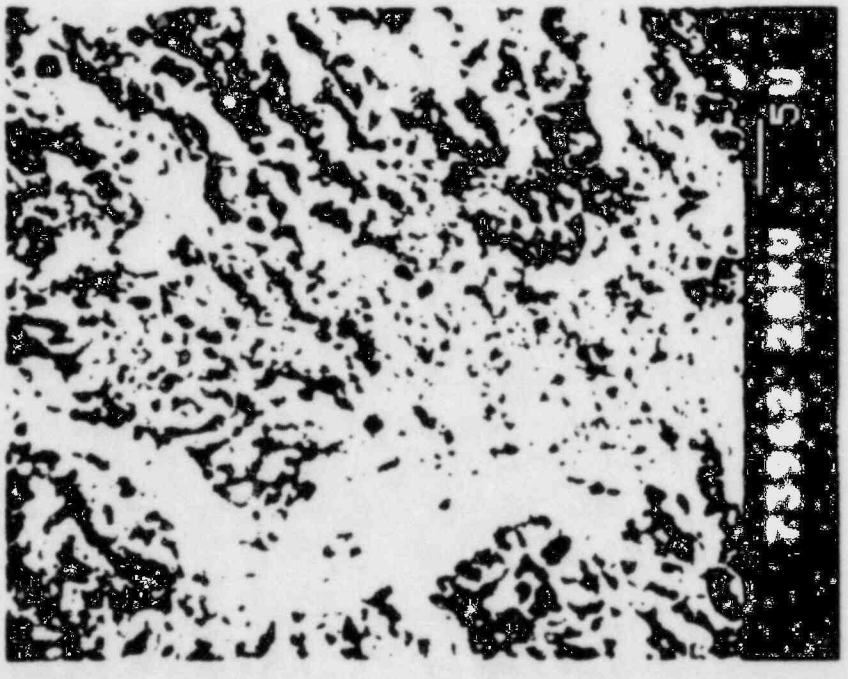

Figure 2-12. Area B of Figure 2-11. This SEM photograph shows an area nearer to the growing crack front than area A in Figure 2-11. It is abraded, but not to the same extent as shown in Figure 2-11. 2KX

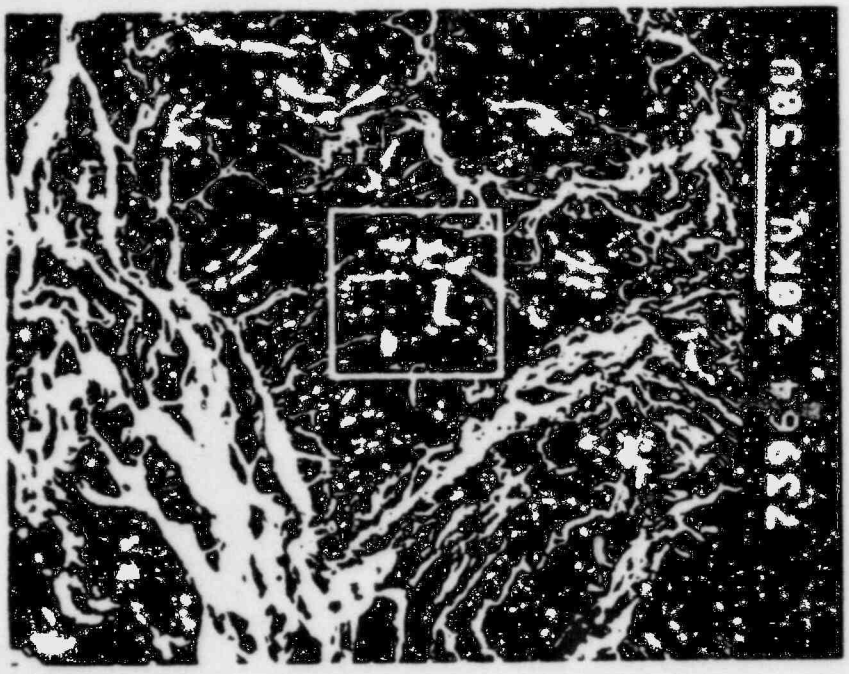

Figure 2-13. A low magnification photograph of area C in Figure 2-10. This SEM photo shows the end of the crack front and a highlighted region, 50μm behind the crack front which is shown at higher magnification in subsequent figures

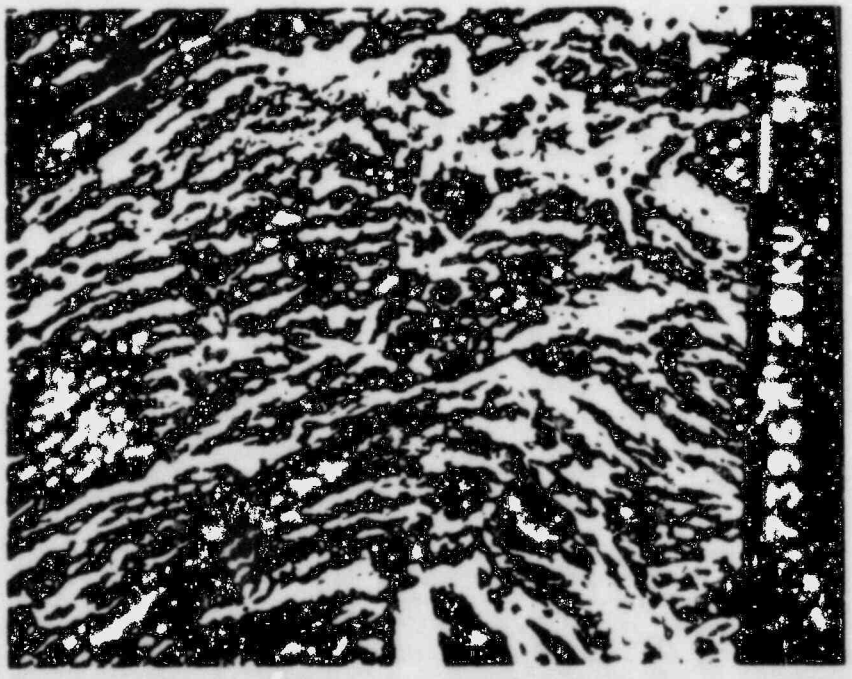

Figure 2-14. SEM photograph that shows the center region of Figure 2-13 at higher magnification. Fatigue striations are visible at center of the picture. 2Kx

FaAA-84-2-14

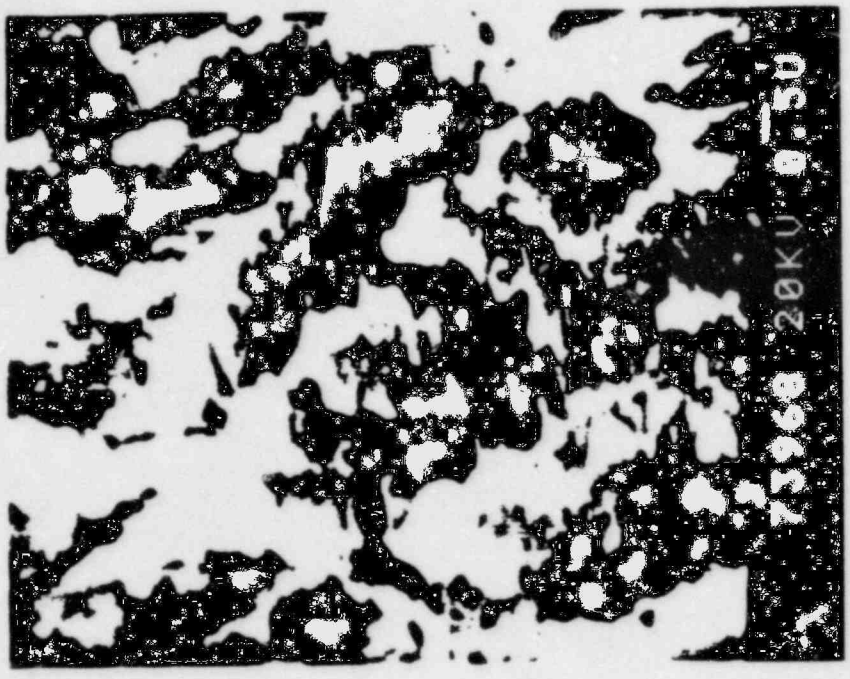

Figure 2-15. This SEM photograph is of the center region of Figure 2-14. Fatigue striations, ~1 × 10^{-5} in./cycle, are clearly visible. 10KX

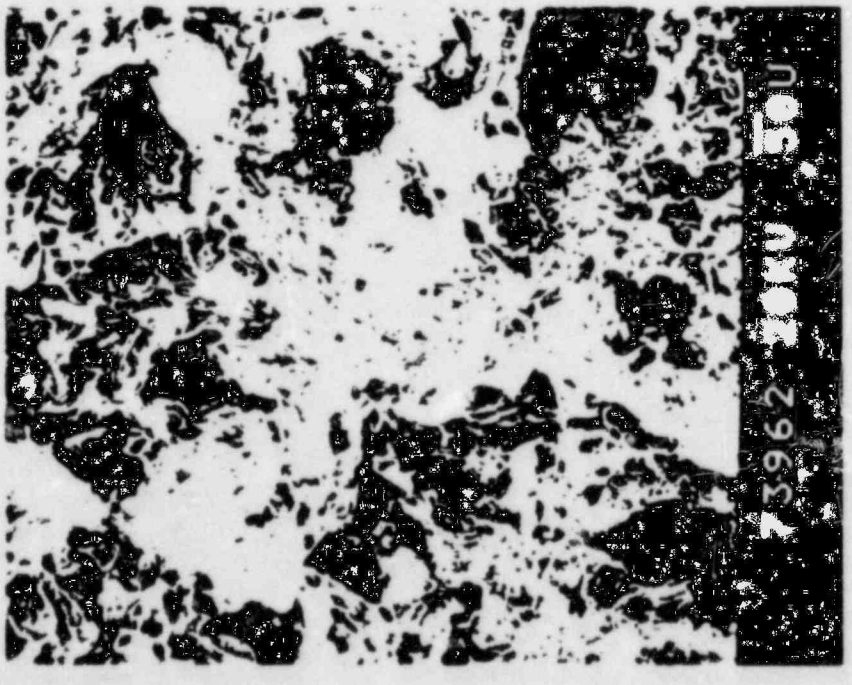

Figure 2-16. This SEM photograph shows an exemplar overload fracture area from the EDS #101 piston shown in Figures 2-10 to 2-15. Note the cleavage of the matrix, the shallow secondary cracks, and the disturbed graphite nodules.

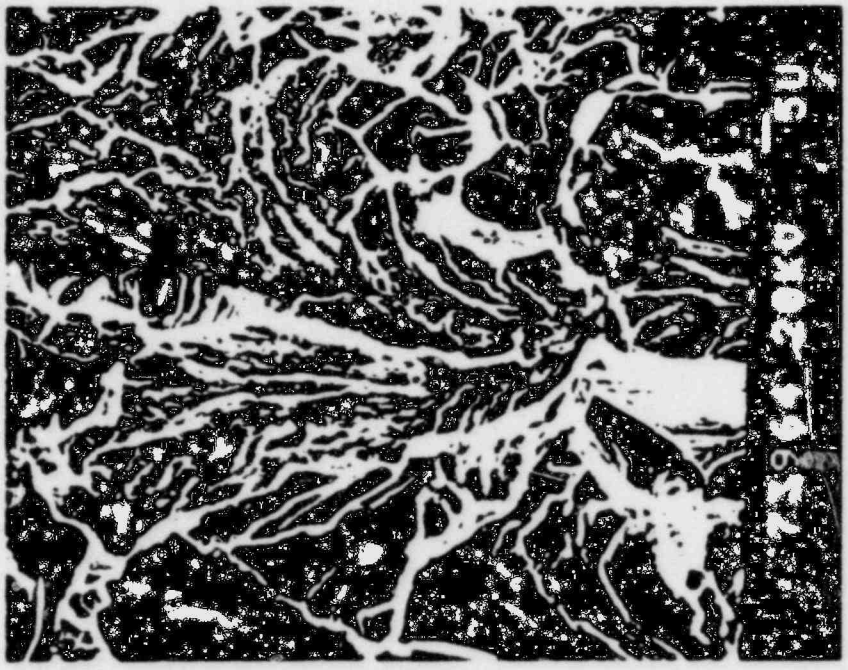

Figure 2-17. This SEM photograph shows a region of matrix cleavage in the center of Figure 2-16. 1KX

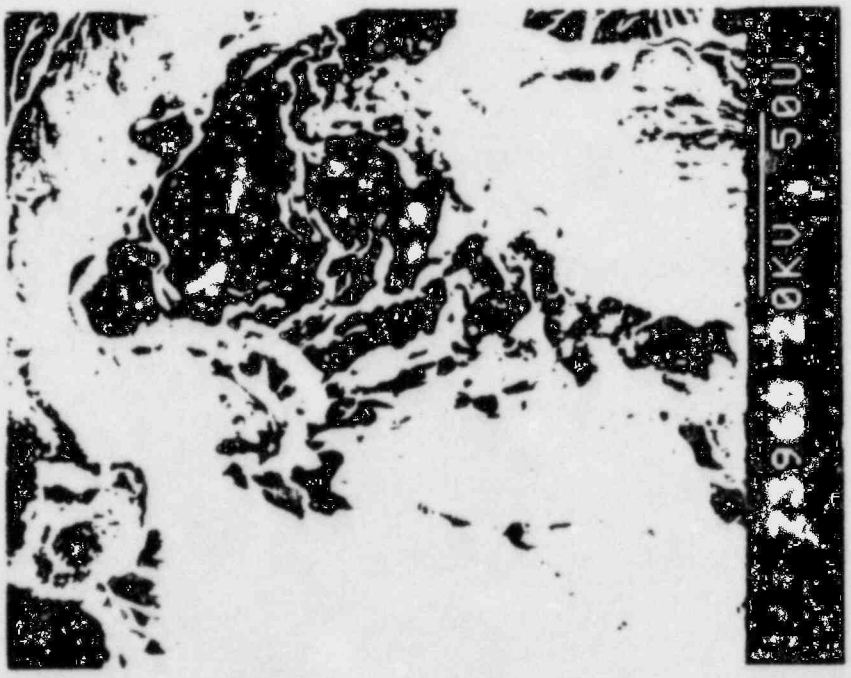

Figure 2-18 - A disturbed graphite nodule is shown in this SEM photograph of the overload region of the fracture shown in Figure 2-16. 500X

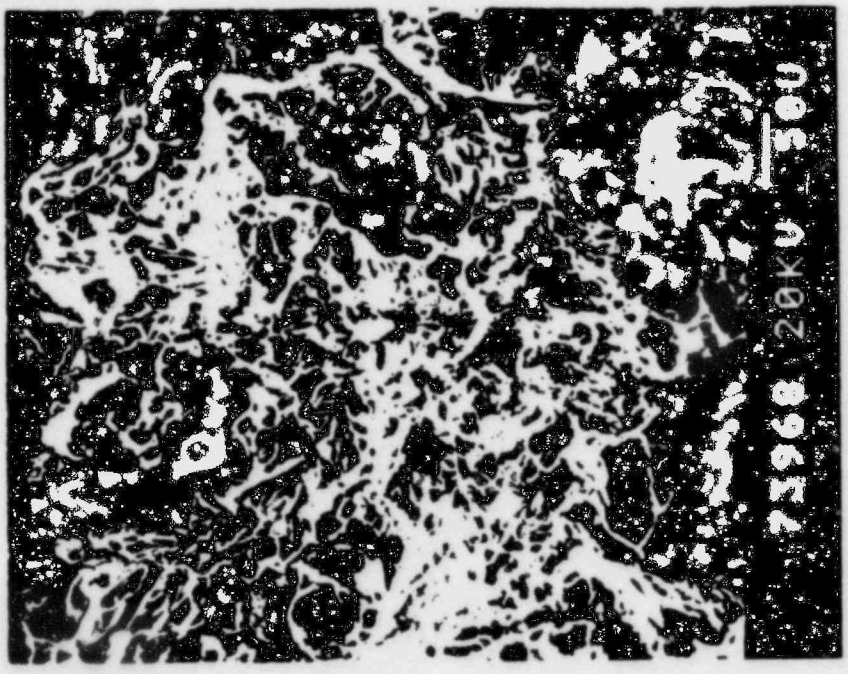

Figure 2-19. Another SEM photograph of an overload fracture region on a sample removed from EDG #101 and fractured. 200X

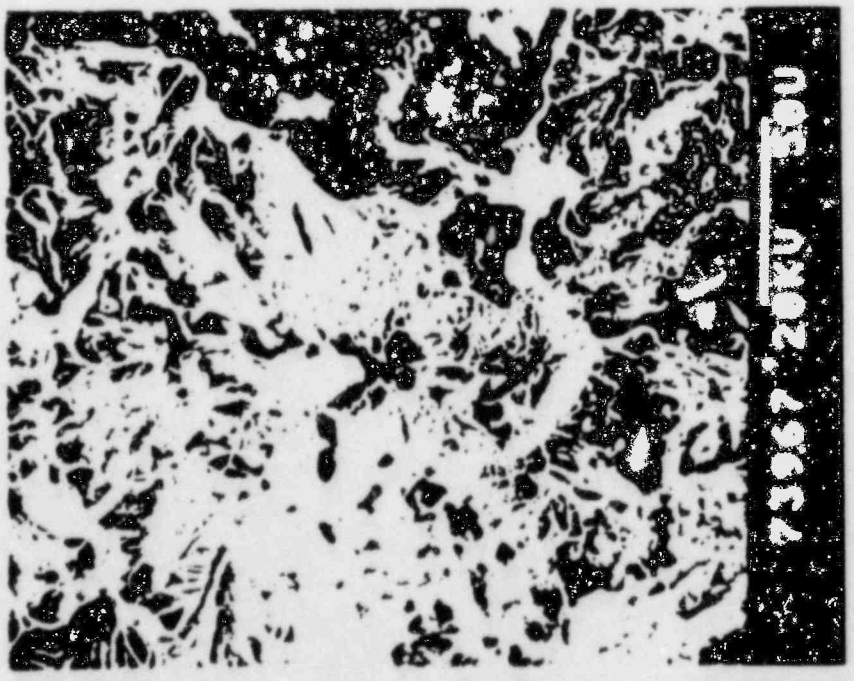

Figure 2-20. A higher magnification SEM photograph of the center of the area shown in Figure 2-19. Note the mixture of cleavage and dimpled rupture seen here; this was not on the pre-existing fatigue crack areas. 500X

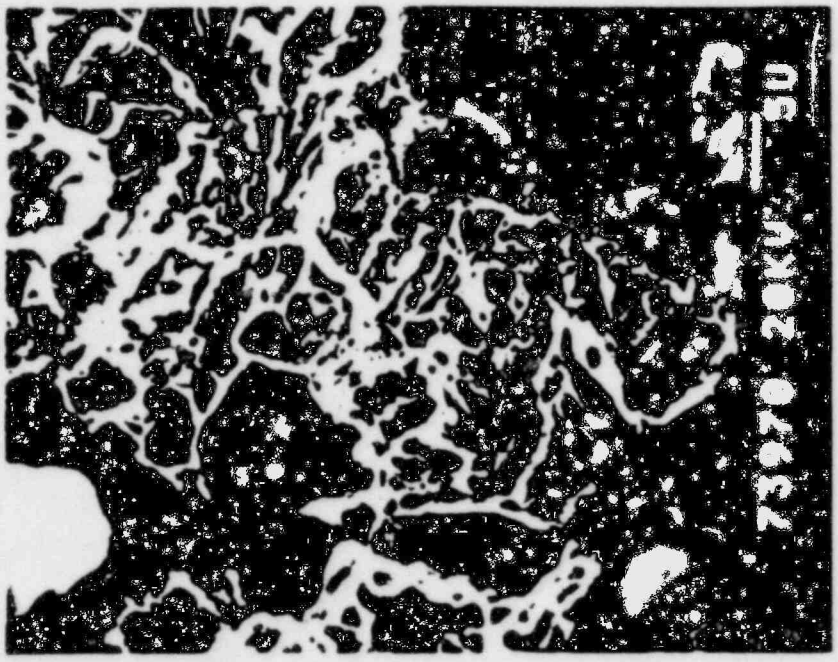

Figure 2-21. Still higher magnification SEM photograph of the center of Figure 2-20. Note the pattern of fractured pearlite. 2KX

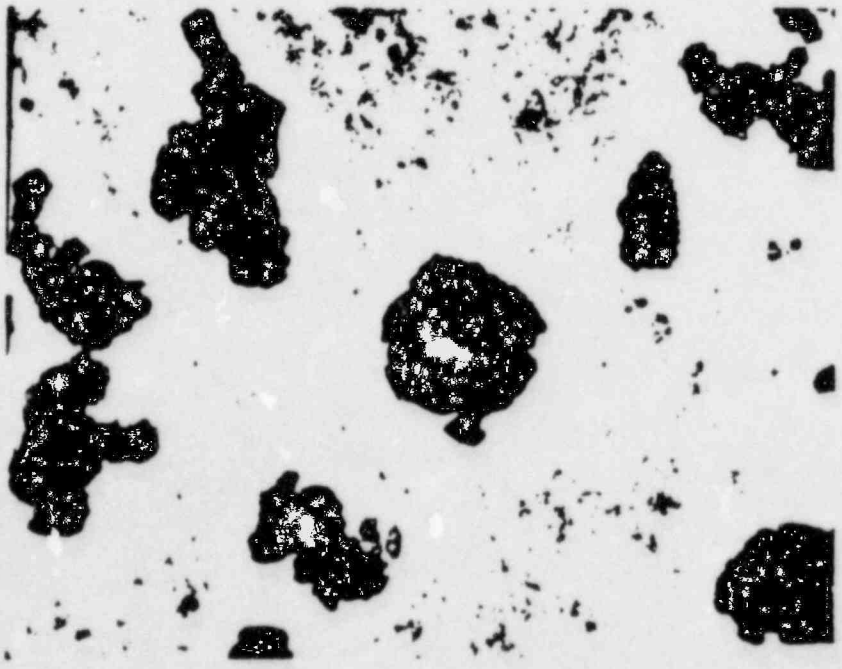

Figure 2-22. This is a metallographic photograph of a polished and etched specimen taken from EDG #102. The dark areas are graphite nodules surrounded by white ferrite. About 80% of the matrix is pearlite. 185X

3.0 EXPERIMENTAL STRAIN MEASUREMENTS

The preceding section described cracking observed in the modified AF piston skirts. Section 4 provides the results of finite element analysis of the AF skirt, along with corresponding results for the more recently designed AE piston skirt. The AE design has been supplied by TDI as a suitable replacement for the AF skirt. This section presents the results of experimental measurements of strain under static load in the AE and AF skirts. These measurements provide a means of assessing the suitability of the AE skirt as well as benchmarks for the finite element calculations.

The experimental strain measurements show that the peak stresses in the AF skirt are much larger than those in the AE skirt. The strain measurements also provide information on the pressure required to close the gap between the outer contact ring of the skirt and crown as well as the influence of such closure on the peak stresses.

3.1 Comparative Description of Piston Skirts

The AF piston skirt and crown were described in Section 2. A comparative description of the AE and AF skirts is provided in this section. Basically, the two skirt designs are similar, and only the major differences need be discussed here.

The major differences between the AF and the AE designs are concentrated in the region of the bosses through which studs extend to attach the crown to the skirt. The stud attachment bosses were considerably enlarged in the AE design. Figure 3-1 provides direct comparison of the two designs in this region. The thickness of the material around the stud hole for the AE design was substantially increased (from 1.44 to 2.62 inches), and the extent of the thickened area around the stud hole was increased (bottom portion of Figure 3-1). In addition to this modification, the following changes were made:

- Thickening of the walls of the cavity that extends from the top of the wrist pin boss to the top of the skirt. This thickening is shown in the bottom portion of Figure 3-1.

- Thickening and filling in of material around the wrist pin hole.
- Thickening and tapering of the circumferential rib that runs between the wrist pin bosses.

The complete piston consists of a skirt (either AE or AF) and a crown, as shown in Figure 2-1. Figure 3-2 shows the crown-skirt mounting. When the crown is mounted on the skirt, contact occurs only over a ring located just inside the stud bolt circle. To compensate partially for thermal distortion of the crown the outer edge of the crown is manufactured so that there is a clearance of about 0.003 inch between the outer contact rings on the crown and skirt.* Hence, there is no contact between the crown and skirt at the outer rim at room temperature when no pressure is applied. The pressure at which the gap closes, the proportion of the load carried by the two load rings and stresses resulting from loading are not well known, and are therefore of interest in the experimental work. The gap closure pressure, load split between the contact rings and peak stresses are useful in comparison with the results of finite element calculations presented in Section 4.

3.2 Test Set-Up

The loading which produces the largest stress in the piston skirt is the firing pressure. The loading due to pressure is much larger than that imposed by inertia loading or friction. Apart from contributing to the closure of the gap and consequent redistribution of the pressure load, temperature gradients will play a relatively minor role -- since they do not contribute to the cyclic stress range. The major portion of cyclic stress levels in the piston skirt can therefore be simulated by pressurizing the top of a piston crown and reacting the resulting force through the connecting rod.

Static stress coat and strain gage tests were performed on AE and AF piston skirts which were subjected to hydraulic pressures as high as 2000 psig. This is well above any reported peak firing pressures for either the R4 or RV4 engines. The tests were conducted at the Transamerica Delaval Inc.

* TDI Drawing No. 03-341-7319, Assembly Procedure 1, dated 11-8-82 specifies a gap between 0.007 and 0.011 inch.

(TDI) facilities in Oakland. TDI participated in the conduct of the tests, and also performed some parallel testing that provided results that were virtually identical to those obtained in the joint tests to be reported here.

An actual cylinder liner was used in the test, with two opposing pistons placed crown-to-crown within the liner. The region between the crowns was pressurized with a hydraulic pump, and the pressure load on the instrumented skirt was reacted through the wrist pin and a short piece of connecting rod to a support plate. The connecting rod was in a vertical position, thereby simulating the top center position of the piston. A rubber O-ring was placed in a specially machined groove in the piston crown in order to seal the pressurized oil, and the pressure was read from a pressure gage. The leakage past the O-ring was very small so that constant pressure on the crown was easily maintained.

As reported in Section 3.3, a brittle lacquer, or stress coat, test was performed on the AE skirt in order to identify regions of peak stress. These regions were then concentrated upon in the strain gage tests. A stress coat test was not performed on the AF piston skirt; the locations of cracking discussed in Section 2 provided indications of locations of peak stresses in this skirt design.

Strain gages were mounted on the piston skirts and connected to the data acquistion and recording equipment. Several different strain gage sizes and configurations were employed, as will be discussed in Section 3.4 - Strain Gage Tests.

The instrumentation used to measure and record the strain readings was a Micro-Measurements Vishay System 4000, which included an HP 9825 Computer for the "executive unit," a Vishay 4220 Controller, and three Vishay 4270 Strain Gage Scanners. The System 4000 is a computer-controlled data acquisition system which can acquire the raw data as well as use the computer to provide appropriate data reduction.

The system software is loaded in the executive unit, and essential data (such as gage factor and which channels have gages) are input by the user and

recorded on magnetic tape in the executive unit. The executive unit also contains a built-in printer to document the input of parameters and the recorded data.

The 4220 Controller, including its interface with the executive unit, provides the logic and timing conversion between the executive unit and the scanners. The 4220 Controller digitizes the analog signal from the scanners and routes it to the executive unit for recording. The controller also provides the logic for the scanners.

The 4270 Strain Gage Scanners contain 20 channels per scanner. The scanner can scan at a rate of 30 channels per second based on a 60 Hz power line. The scanner also provides internal shunt calibration to check each channel. At each pressure that strain gage data was gathered, the strain reading from each of the strain gages was recorded upon command on magnetic cassette tape. Selected magnetic tape data was also printed on paper tape for displaying of test results and to provide checks on the storage of data. The magnetic cassette was interfaced through the HP9825 computer to an IBM personal computer. The IBM unit was then used for data storage, manipulation and printing and plotting of test results.

3.3 Stress Coat Test

In order to identify with confidence and accuracy the areas of highest stress in the AE skirt, a brittle lacquer, or stress coat, test was performed to identify precisely the highly stressed regions of this skirt design. These results were used to provide guidance in the placement of strain gages for subsequent quantitative evaluation of skirt strains. The serial number and heat number of the skirt that was tested with stress coat were G80 and 342K, respectively.

A stress coat test was performed on an AE piston skirt with attached crown. The gap between the crown and skirt was measured with a feeler gage to be uniform and between 0.007 and 0.008 inch. The region of the four crown stud mounting bosses was sprayed with Tens-Lac. Calibration blocks were also

prepared in order to provide estimates of the threshold strain for cracking of the brittle lacquer.

The strains in the piston skirt are primarily compressive, whereas cracking of brittle lacquer occurs when subjected to tensile strain. In order to use the brittle lacquer for evaluation of compressive strains, the pressure was applied to a given level, held for approximately 15 minutes, and then rapidly released. The hold time allowed the brittle lacquer to creep so that it would be placed in tension when the pressure was rapidly released. Tests on the calibration blocks that were tested under the same conditions (compression, hold, rapid release) showed a cracking threshold of 1500 to 2000 uin/in.

A pressure of 500 psig was first applied, held, and then rapidly released. A careful inspection revealed no cracking of the lacquer. The same procedure was followed with a pressure of 1000 psig, and again no cracking was observed. The pressure was then increased to 2000 psig, and localized cracking was observed in the stud boss region. Figure 3-3 presents a photograph of the cracked region, which was observed on three of the stud bosses. A roughly circular region of about 1/2 inch diameter was observed on the three stud bosses that exhibited cracking of the brittle lacquer. This served to closely define the region with largest strains, which was then concentrated upon in the placement of strain gages for obtaining quantitative strain levels.

3.4 Strain Gage Test

An AF and AE skirt were instrumented with foil-resistance strain gages. Attention was concentrated on the regions of peak stress as well as on locations that provide information on gap closure and load transfer between the inner and outer loading rings.

3.4.1 AE Piston Skirt

An unused AE piston skirt was instrumented with rectangular rosettes with one arm of the rosette oriented in the direction along the axis of the piston. The serial number and heat number of the instrumented piston skirt were G73 and 388K, respectively. Fifteen rosettes were mounted; Figure 3-4

summarizes the locations and Table 3-1 summarizes the description of the locations. Two rosettes were placed on each stud mounting boss in the region where the brittle lacquer was observed to crack (for a total of eight rosettes). All gages in these highly stresses regions had a gage length of 0.030 inch. As indicated in Figure 3-4, two rosettes (A and J) were mounted in the stud boss region away from the location of the peak stress. These "column gages" provide an estimate of nominal stresses in the wrist pin cavity wall. The K and M rosettes were placed on the longitudinal ribs between the wrist pin bosses. Rosettes P and R were placed in the wrist pin cavity. Rosette N was placed on the skirt wall 90° from the wrist pin. These rosettes provided information on the pressure required to close the gap between the outer load ring and the crown, as well as to estimate how the load was divided between the two loading rings. Some of the gages located in regions of lower strain gradients had gage lengths of 0.060 inch.

Tests were conducted by applying the pressure in steps. At each step, the pressure was held constant while the strain gage readings were automatically recorded by the instrumentation system. Data was recorded for both increasing pressure steps and decreasing pressure steps. Several cycles of loading were recorded.

Two separate test series were conducted; one with a conventional crown, and one with a crown that was machined to widen the gap so that it would not close under an applied pressure of 2000 psig. Thus, the loading was known to be only on the inner ring in the test with the modified crown.

The strain gages were zeroed prior to installing the crown on the skirt. The TDI-specified crown installation procedures were followed, and strain gage readings then taken. Only very small strains were recorded at this point. Pressure was then applied in steps, as mentioned above, and strain gage readings recorded.

The maximum stresses in the piston skirt under peak firing pressure are of primary interest. This pressure is approximately 1670 psig as independently measured by FaAA and reported by TDI [3-1]. Some of the circumferential gages in the rosettes in the stud boss region did not work; however, enough

were operable to provide accurate and representative results. Table 3-2 summarizes the strain readings for the stud boss rosettes that were complete. The results are for 1600 psig on the first cycle of rising load for a conventional crown. The principal strains were calculated from the rosette readings using the conventional equations for a rectangular rosette [3-2]. The following elastic constants were used to calculate the stresses from the strains.

$$E = 23.6 \times 10^6 \text{ psi}$$
$$\nu = 0.3$$

These values are reported in Reference 3-3, and the value of E is in accordance with the value suggested by TDI.

The results presented in Table 3-2 show that the principal stresses and strains are very closely aligned with the z and θ (axial and circumferential) directions in the skirt, because ε_z and ε_θ are nearly equal to ε_{II} and ε_I, respectively. Additionally, the stresses are nearly uniaxial, and the value of σ_{III} is well below the yield strength of the material.

The stress levels for the rosettes which had inoperable circumferential gages can be estimated by assuming $\varepsilon_\theta/\varepsilon_z = 0.17$, which is the average value for the rosettes included in Table 3-2. This allows the results presented in Table 3-3 to be obtained. A comparison of the results from the two tables show that the stress values are comparable; the smallest value (37.8 ksi) being 78% of the largest value (48.4 ksi). Hence, the results do not show a large variation from rosette to rosette nor from stud boss to stud boss. Therefore, the values measured should be close to the largest values present in the skirt, and are the values to be compared with the peak stresses calculated by finite elements (once adjustments are made for differences in pressure and load splits between inner and outer rings).

The absolute value of σ_{III} ($\sim\sigma_z$) for Rosette C is plotted in Figure 3-5 for the three pressurization cycles applied and for increasing pressure between steps (up) and decreasing pressure (down). The upper part of the figure presents results for a conventional crown, and the lower part of the figure is

for the modified crown (in which gap closure does not occur). These figures show the degree of reproducibility and hysteresis in the test results.

The solid line in the upper part of Figure 3-5 is through the data for Run 1 up. A bilinear variation of stress with pressure is observed, with a slope change at just below 1000 psig. This slope change is believed to be due to closure of the crown-skirt gap at the outer loading ring. Evidence of this is shown in the lower portion of Figure 3-5, which presents corresponding results obtained by use of the modified crown. In this case a linear σ_{III} versus p variation is observed, with a slope equal to that for a conventional crown at pressures below 1000 psig. The 12% difference at the peak firing pressure between the modified and conventional crown indicates that approximately 88% of the pressure load is carried on the inner ring at the peak firing pressure. This result is for room temperature. A greater percentage of the load is expected to be applied on the outer ring at operating temperature. This is because the top of the crown is hotter than the underside thereby producing thermal distortion whose effect will be to partially (or totally) close the gap. This results in more load being transmitted through the outer ring. Since the stress in the stud attachment boss is governed by the load applied to the inner contact ring, the effect of thermal distortion is to reduce the peak stresses due to firing pressure.

Further evidence of a gap closure pressure of about 1000 psig (at room temperature) is provided by considering the strain data from the rosettes in the wrist pin cavity (P at inner ring, R at outer ring) and at the top of the skirt 90° from the wrist pin (N). Figure 3-6 presents the axial strain (ε_z) measured in the inner part of the wrist pin cavity (P) with a conventional crown. Once again, a bilinear relation with pressure is observed, with the slope change occurring at about 1000 psig. In this instance, the slope change is not as large.

Figure 3-7 shows results for axial strain with conventional and modified crowns for the rosette at the outer edge of the wrist pin cavity (R). Once again, a bilinear variation with pressure is observed for the complete crown, with the slope at low pressure being equal to that for a modified crown. The slope change again occurs at 1000 psig and is particularly marked

in this instance. Apparently, once the outer gap is closed, relatively large loads are transmitted through the outer ring over the wrist pin.

Figure 3-8 presents results for the rosette 90° from the wrist pin (N). The bilinear relation is again observed, with a slope change at about 1000 psig -- which is the same behavior observed on all other rosettes. A comparison of the rosettes under the outer ring (N and R) shows that the slope change is in opposite directions for the 90° position versus the wrist pin. The marked increase in the slope for the wrist pin results (Figure 3-7), in conjunction with the less marked decrease at 90°, indicates that (once the gap closes) most of the load on the outer ring is reacted over the wrist pin, with a smaller portion of the load being transmitted in the portion of the outer ring away from the wrist pin. Such behavior is explainable if each of the contact rings on the crown is considered to remain planar when the crown/skirt is pressurized. The vertical displacement (u_z) in each of the contact rings would be uniform, and "dishing" distortion of the crown is responsible for gap closure and varying load split between the inner and outer loading rings. A uniform vertical displacement over the outer ring would result in most of the outer ring load being reacted over the relatively very rigid wrist pin boss, with much less load over regions away from the wrist pin boss. This would explain the difference in direction of the slope change for the wrist pin (R) and 90° rosette (N).

Finite element results that include the crown and the skirt, as discussed in Section 4.4, provide additional insight into the behavior of the crown and skirt in the contact regions.

3.4.2 AF Piston Skirt

A used AF piston skirt which had been stress relief heat treated was supplied by TDI for strain gage testing. The serial number and heat number of the skirt were K88 and 292M, respectively. A variety of different strain gage types was used. The compound curvatures present at the locations where cracks have been observed, as can be seen in Figure 2-4, precluded the use of rosettes in the high strain regions. Therefore, a single gage was mounted in the high strain regions of each stud boss. In one case, a rectangular rosette

(U) was placed as close as possible to the gage in the high strain location in order to provide a check on the degree of uniaxiality of the stresses in the stud boss region. The results of the strain gage measurements on the AE piston skirt showed that the stresses are all nearly uniaxial. Hence, the use of a rosette is not necessary in order to characterize the stress at a given location.

Figure 3-9 identifies the strain gage location on the AF skirt, and Table 3-4 summarizes gage lengths and configuration employed. The particular skirt employed for this test exhibited a noticeable lack of symmetry which was apparently due to core shift during the casting process. Therefore, as shown in Figure 3-9, both wrist pin cavities were instrumented in order to provide information on the symmetry of the loading through the wrist pin bosses.

Tests were conducted in the same manner as for the AE skirt. Two separate test series were conducted; one with a conventional crown, and one with a conventional crown with a 0.005 inch shim placed between the crown and the top of the skirt along the inner contact ring. The gap between the crown and the skirt (without the shim) was measured with a feeler gage. The gap was found to be between 0.0075 and 0.0095 inch, with some variation around the circumference.

The skirt was placed on the crown and inserted into the test cylinder. The crown was not bolted to the skirt; results on the AE skirt showed that stud loads did not produce appreciable strain for the loading case considered. Pressure was applied in steps and strain gage readings recorded. The following pressure cycles were applied:

2 cycles to 1200 psig with no shim,
1 cycle to 2000 psig with no shim, and
2 cycles to 2000 psig with shim.

The maximum stresses in the piston skirt under peak firing pressure are of primary interest. Table 3-5 summarizes the strain readings and stresses for the four stud boss gages. Also included in the table are the corresponding results for the column rosettes (A and J), the rosette near Gage B, and

the wrist pin cavity rosettes (P, R, S, and T). The results are for 1600 psig under rising pressure conditions. The rosette results in the stud boss regions (A, J, and U) show that the stresses are nearly uniaxial which is in agreement with the observations on the AE skirt.

A comparison of the results in Table 3-5 for the ligament gages (B, D, F, and H) show a large variation from stud boss to stud boss. Gage B shows elastically calculated compressive stresses well in excess of the ultimate tensile strength of the material. Hence, it is apparent that yielding was taking place in the ligament. This will be discussed more fully below. Even ignoring the results for Gage B, a large variation between locations is shown in Table 3-5; the smallest value of σ_{III} with no shim (35.9 ksi) is 72% of the largest value (49.7 ksi). Hence, there is more variation between locations than was observed in the AE skirt.

This larger variation in the AF skirt could result from four factors.

(i) Geometrical variations from stud boss to stud boss are larger in the AF than the AE, because the ligaments are hand-ground in the AF and are as-cast in the AE.

(ii) Geometrical variations resulting in lack of symmetry of the skirt were considerably larger in the particular AF skirt tested than were present in the AE skirt. Such variations can produce non-symmetrical loading in the wrist pin areas.

(iii) The gap measured in the AF piston showed more circumferential variation than the AE. This is another source of asymmetrical loading.

(iv) Strain gradients on the surface of the AF are larger than than AE so that is is easier to miss the location of peak stress in the AF when strain gages are applied.

The larger strain gradients at the surface in the AF are apparent by considering the results in Table 3-5 for the rosette near Gage B (Rosette U). Even through B and U were quite close to one another (~1/4 inch), there is a factor of over three between their strain values. In marked contrast to this,

rosettes in the AE placed adjacent to one another showed very similar results (see Tables 3-2 and 3-3).

Asymmetry of the load paths into the wrist pin boss may be a major contributor to the stud boss variations. Table 3-5 shows that the column rosette on the high strain side of the skirt (A on the B-D side) had lower strains than the column rosette on the opposite (lower strain) side (J). This indicates that asymmetry is not a contributor. In contrast to this, the rosette on the inner wall of the wrist pin cavity on the high strain (B-D) side showed strain levels almost twice those of its counterpart on the opposite side (P). This large difference suggests that asymmetry of the skirt response is appreciable -- even though it doesn't show up in the column gages. The strain levels of the rosettes on the outer wrist pin wall are also included in Table 3-5. The strain levels are quite low and approximately the same. This indicates that much more of the load under the test conditions is being transmitted down the inner wall of the wrist pin cavity than down the outer wall (an expected result).

Returning to the topic of yielding in Ligament B, Figure 3-10 presents the pressure-axial strain results for each loading and unloading for each of the pressurization cycles applied. Pressure is used as the vertical axis for this figure so that it is analogous to a stress-strain curve. The nonlinearity of the curves is due to two sources; gap closure and yielding of the material. Gap closure increases the pressure required for a given strain at the gage location. Hence, gap closure results in a p-ε curve that is concave upward (in Figure 3-10). Yielding decreases the pressure required for a given strain and results in a p-ε cuve that is concave downward (like a conventional stress-strain curve). The hysteresis in the curve is due to crown/skirt friction and plastic deformation. The observance of high strain in conjunction with a concave downward p-ε curve during the first cycle for a given condition (when p_{max} = 2000 psig) shows that plastic deformation is occurring. The relatively large zero offsets (plastic offset) and bilinear behavior during subsequent cycles is further evidence of plastic deformation, rather than gage abnormalities or complex skirt/crown interaction.

The absolute value of the elastically calculated stress ($E\varepsilon$) for each of the stud boss gages is plotted in Figures 3-11 through 3-14. Results are shown for a conventional gap (no shim) and with a 0.005 inch thick shim (with shim). The stud boss to stud boss variation at 1600 psig discussed above is readily apparent by comparison of these figures. The bilinear variation of stress with pressure that was observed for the conventional crown with the AE piston skirt (Figures 3-5 through 3-8) is again observed for the AF. The slope changes in these figures are due to gap closure. In contrast to the AE results, the AF results are for two different gap sizes and shows the influence of gap size on the gap closure pressure. For a given gage, the slopes of the linear positions of the curves are nearly the same with and without the shim, but the pressure at which the slope changes is dependent on the presence or absence of the shim. The results invariably show that the slope change occurs at a higher pressure when the shim is present. This is expected because a higher pressure is required to close a larger gap.

The "load split" between the inner and outer rings at the peak firing pressure of 1670 psig can be estimated from the results in Figures 3-11 through 3-14. (The percent load split values shown have been compensated for zero offset on the line for low pressure.) Table 3-6 summarizes the results from the figures. Large variation in the load splits are not observed, and (as expected) a greater share of the load is on the inner ring when the gap is larger (shim inserted).

Further evidence of gap closure is provided by considering the strain data from the rosettes in the wrist pin cavity (P, R, S, and T) and at the top of the skirt 90° from the wrist pin (N). Figures 3-15 through 3-19 present the values of the axial strain as a function of pressure for these rosettes. The observed behavior is the same as observed in the AE skirt; the discussion at the end of Section 3.4.1 therefore also applies to the AF skirt, except that larger variations of the indicated gap closure pressure from gage location to gage location is observed in the AF skirt. This is again due to asymmetry of the piston and circumferential variations of the initial crown/skirt gap. Table 3-7 summarizes the gap closure pressure (pressure at slope change) for the gage locations included in Figures 3-11 through 3-19. For

comparison purposes, corresponding results for the AE skirt (as obtained from Figures 3-5 through 3-8) are also included in this table. Table 3-7 shows that there is some variation in indicated gap closure pressure for both skirt designs, depending on which gage location is used. Selected nominal values of the gap closure pressures are shown in the bottom line of Table 3-7. The results for the AF skirt show an approximately linear variation of gap closure pressure with gap (800 psig for ~8 mils, 1300 psig for ~8+5 = 13 mils), and the gap closure pressure for the AE skirt is higher than the AF skirt. The linear variation of gap closure pressure with gap is expected. The higher gap closure pressure for the AE is also expected; the top of the AE skirt is stiffer than the AF because of the additional material around the stud bosses and wrist pin cavity (see Figure 3-1).

A comparison of the peak stress magnitudes reveals that the peak stresses in the AF are generally higher than the corresponding AE values, even when no compensation is made for the different load splits (~80% versus 88%). The largest strains measured in the AF were well into the plastic range, whereas all strains measured in the AE were elastic. Additional comparisons between the two skirt designs are presented in Section 5 in which comparisons with finite element calculations are made.

3.5 Section 3 References

3-1 TDI Reported Values for Unit 1, Division 2, of DSRV-16-4 Engine at Grand Gulf Nuclear Station.

3-2 R.C. Dove and P.H. Adams, Experimental Stress Analysis and Motion Measurement, Charles E. Merrill Books, Inc., Columbus, Ohio, 1964.

3-3 Iron Castings Handbook, edited by C.F. Walton and T.J. Opar, Iron Casting Society, Inc., 1981.

Table 3-1

DESCRIPTION OF STRAIN GAGE LOCATIONS ON AE PISTON SKIRT
(Refer to Figure 3-4)

Location	Gage Identification
Stud Boss	B, C, D, E, F, G, H, I
Column	A, J
Rib	K, M
Inner Wall of Wrist Pin Cavity	P
Outer Wall of Wrist Pin Cavity	R
Top at 90° from Wrist Pin	N

Table 3-2
STRAIN READINGS AND CALCULATED STRESSES FOR AE PISTON SKIRT FOR THE COMPLETE STUD BOSS ROSETTES AT 1600 PSIG WITH A CONVENTIONAL CROWN
(all strain values are in μin/in)

	C	D	E	F	H
ε_z	-1740	-1668	-1722	-1605	-1583
ε_θ	270	366	304	270	246
ε_{45}	-732	-787	-815	-602	-632
ε_I	270	375	310	272	247
ε_{II}	-1740	-1677	-1728	-1607	-1584
σ_{II}, ksi	-6.5	-3.3	-5.4	-5.5	-5.9
σ_{III}, ksi	-43.0	-40.6	-42.4	-39.6	-39.24

Table 3-3

STRAIN READINGS AND CALCULATED STRESSES FOR THE AE PISTON SKIRT FOR THE STUD BOSS ROSETTES WITH MISSING ϵ_θ FOR A CONVENTIONAL CROWN AT 1600 PSIG
(all strain values are in μin/in)

	B	G	I
ϵ_z	-1930	-1768	-1471
$\epsilon_\theta = 0.17\ \epsilon_z$	328	301	250
ϵ_{45}	-1145	-798	-1014
ϵ_I	379	303	340
ϵ_{II}	-1981	-1770	-1561
σ_{II}, ksi	-5.6	-5.9	-3.3
σ_{III}, ksi	-48.4	-43.6	-37.8

Table 3-4

DESCRIPTION OF STRAIN GAGE LOCATIONS, CONFIGURATIONS AND GAGE LENGTHS ON THE AF PISTON SKIRT
(Refer to Figure 3-9)

Location	Gage Identification	Configuration	Gage Length, inch
Stud Boss	B, D, F, H	Single	0.015
Near Stud Boss	U	Rosette	0.030
Column	A, J	Rosette	0.060
Rib	K, M	Single	0.030
Inner Wall of Wrist Pin Cavity	P, T	Rosette	0.060
Outer Wall of Wrist Pin Cavity	R, S	Rosette	0.060
Top at 90° from Wrist Pin	N	Rosette	0.060

Table 3-5

STRAIN READINGS AND STRESSES FOR SELECTED LOCATIONS ON AF PISTON SKIRT
FOR 1600 PSIG UNDER RISING PRESSURE CONDITIONS

		$-\varepsilon_z$, μin/in			$-\sigma_{III}$, ksi			$-\sigma_{II}$, ksi		
		No Shim	Shim Cycle 1	Shim Cycle 2	No Shim	Shim Cycle 1	Shim Cycle 2	No Shim	Shim Cycle 1	Shim Cycle 2
inner cavity	T	1236	1491	1517	30.9	37.6	38.3	5.3	6.9	7.1
outer cavity	S(1)	153	78	81	3.1	1.1	1.2	-1.8	-2.5	-2.4
column	A	395	456	427	10.3	11.5	10.7	0.1	0.6	0.5
near B	U	1071	1272	1260	26.9	32.6	32.6	1.1	4.4	4.8
ligament	B	3872	4970	5271	91.4	117.3	124.4	--	--	--
	D	2104	2589	2602	49.7	61.1	61.4	--	--	--
ligament	F	1520	1823	1784	35.9	43.0	42.1	--	--	--
	H	1636	1927	1867	38.6	45.5	44.1	--	--	--
column	J	471	498	509	12.9	12.9	13.1	-0.5	-0.2	-0.2
inner cavity	P	658	801	822	15.5	18.9	19.4	--	--	--
outer cavity	R	143	69	54	2.9	1.2	0.6	-1.9	-1.7	-2.3

σ_{III} for B, D, F, H, P $-E\varepsilon_z$

(1) Relatively large zero shift when shim was installed (see Figure 3-18).

Table 3-6

SUMMARY OF LOAD SPLITS BETWEEN INNER AND OUTER RING WITH AND WITHOUT SHIM FOR AF SKIRT
(Data from Figures 3-11 through 3-14)

Gage	No Shim	With Shim
B	75%	90%
D	79	96
F	82	91
H	77	91

Table 3-7

SUMMARY OF GAP CLOSURE PRESSURES AS ESTIMATED FROM GAGES AT VARIOUS LOCATIONS FOR THE AE AND AF PISTON SKIRTS

(all pressures are in psig)

		AF					AE	
		BD Side		FH Side				
		No Shim	With Shim	No Shim	With Shim			
Boss Gages	B	700	1300	800	1300	F	C	1000
	D	700	1400	800	1350	H		
Wrist Pin Cavity								
Inner Wall	T	900	1300	900	1050	P	P	820
Outer Wall	S	800	1500	1000	1650	R	R	1050
Top 90°	N	700	1250	700	1250	N	N	900
Nominal Values		800	1300	800	1300			1000

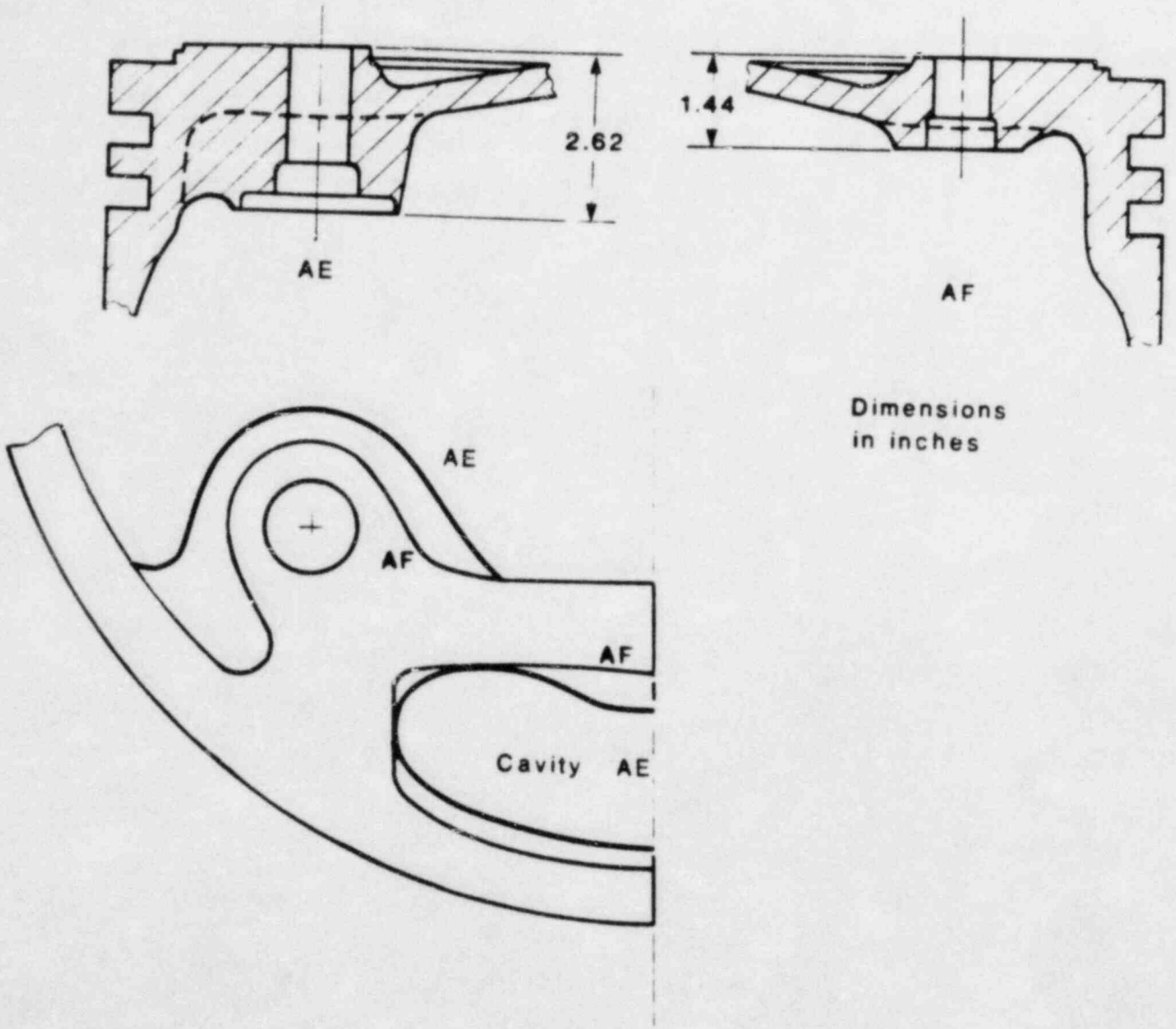

Figure 3-1. Comparison of AE and AF piston skirts in the regior of the stud attachment bosses.

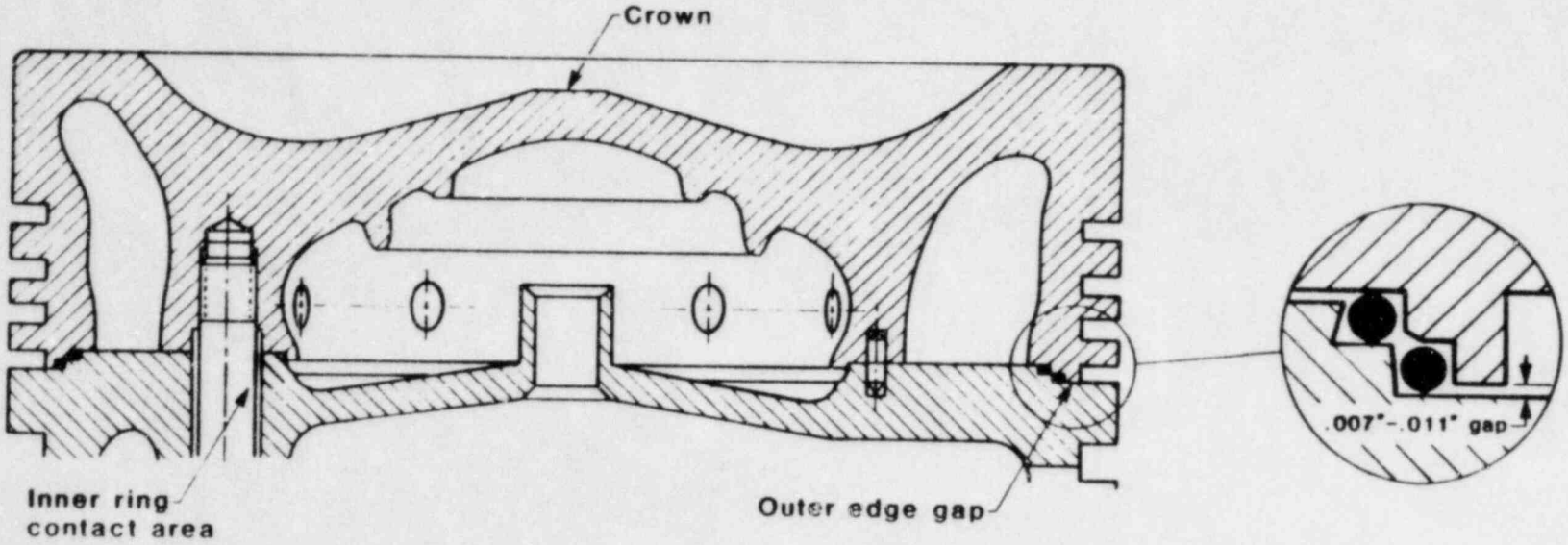

Figure 3-2. Cross section of crown and skirt indicating the two areas of load transfer from the crown to the skirt.

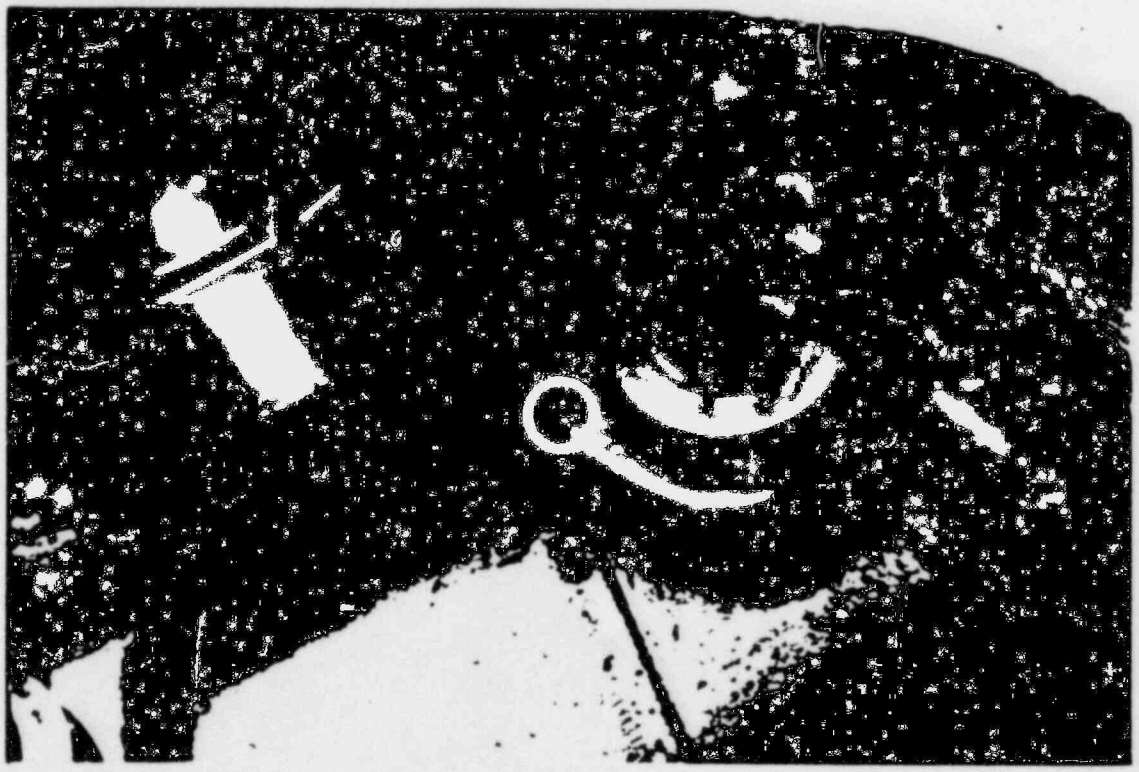

Figure 3-3. Photograph of cracked lacquer.

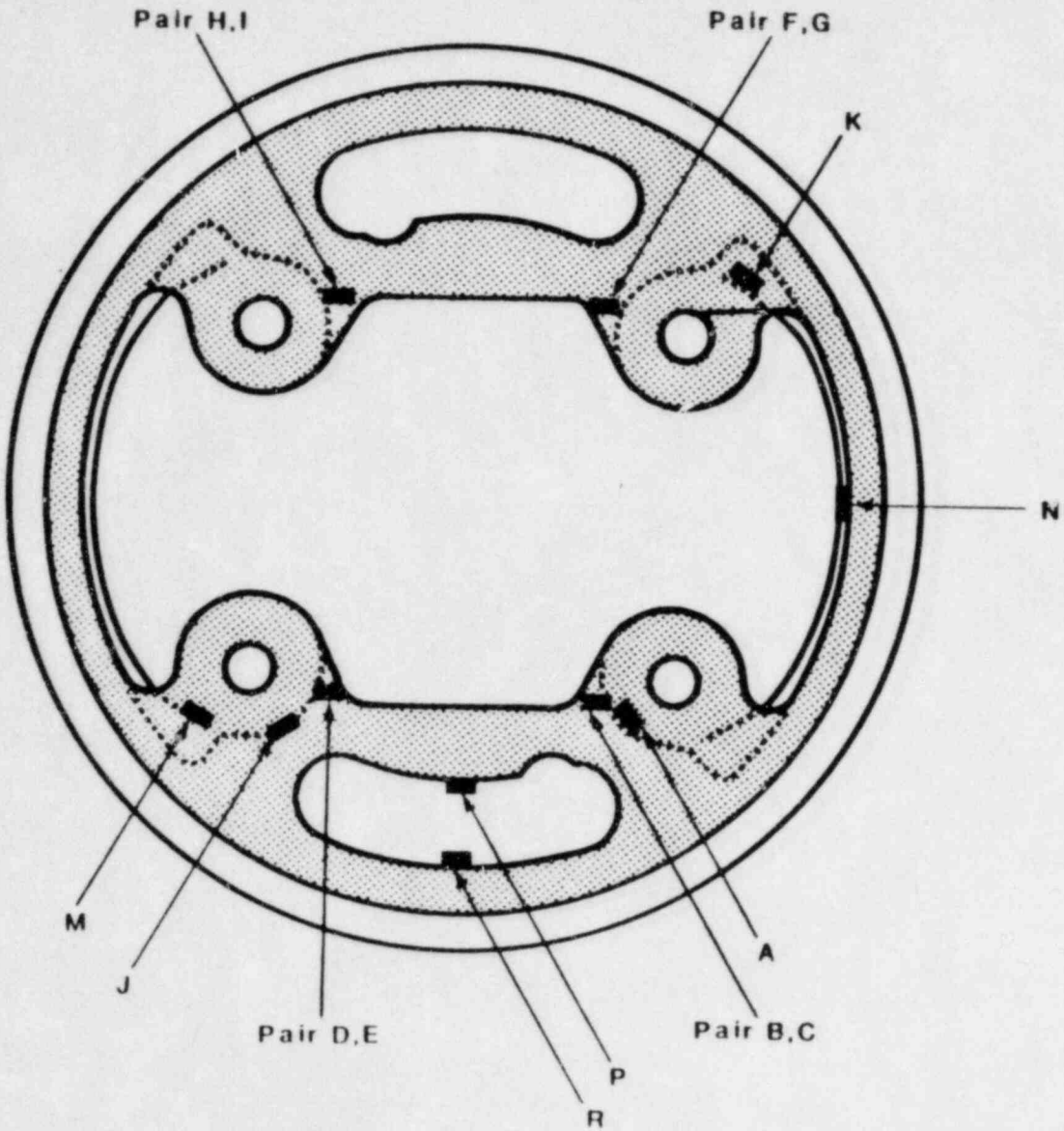

Figure 3-1. Location of strain gage rosettes on instrumented Al skirt.

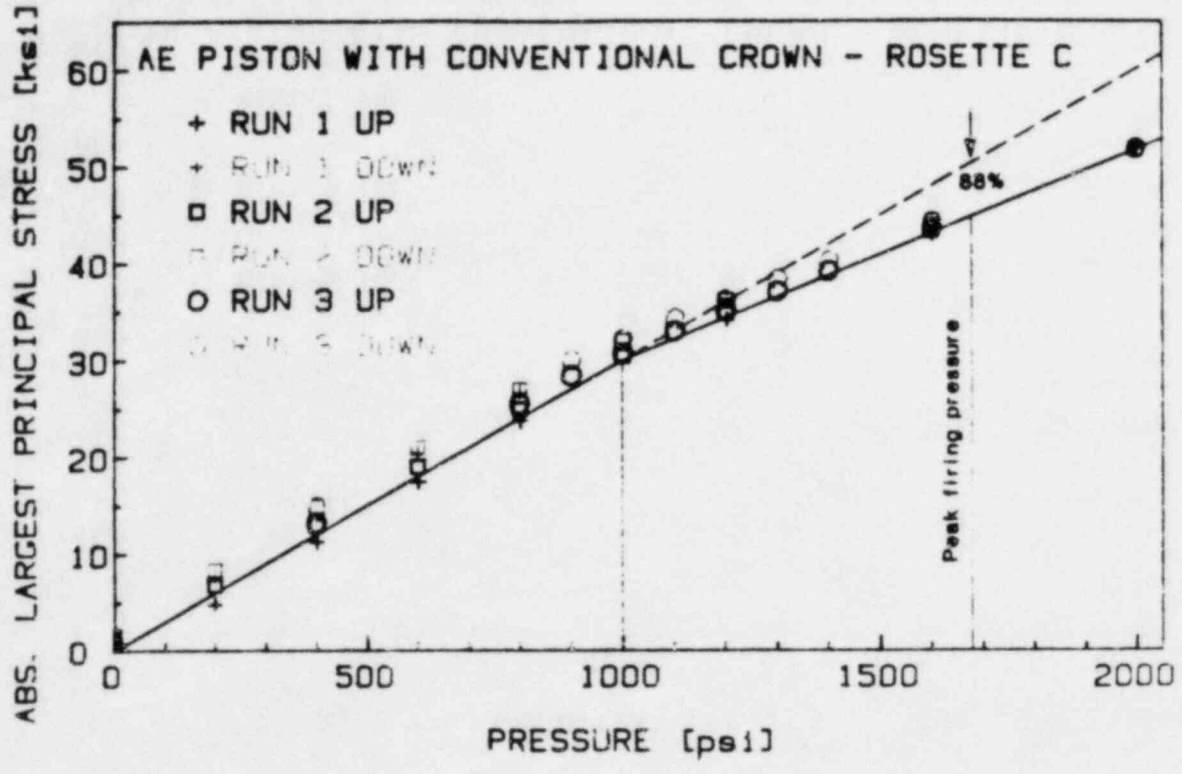

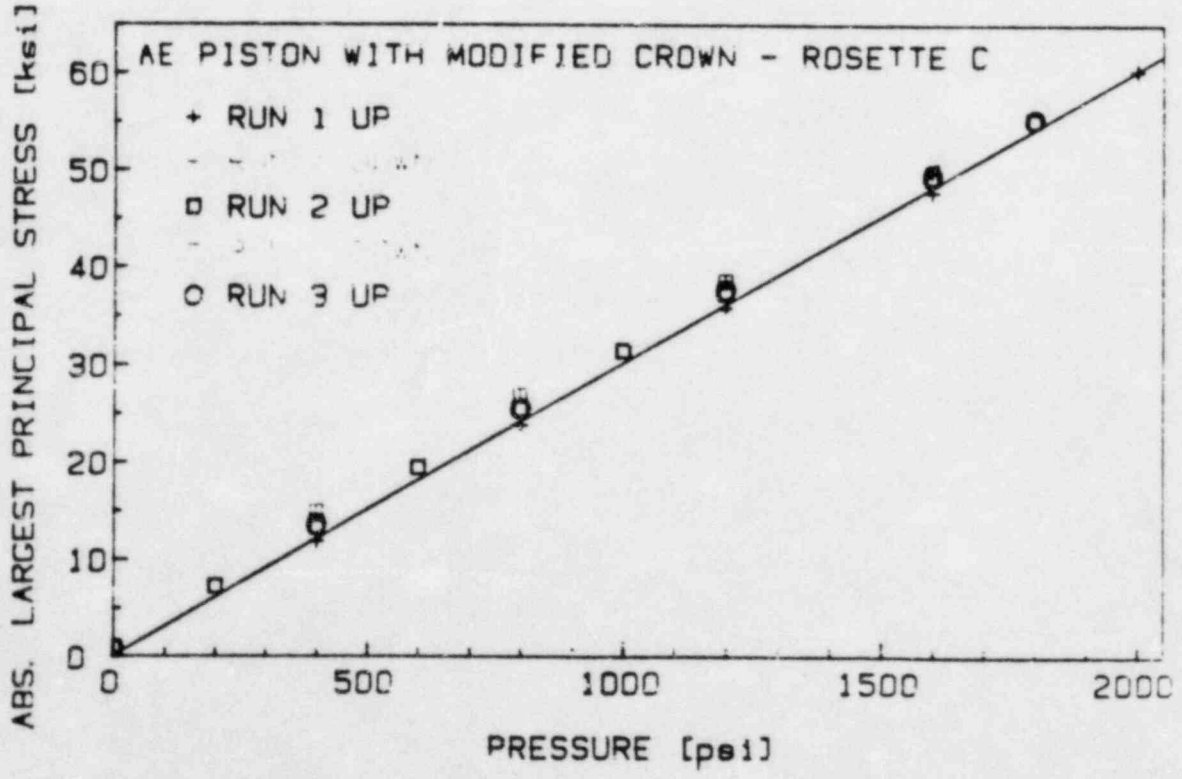

Figure 3-5. σ_{III} as a function of pressure for stud boss rosette C with conventional and modified crown.

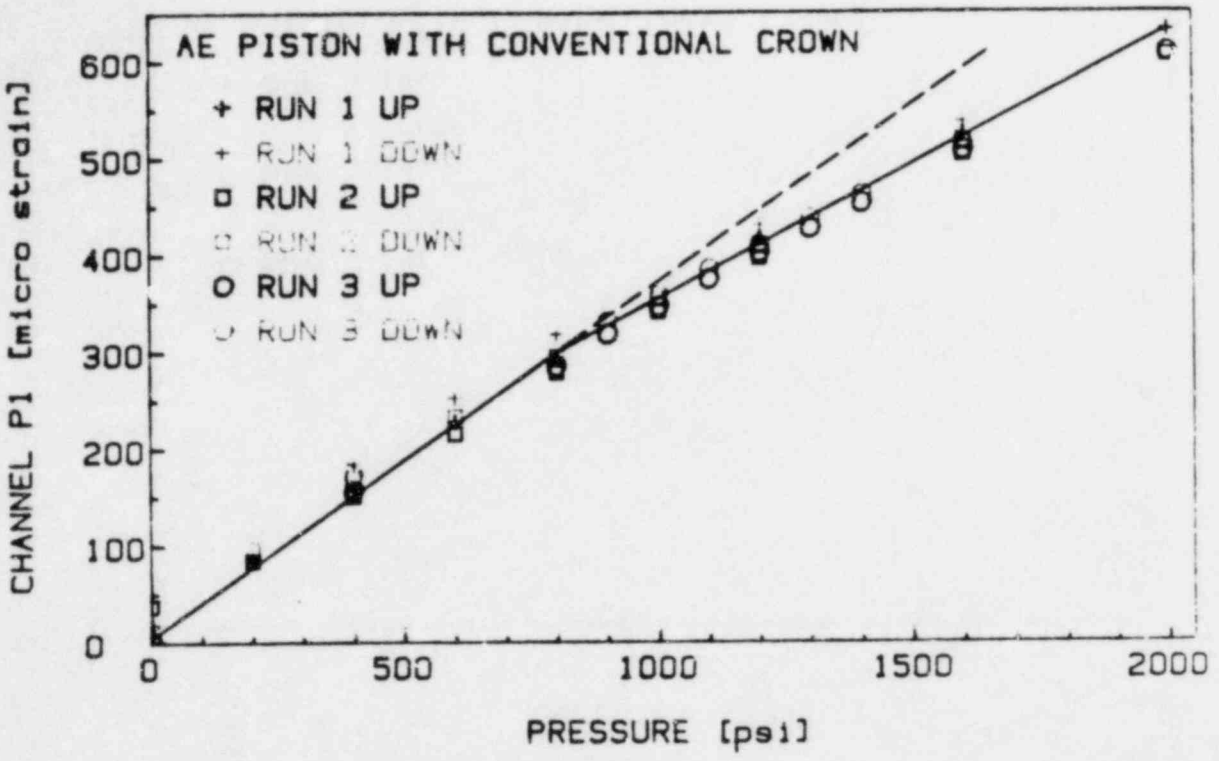

Figure 3-6. Axial strain as a function of pressure for strain gage rosette P located at inner portion of wrist pin cavity.

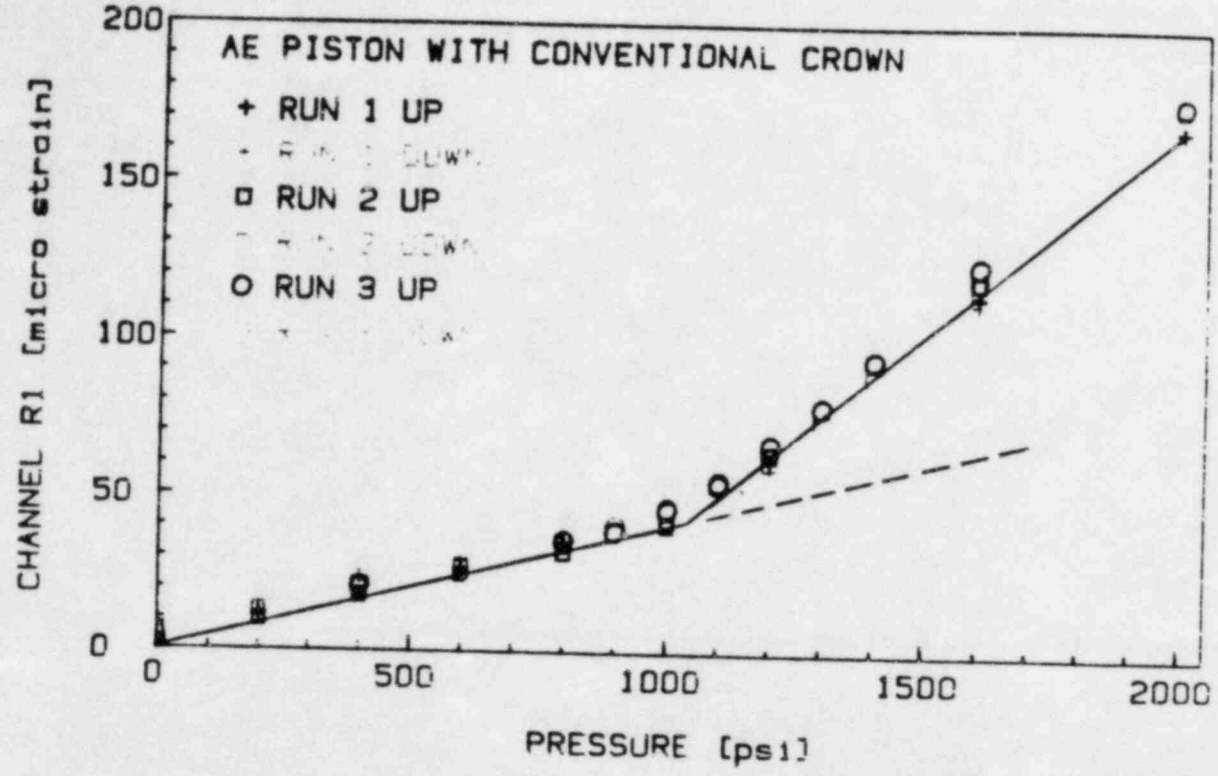

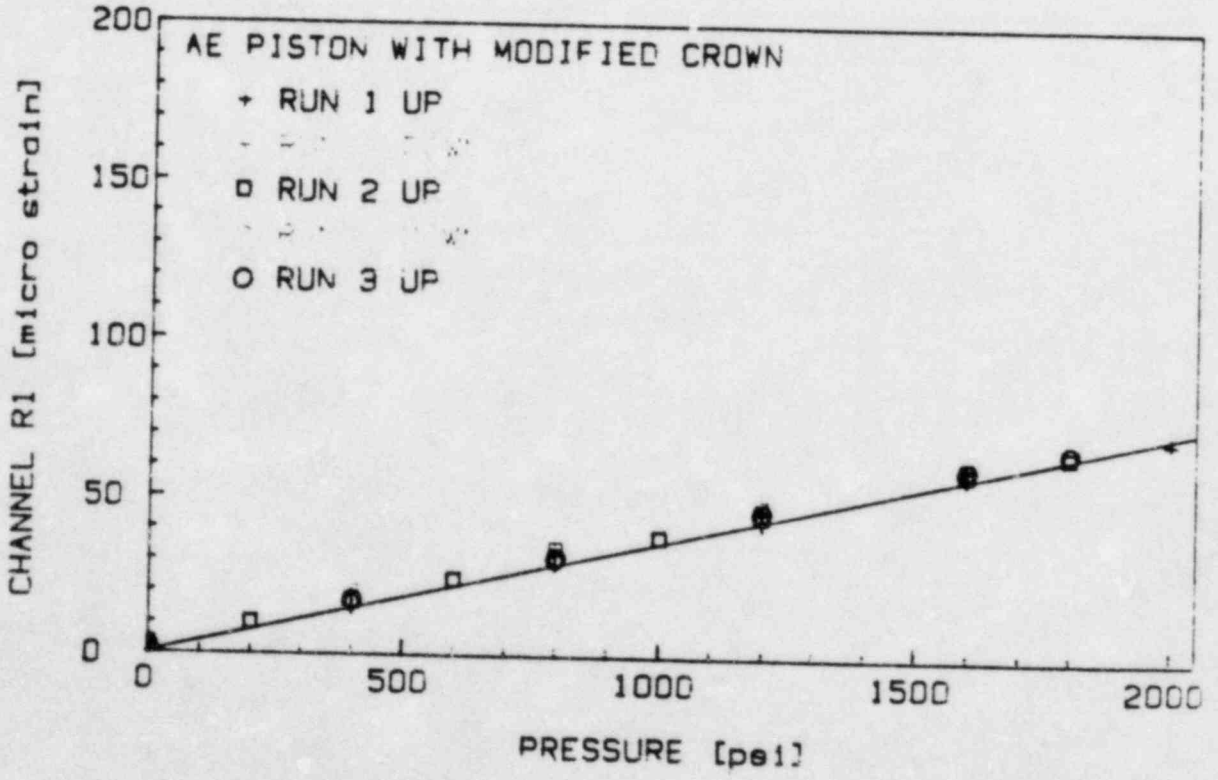

Figure 3-7. Axial strain as a function of pressure for strain gage rosette R located at outer portion of wrist pin cavity.

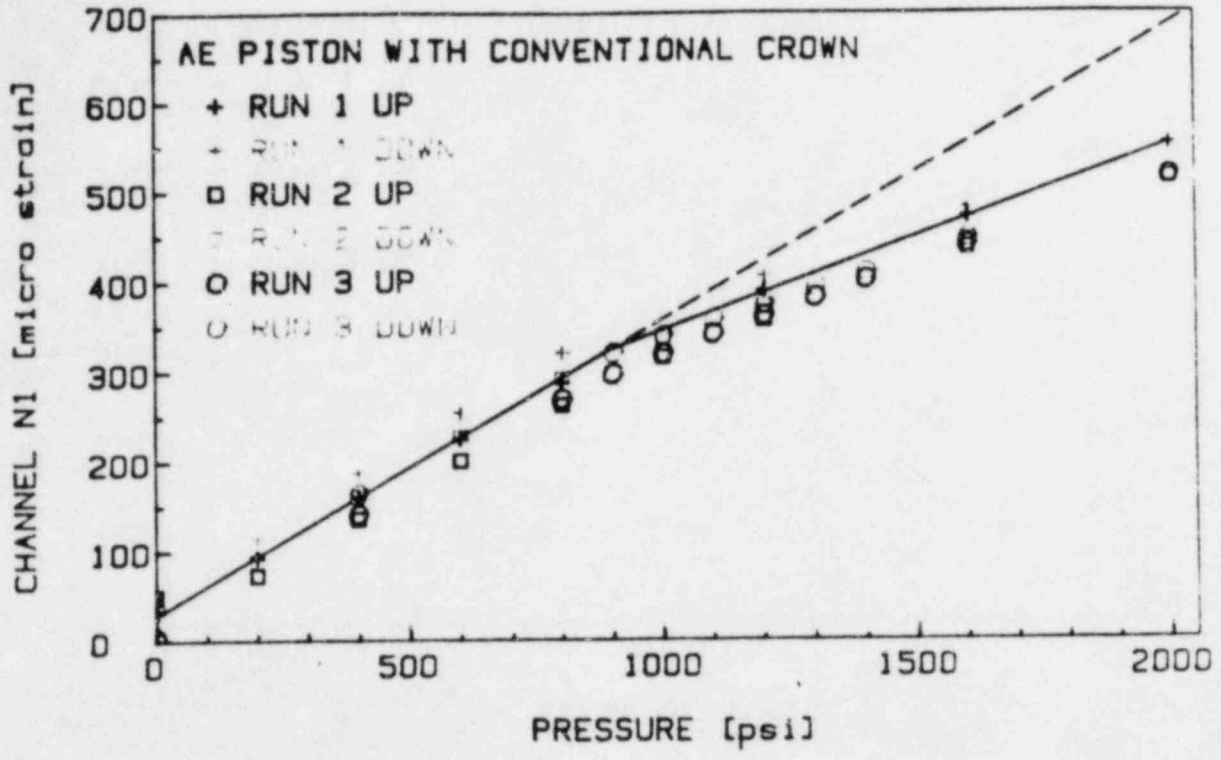

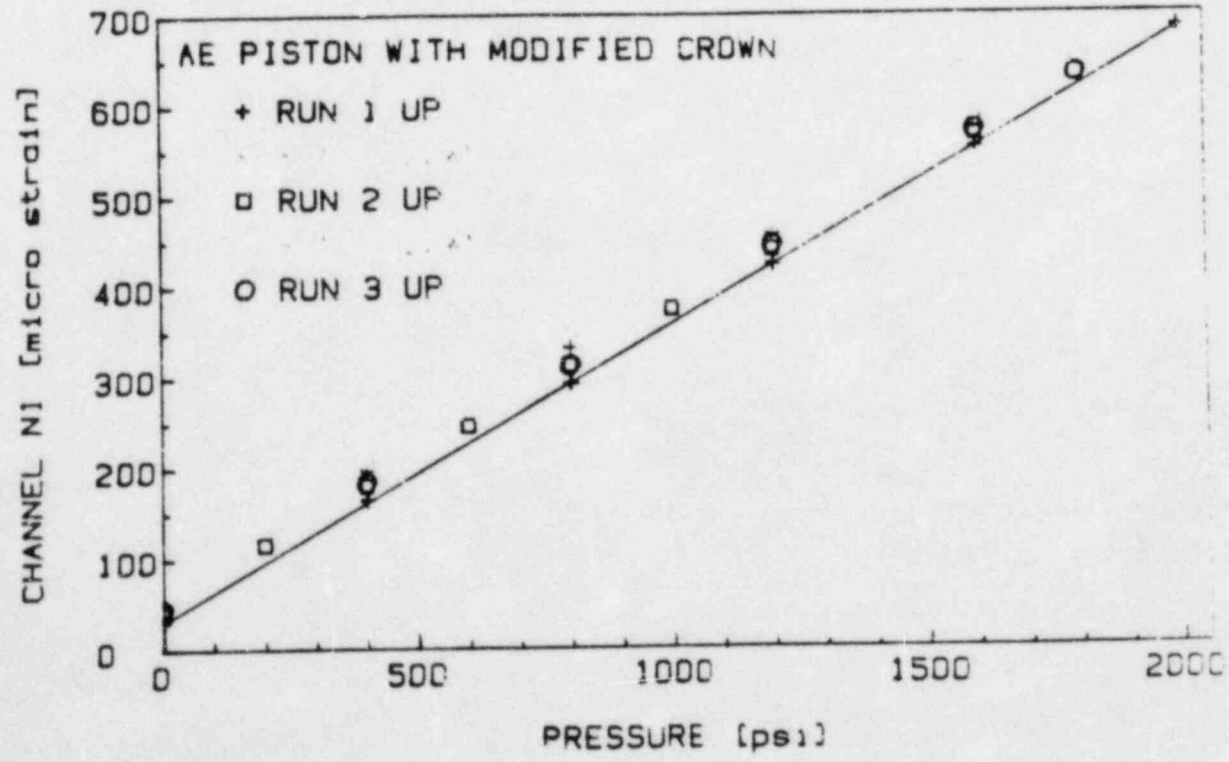

Figure 3-8. Axial strain as a function of pressure for strain gage rosette N located near outer ring at 90° from wrist pin cavity.

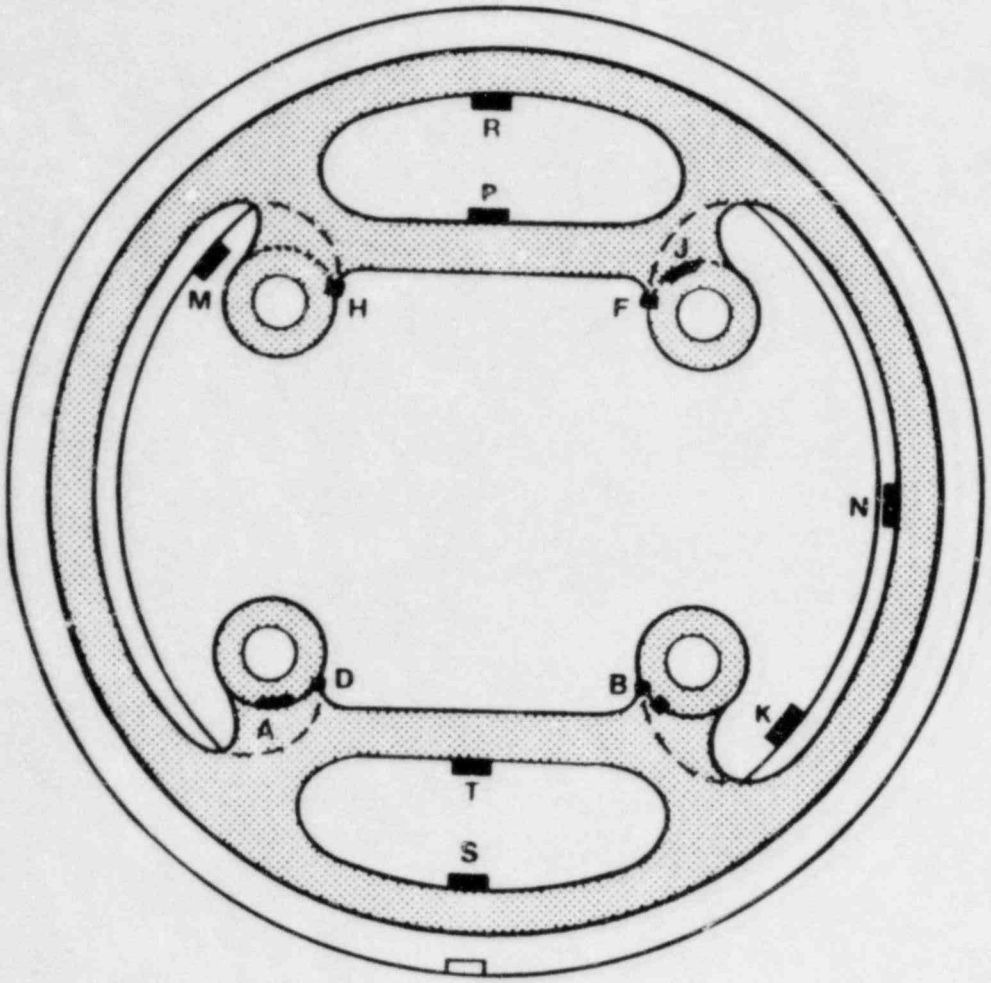

Figure 3-9. Location of strain gage rosettes on instrumented AF skirt.

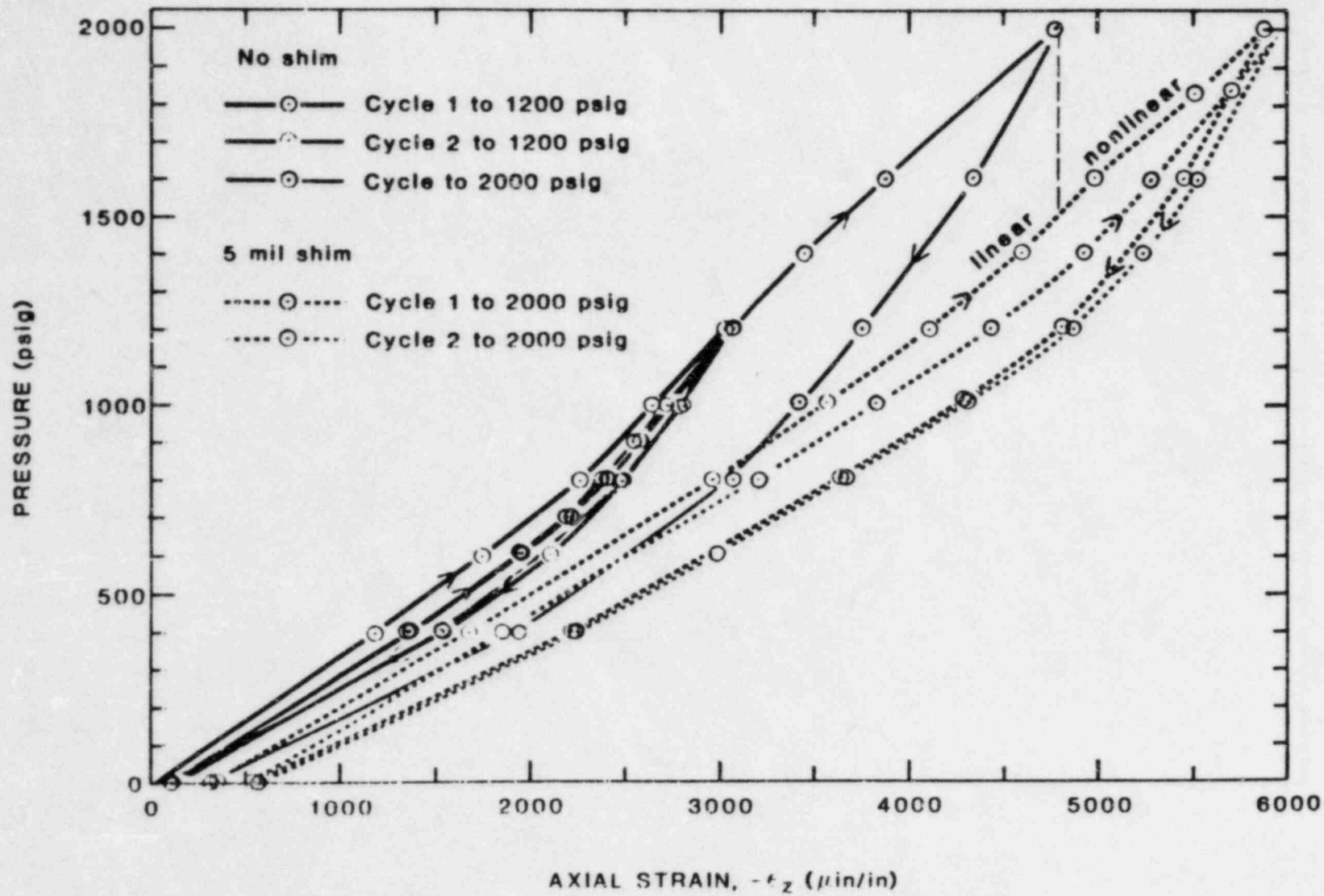

Figure 4.10. Pressure-axial stress results for various cycles of loading and unloading for stud boss B in the AF skirt.

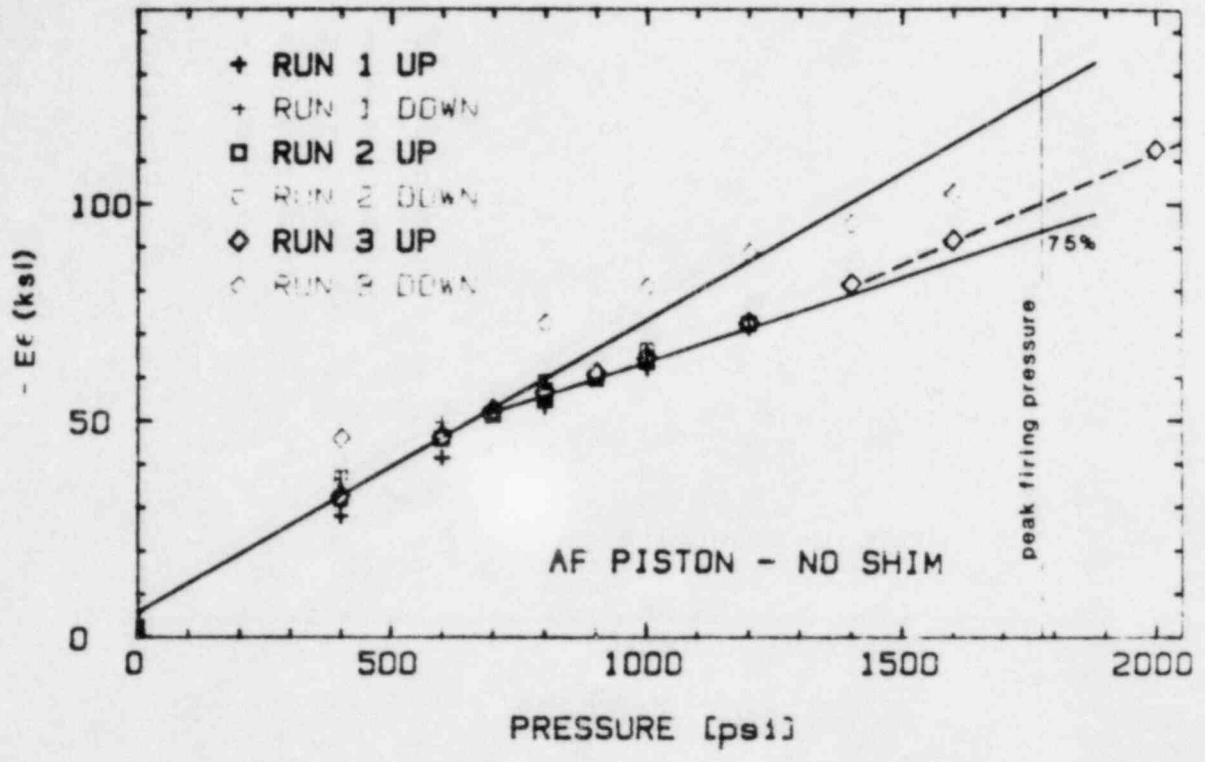

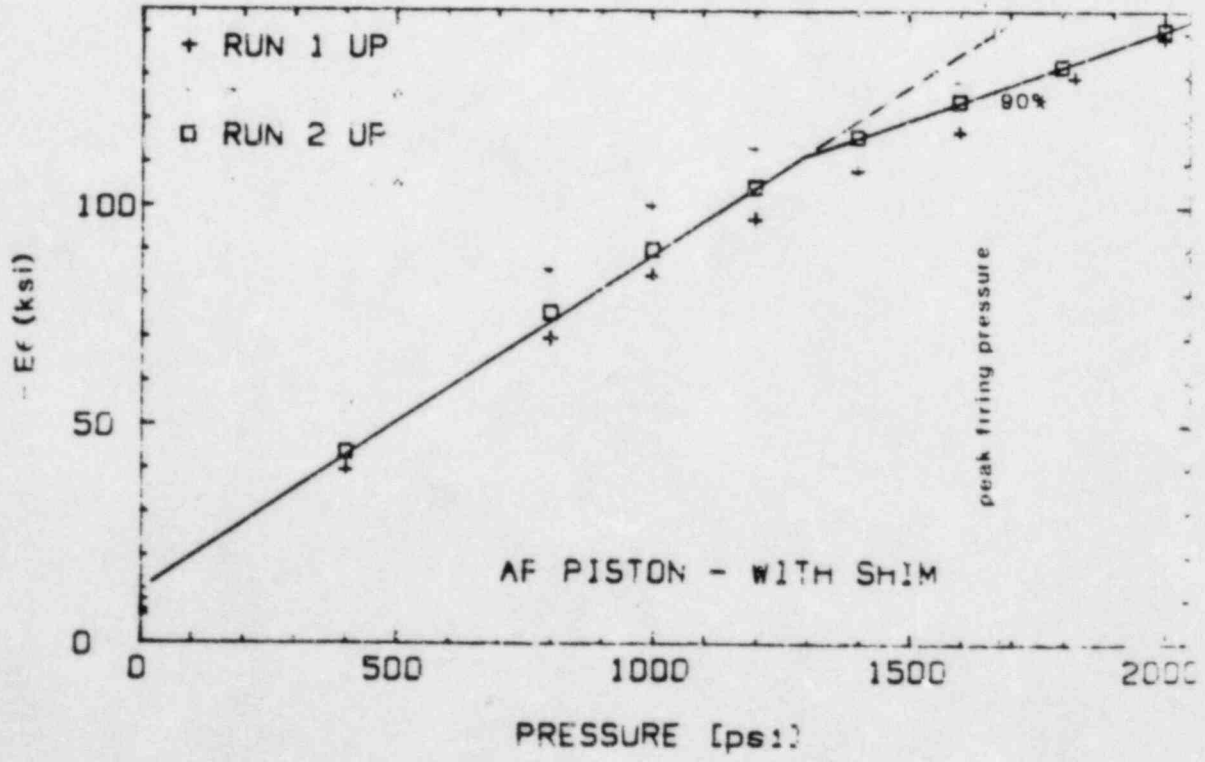

Figure 3-11. Elastically calculated stress as a function of pressure for stud base gage B with and without shim

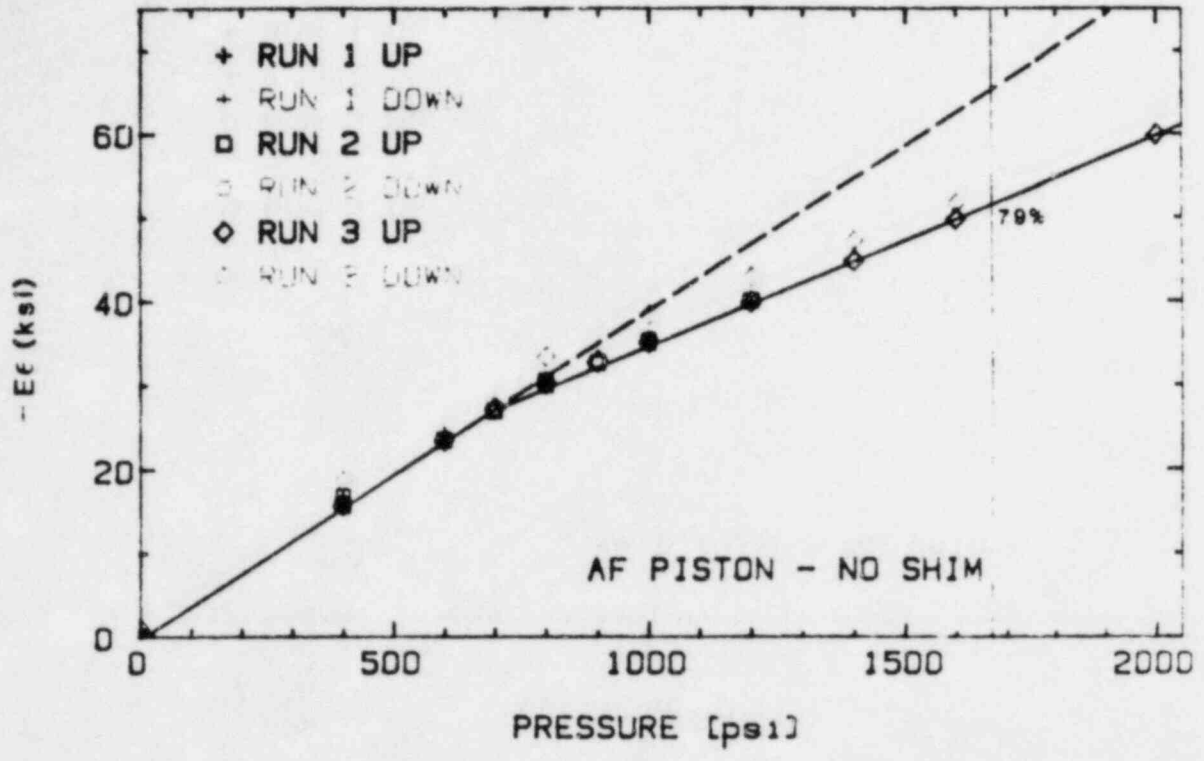

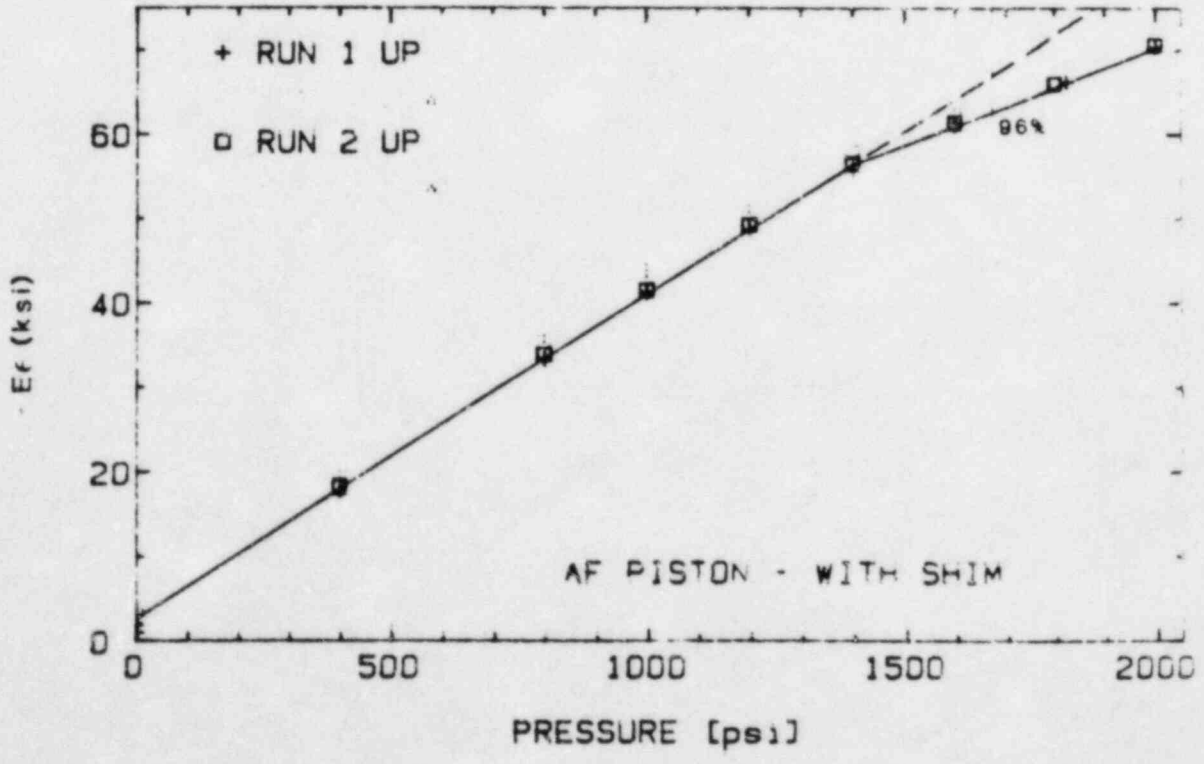

Figure 3-12. Elastically calculated stress as a function of pressure for stud base gage D with and without shim

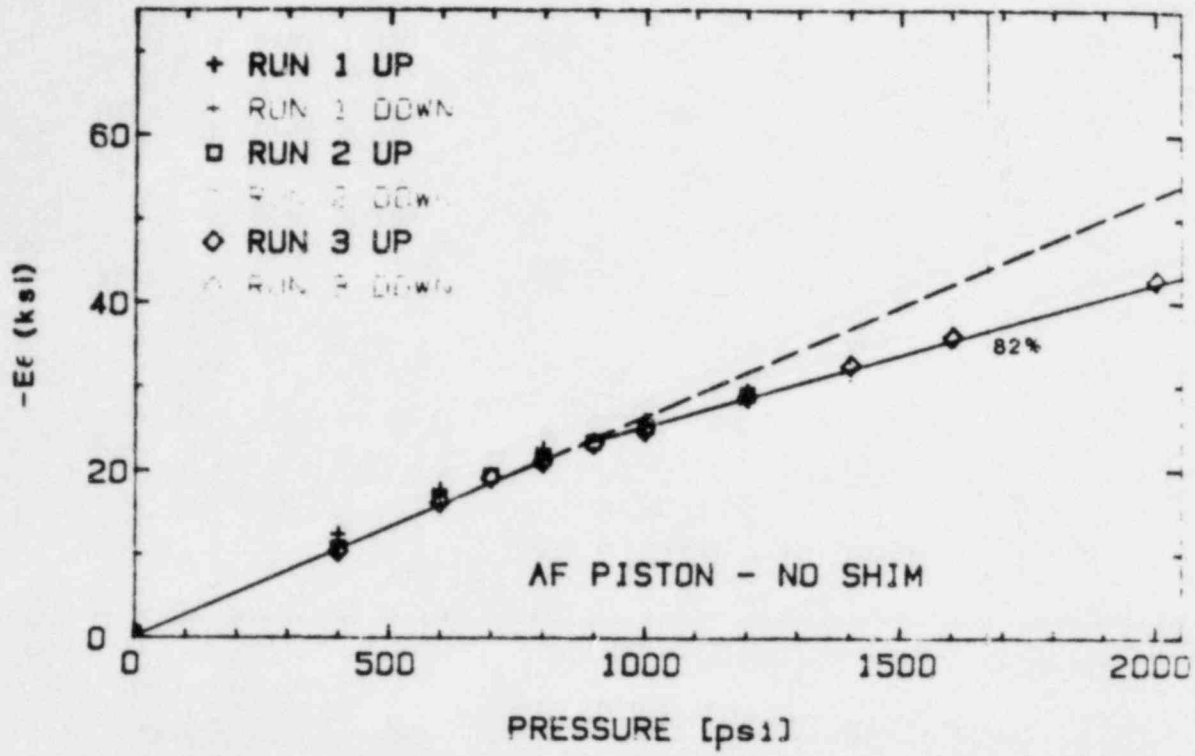

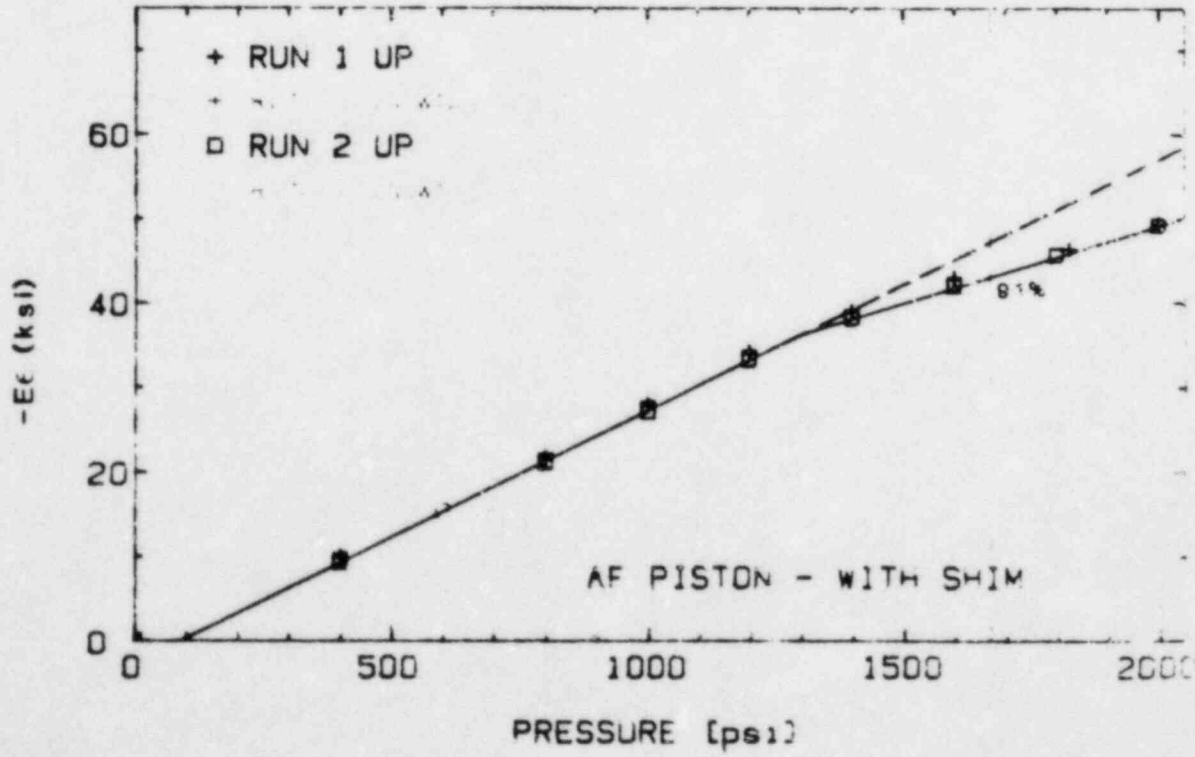

Figure 3-13. Elastically calculated stress as a function of pressure for stud base gage F with and without shim.

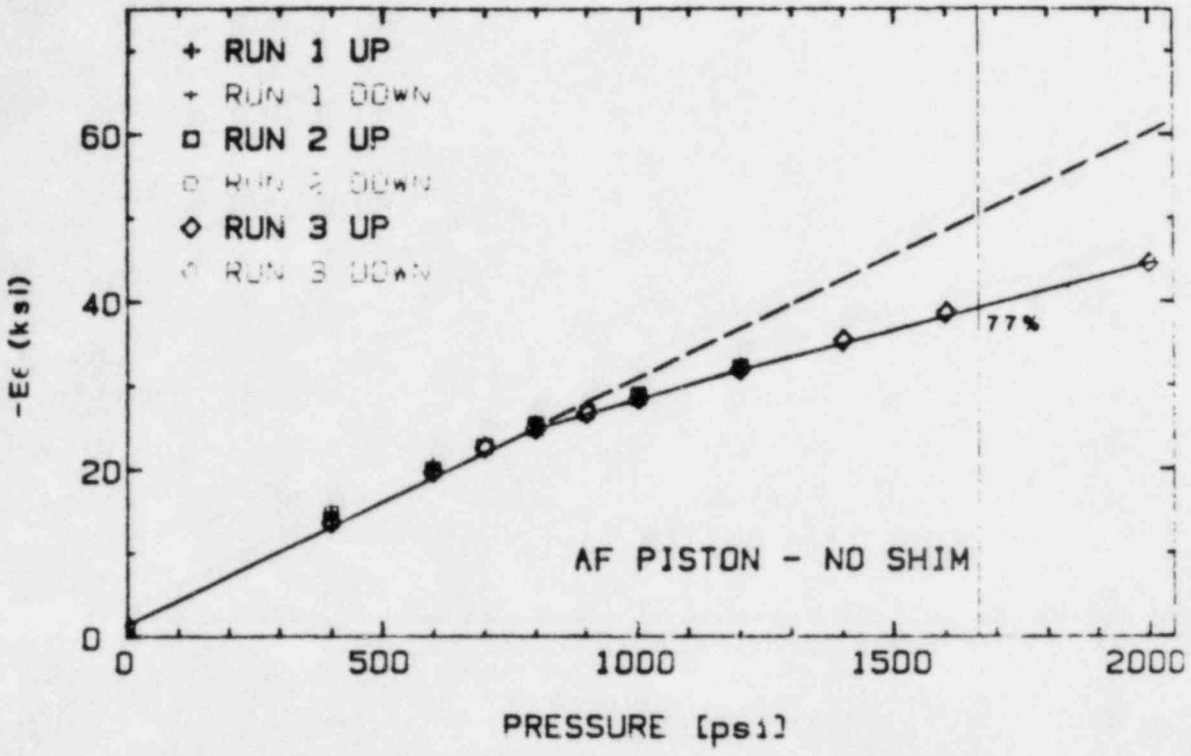

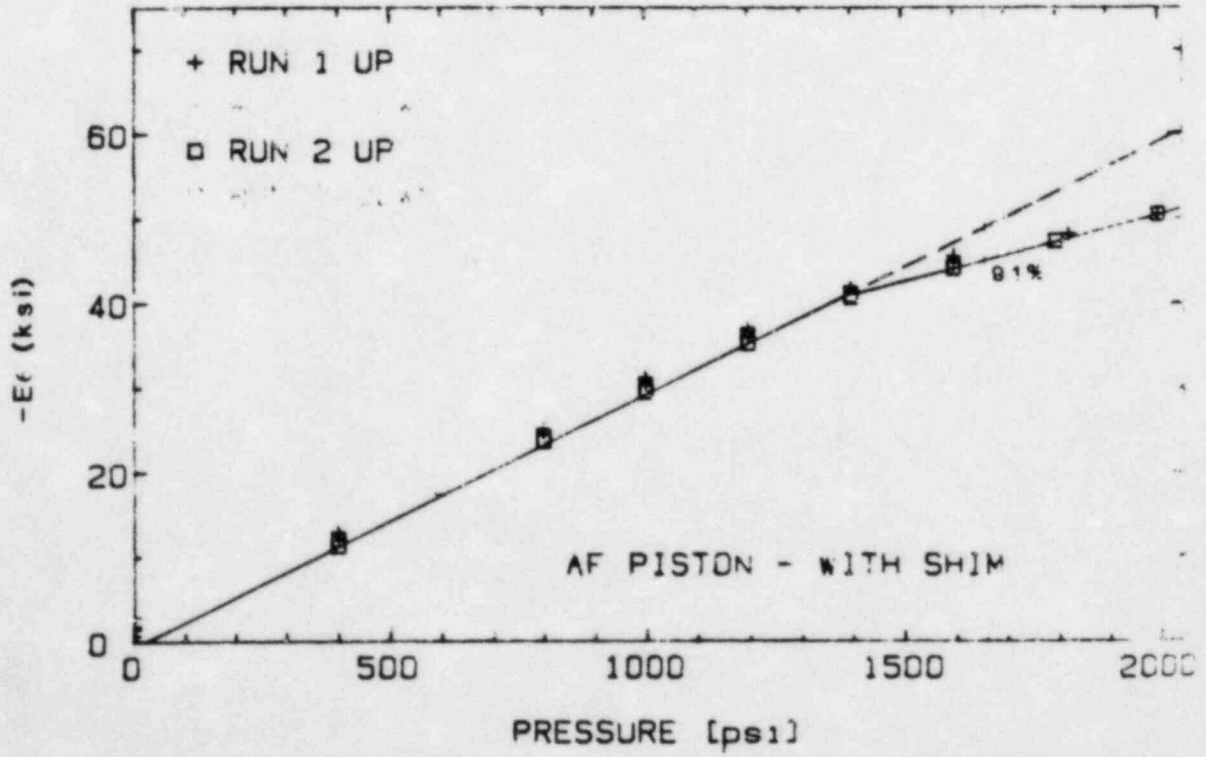

Figure 3-14. Elastically calculated stress as a function of pressure for stud base gage H with and without shim.

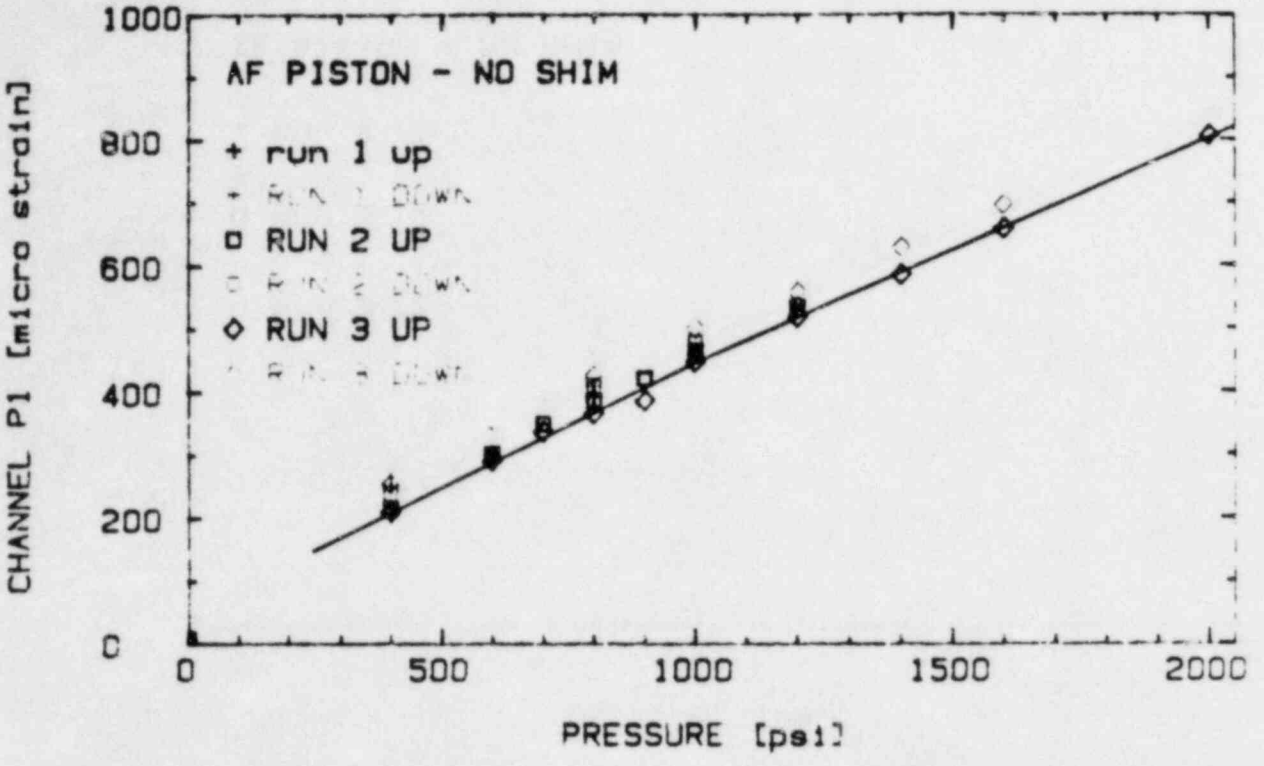

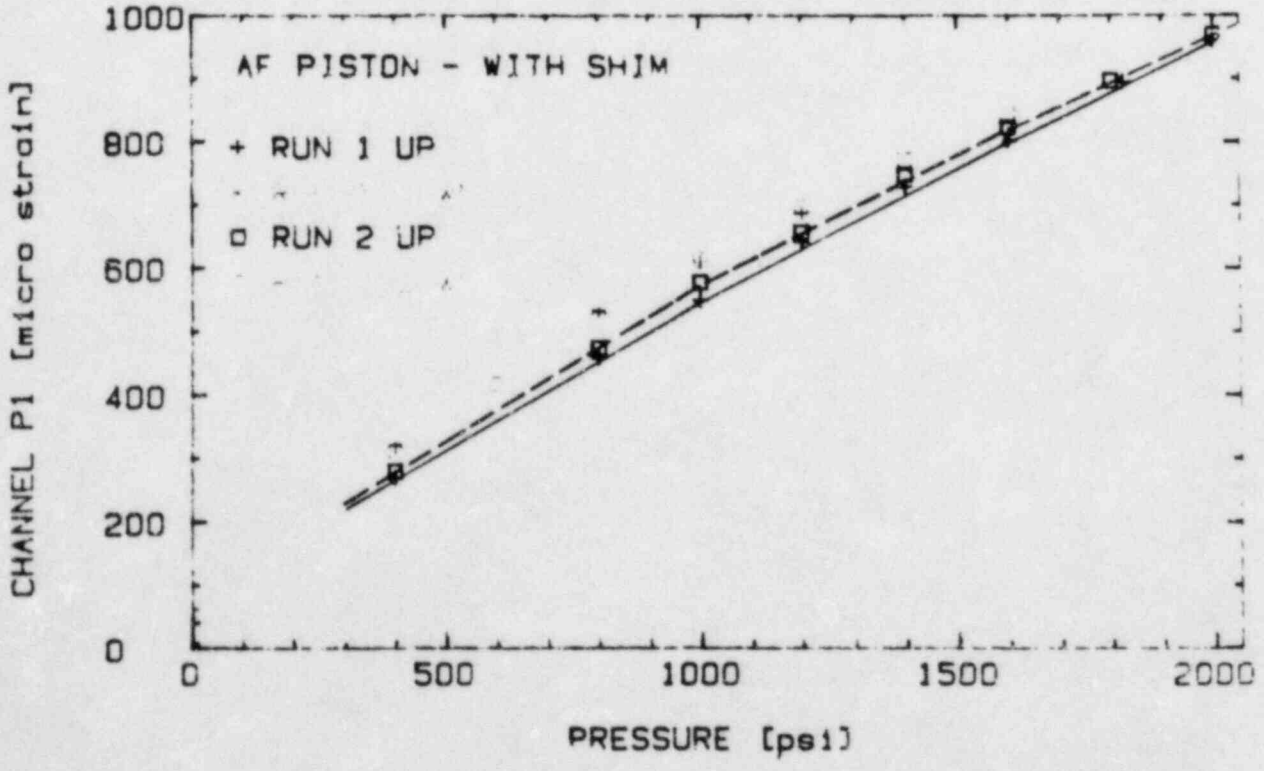

Figure 3-15. Axial strain as a function of pressure for strain gage rosette P located at inner portion of wrist pin cavity.

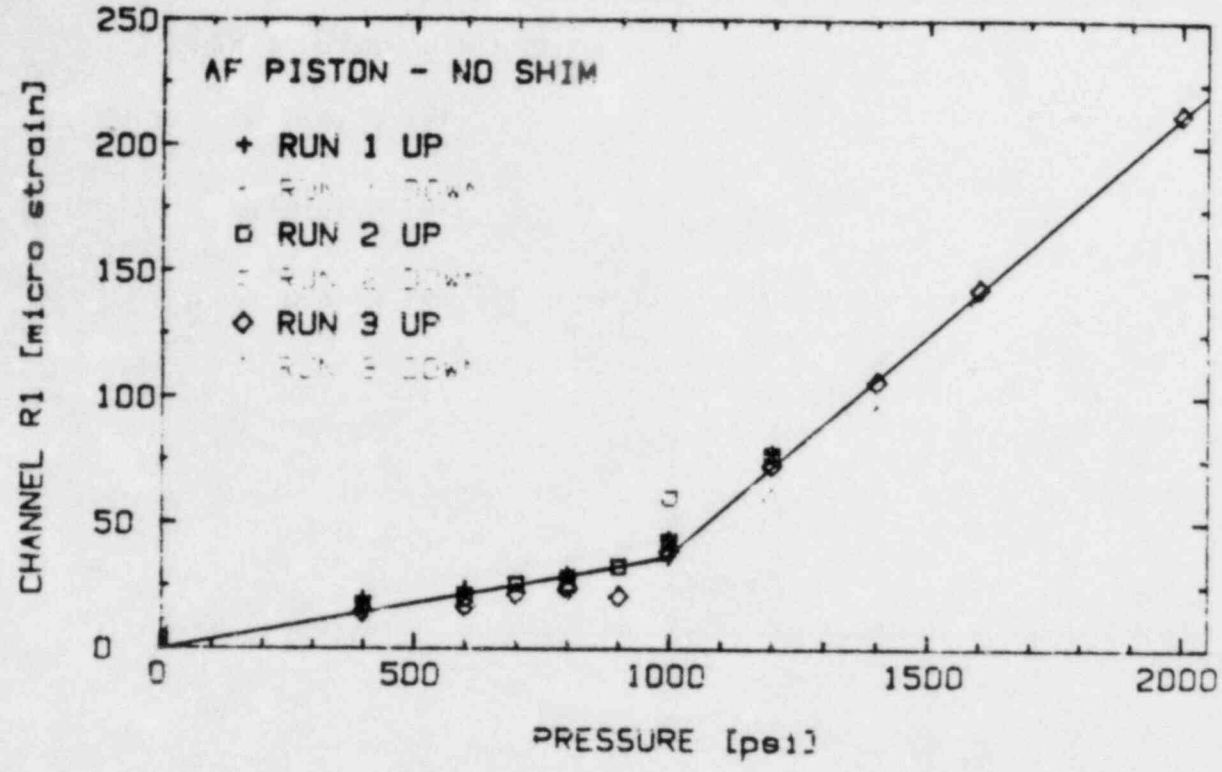

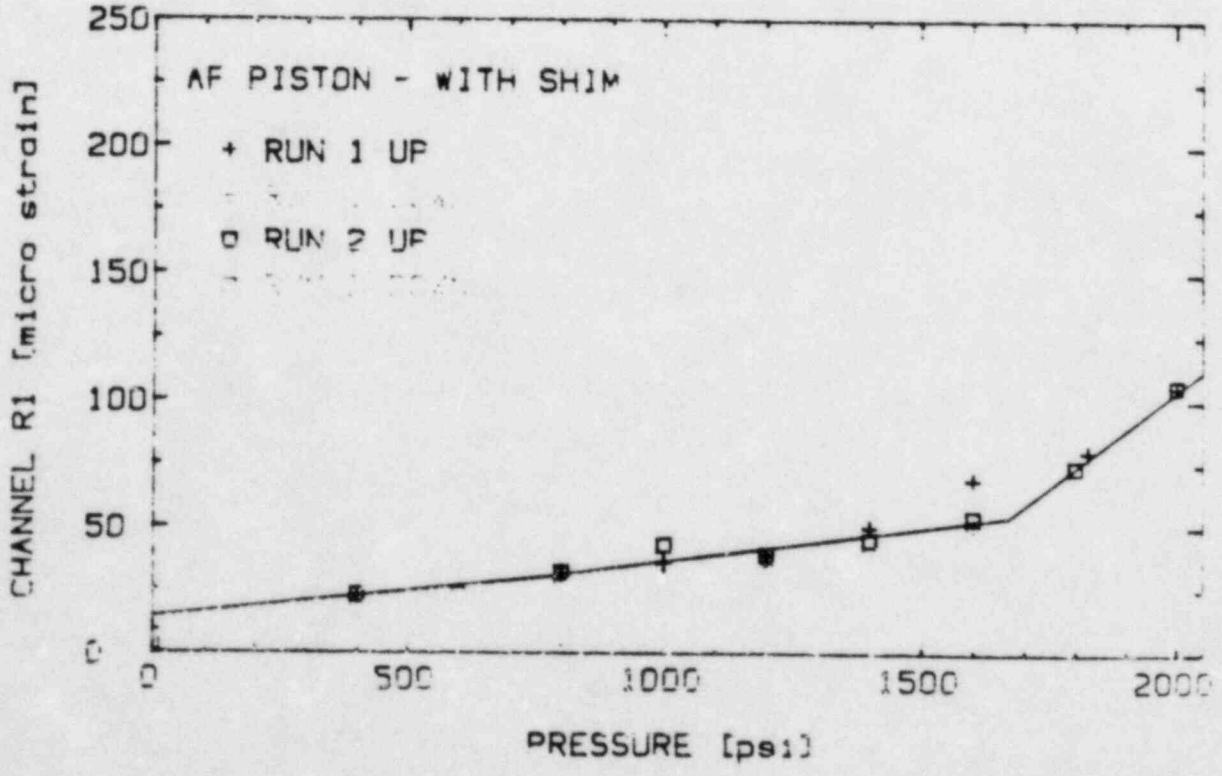

Figure 3-16. Axial strain as a function of pressure for strain gage rosette R located at outer perimeter of wrist pin cavity.

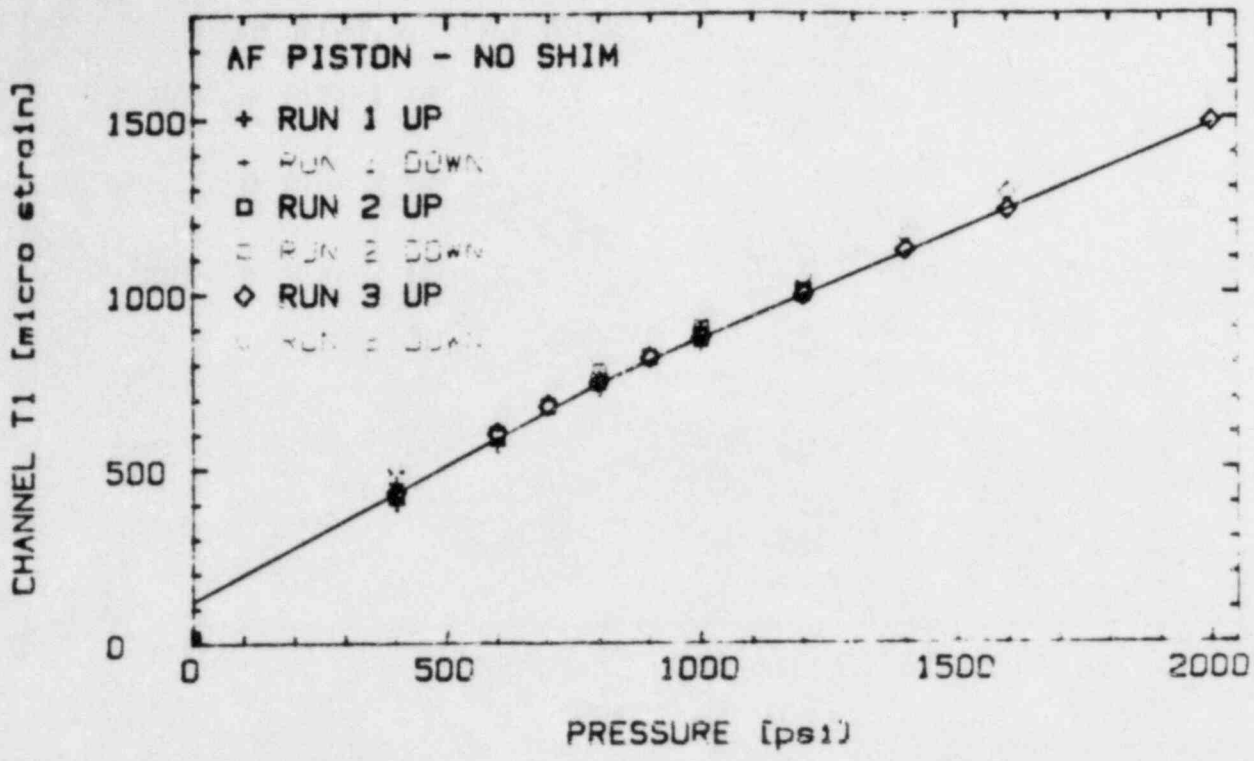

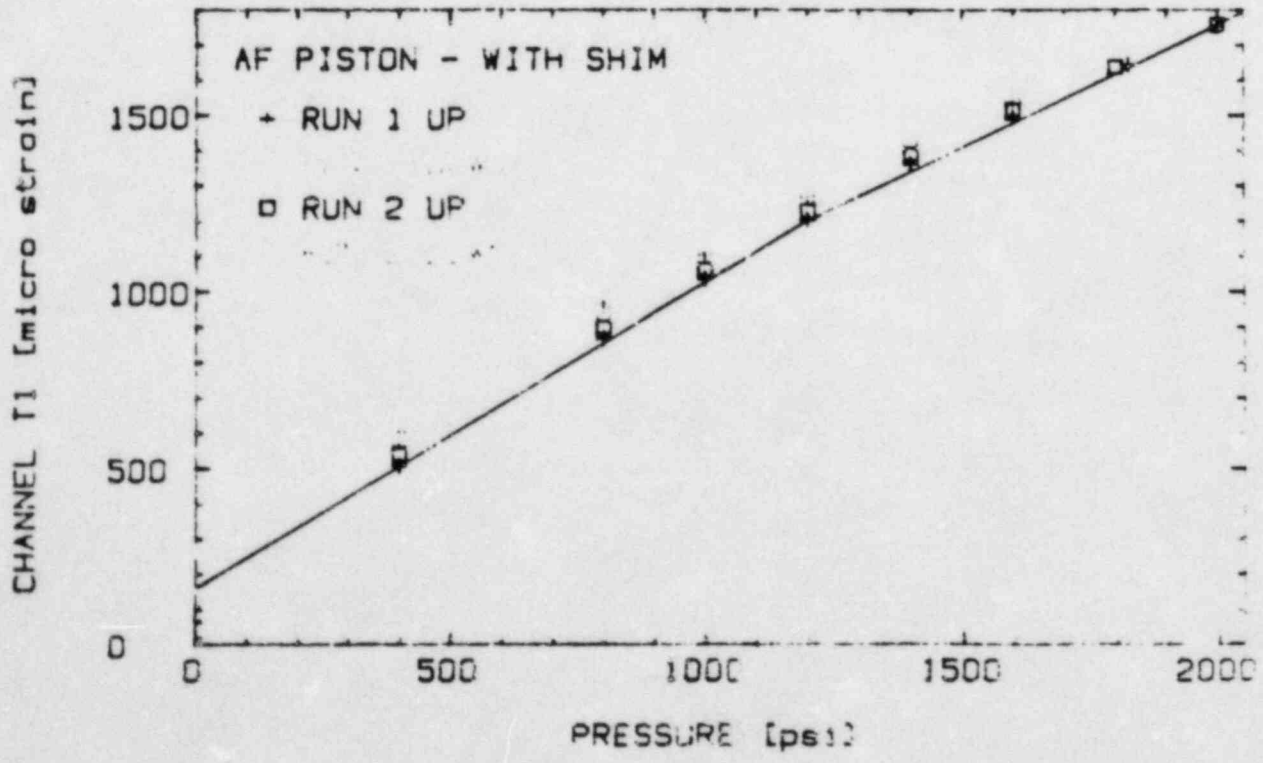

Figure 3-17. Axial strain as a function of pressure for strain gage rosette T located at inner wall of wrist pin cavity.

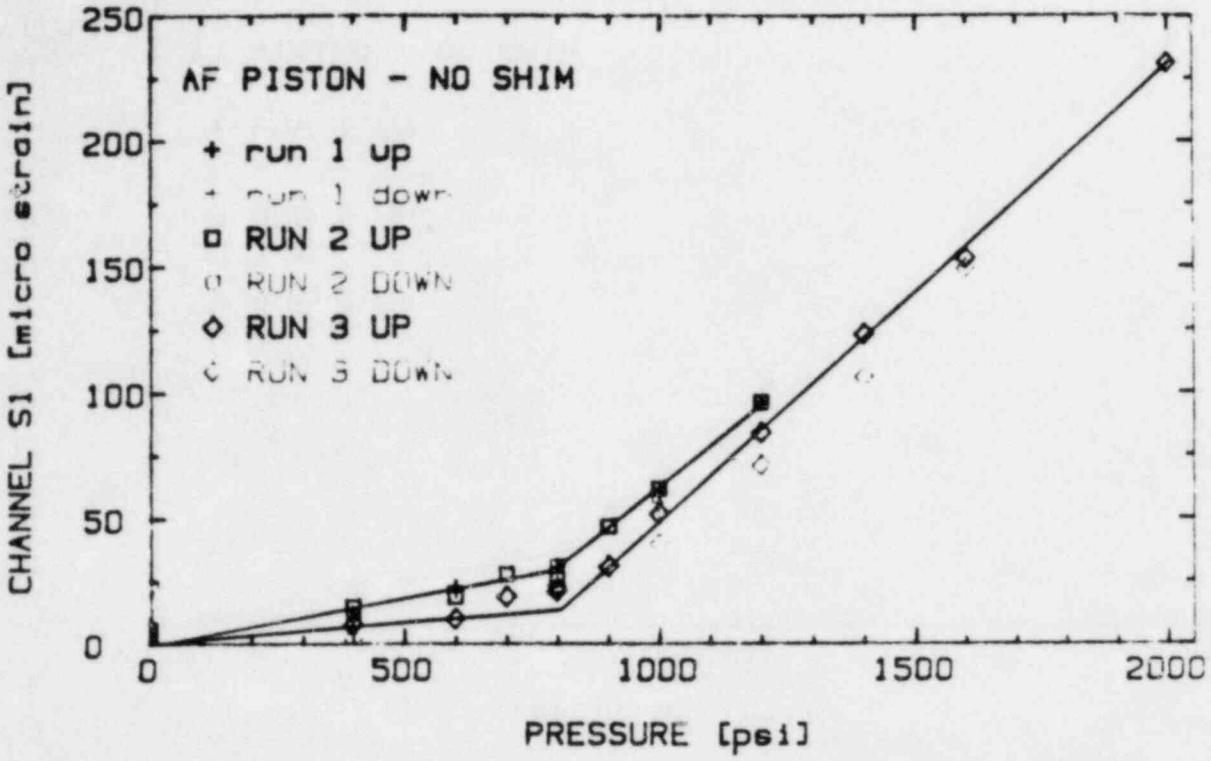

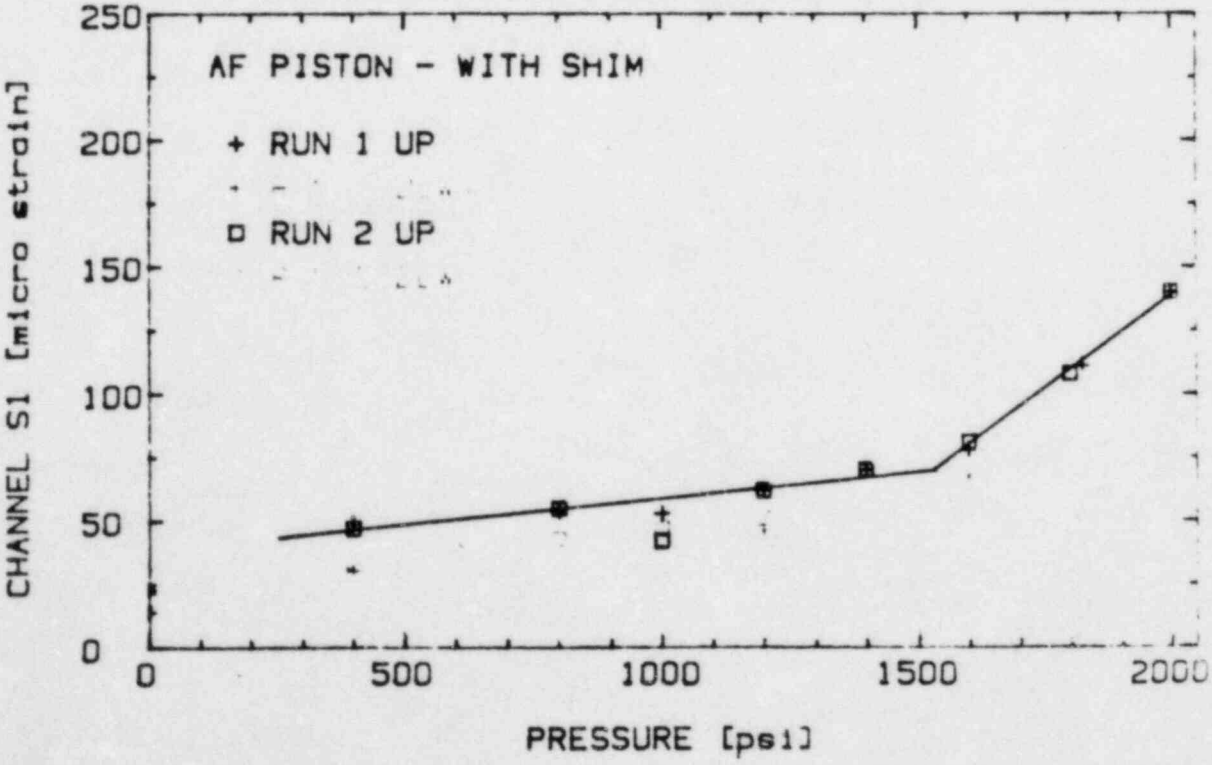

Figure 3-18. Axial strain as a function of pressure for strain gage rosette S located at outer portion of wrist pin cavity.

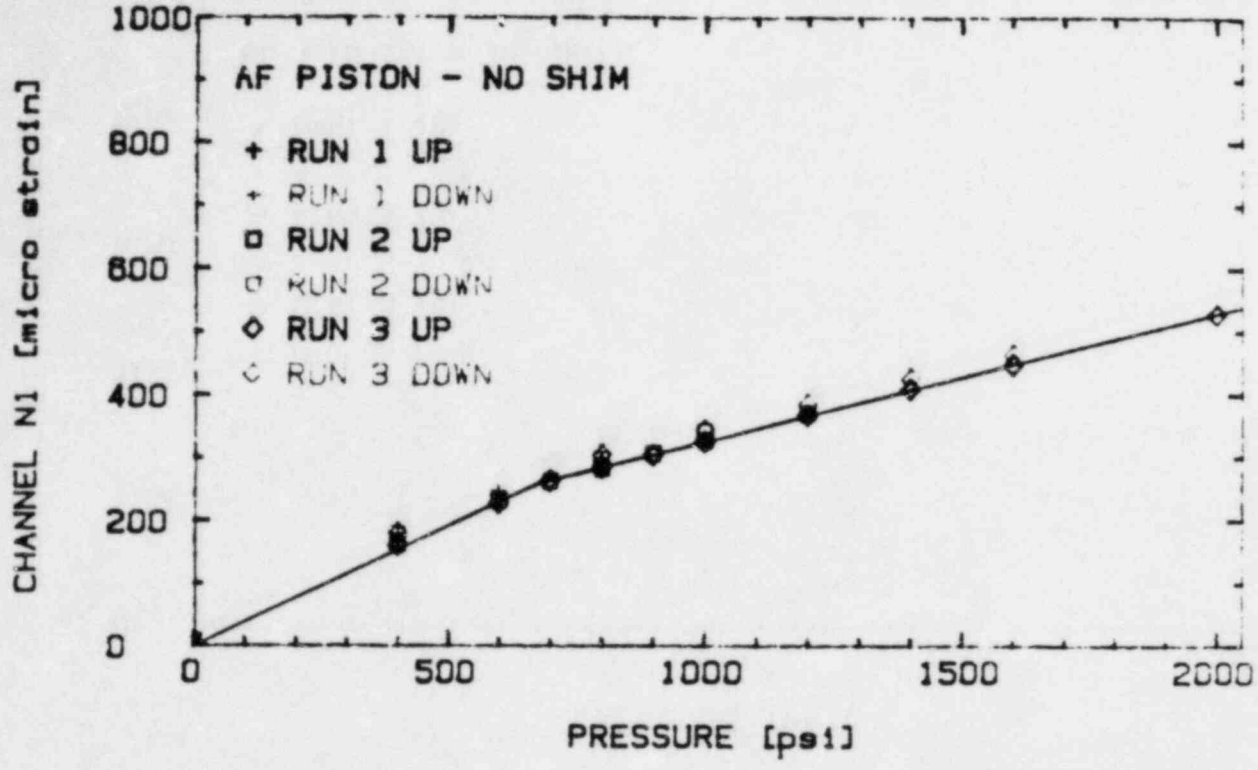

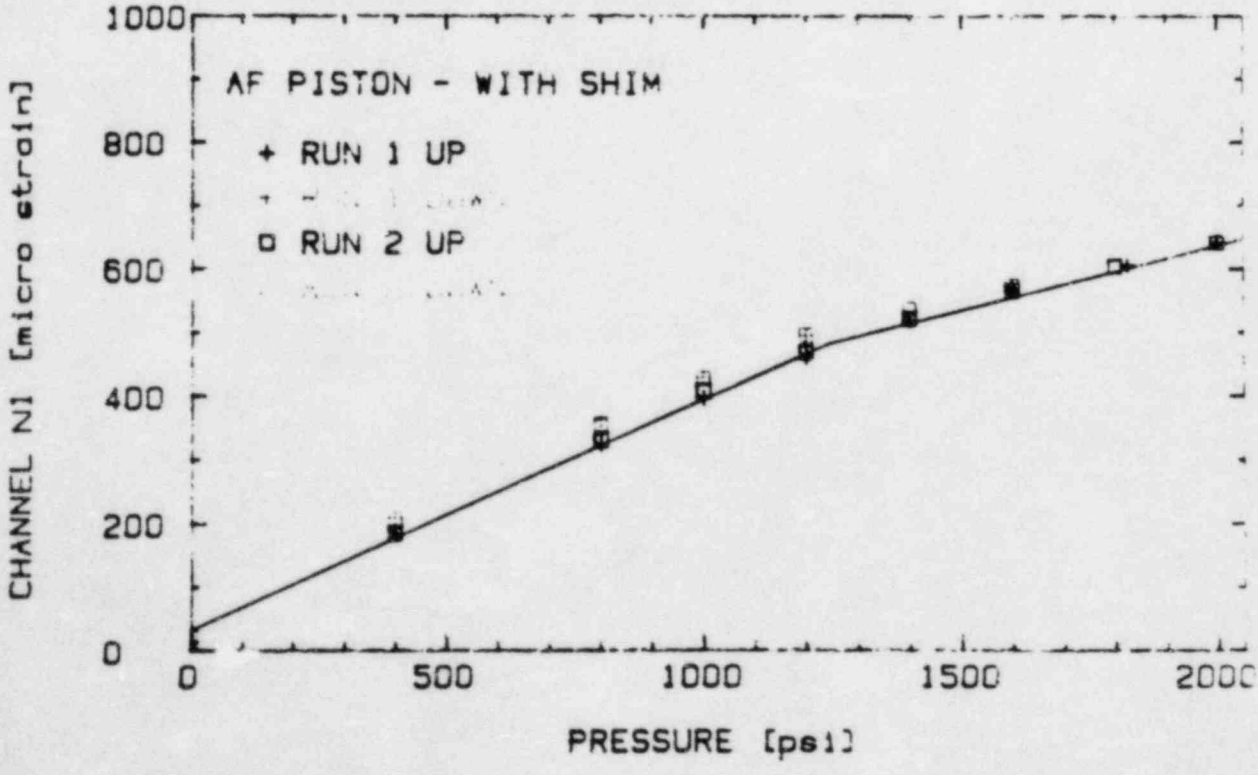

Figure 3-19. Axial strain as a function of pressure for strain gage rosette N located near outer load ring at 90° from wrist air cavity.

4.0 FINITE ELEMENT STRESS ANALYSIS

The results of the finite element stress analysis for both the AE and AF piston skirts are presented in this section along with descriptions of the models employed in the analysis. Calculations were performed for pressure loading on an elastic crown that has a frictionless contact on the inner contact ring on top of the skirt. The finite element calculations show that the peak stresses in the stud boss region are much larger in the AF skirt than in the AE skirt.

4.1 Load Considerations

Three loads were assumed to be acting on the piston: gas pressure, reciprocating inertia, and friction. In addition, since the piston is a two-piece design, initial internal load is associated with the bolt preload. As part of the analysis of the crankshaft of these same engines [4-1], a table of gas pressure, accelerations, and friction was developed that provided values for every ten degrees of rotation of the crankshaft. This covered rotation from 0° to 720°, thereby encompassing all four stokes in a cycle. The combined loading was found to be highest at top dead center during the combustion stroke. At this point, only pressure and inertia are acting on the piston since the velocity (and therefore friction) is essentially zero. A peak firing pressure of 1670 psig was applied when the piston is at top center. This value of the peak firing pressure is based on FaAA measurements at Shoreham [4-1] as well as values reported by TDI [4-2].

The gas pressure load acts on the surface of the piston crown. As discussed in Section 3.1 and shown in Figure 3-2, the crown contacts the piston skirt at the inner ring just inside the bolt circle. At the outer edge of the crown there is a specified clearance of 0.007 to 0.011 inch between the crown and the skirt. This gap can close due to pressure and/or thermal distortion of the crown. The strain gage results presented in Section 3.4 for the AE and AF suggest that the gap closes at pressures less than the peak firing pressure when the piston is at room temperature, and that most of the peak load is carried on the inner ring.

The magnitude of the pressure load is obtained knowing the peak firing pressure and cylinder bore. A value of 379,000 pounds is obtained. This load is transmitted from the crown to the skirt through the inner and outer contact rings, as discussed above. At top center of the power stroke, the pressure load is somewhat offset by the inertia load, which is exerted by the crown to the top of the skirt. The piston acceleration at top center was found from the crankshaft analysis to be 26.1×10^3 in/sec^2. The crown weighs 144 pounds. Therefore, the inertia force is $144 \times 26.1 \times 10^3/386.4 = 9727$ pounds. Subtracting this from the pressure force provides the maximum net force on the top of the skirt, 369,300 pounds. This corresponds to an effective pressure of 1627 psig. This pressure was applied to the top of the crown for evaluation of the stresses in the piston skirt due to firing pressure.

The other extreme of the stress cycle in the skirt occurs at top center of the exhaust stroke, at which time a tensile load equal to the inertia force of the crown is applied to the top of the skirt. Provided no gap opens between the crown and skirt at the inner ring, the peak stress under this condition is proportional to the pressure loading, and can be obtained from the results for peak firing pressure by multiplying by $-9727/369,300 = -0.026$.

The boundary condition on the top of the skirt for each skirt design was considered to be a crown mounted on the top of the skirt with a frictionless interface. Pressure is applied to the top of the crown and the crown and skirt are allowed to deform without interfering with each other at the outer loading ring. This boundary condition provides the most realistic estimate of stresses in the skirt in the absence of gap closure and also provides information on the crown/skirt interactions. All finite element runs on the skirt models were performed for uniform room temperature of the skirt and a rigid wrist pin.

The stresses due to bolt preload were evaluated by finite element models and measured on the AE skirt. The bolt preload was found to have virtually no effect on the stresses in the area of the radius between the boss and the vertical wall. The bolt preload was, therefore, omitted from further consideration.

4.2 Stress Analysis

Stresses and displacements under gas pressure and inertia loads were calculated for the AF and AE skirts using the ANSYS finite element computer program. Two models were developed for each piston design: (i) a full (global) model of the skirt, and (ii) a refined local model of the crown-stud boss in the region of highest stress (as defined by the global model). Additionally, a finite element model of the crown was developed for placing on the global skirt models.

The crown is fabricated from cast steel and mounts on the top of the skirt, as shown in Figure 2-1. Figure 3-2 presents a cross-section of the crown and the attachment region at the top of the skirt. The 0.007-0.011 inch gap that is present at the outer load ring at room temperature is shown in Figure 3-2. The crown enters into the analysis of the skirt because the pressure load applied to the top of the crown is transmitted through the crown to the top of the skirt in a manner which corresponds to neither a uniform displacement nor uniform loading boundary condition on the skirt. The crown model need only be suitable for representing the circumferential variation of the crown/skirt interfacial pressure, and can be relatively coarse. The need to place this model on the already large skirt model is further motivation for a coarse crown mesh. This crown model will be discussed in conjunction with the skirt models.

Each of the "global" finite element skirt models was generated with ANSYS eight-node solid elements incorporating trilinear displacement functions along with additional "incompatible displacement modes" to improve the response of the element to stress gradients [4-3]. Each node may have three components of displacement.

Results from the global model analyses indicated highly localized stress gradients at the intersection of the vertical wall and the stud attachment boss in both designs. For this reason, substructured models of this region in both designs were developed with a much greater degree of mesh refinement than was possible in the global models. The substructured models were loaded using a technique known as "displacement recovery." In displace-

ment recovery, the boundaries of the local model, as defined by boundary nodes, describe surfaces in the global model for which nodal displacements can be determined. By imposing the displacements calculated for the global model on the local model, the local model is made to respond as if it were an integral part of the global model. This technique provides results in regions of high stress gradients and small geometric details without incurring prohibitive computer memory allocations associated with high degrees of refinement in large global models.

Calculated values of the AE and AF piston skirt peak stresses are given in Table 4-1 which shows the relevant principal stress and the Von Mises effective stress. The third algebraic minimum principal stress shown is the absolute maximum and is the most pertinent for the fatigue analysis of Section 6. Details of these values are discussed in subsequent subsections.

The gradient of these stresses below the surface as calculated by the local models is shown in Figure 4-1, which shows the normalized stress ($\sigma_{III}/\sigma_{max}$) as a function of distance below the surface. These gradients are necessary for the fracture mechanics calculations of crack growth, as will be discussed in Section 6.

The stress gradients are determined by starting at the surface where the highest stress nodes are located. The stress at the nodes in the next layer beneath the surface are scanned to obtain the node with the highest value. Each subsequent layer is also scanned finally forming a string of nodes along which the highest stress level at any given depth can be found. On both the AE and AF piston skirt local models, this string was a smooth line following a logical trail back to the surface.

4.2.1 AE Piston Skirt Analysis

Global Model. The global model of the AE piston skirt consisted of 1308 solid elements and 2007 nodes. The crown model consisted of 638 elements and 1336 nodes. Figure 4-2 shows the AE global model and the region selected for further analysis using a refined local model. As was also done for the AF

piston, a quarter-section was modeled and symmetric displacement boundary conditions were imposed on the x = 0 and y = 0 planes of symmetry.

Local Model. The local model of the AE skirt stud attachment boss detail consisted of 2960 solid elements and 3712 nodes. Figure 4-3 shows the local model with shaded planes representing those on which displacements from the global analysis were imposed.

Stress Results. The global AE piston skirt model showed peak values of the third principal stress to be located in the area of the intersection of the vertical wall and the stud attachment boss. The peak value of the third principal stress in this area for the global model with a crown was -42.7 ksi. Figure 4-4 shows a color schematic of the stress contours on the surface of the global skirt model with pressure applied on the crown.

To accurately evaluate the stresses and to determine the stress gradient under the surface, a local model was produced (shown in Figure 4-3) which more accurately models the geometry. Displacements from the global model were used as the boundary condition for the local model. The principal stress peak is in the radius between the vertical wall and the stud attachment boss. The stress contours on the surface for the local model are shown in Figure 4-5. The peak third principal stress at the surface in that region was found to be -68.1 ksi.

4.2.2 AF Piston Skirt Analysis

Global Model. The global model of the AF piston skirt consisted of 1070 solid elements and 1746 nodes. The crown model consisted of 493 elements and 1046 nodes. Figure 4-6 shows the AF global skirt model with a crown and the region selected for substructuring. The global model represents a quarter-symmetric section of the piston skirt. Symmetric displacement boundary conditions were imposed on the two planes of symmetry: x = 0 and y = 0. The z-axis coincides with the centerline of the piston skirt.

Local Model. The local model of the AF skirt stud attachment boss detail consisted of 720 solid elements and 1021 nodes. Figure 4-7 shows the

AF local model; the shaded planes are those on which displacements from the AF global model analysis were imposed.

Stress Results. The global AF piston skirt model indicated that the maximum third principal stress occurred in the area of the bosses and had a peak value of -41.3 ksi for a skirt with a pressurized crown. This peak stress was at the intersection of the vertical wall and the stud attachment boss. Figure 4-8 shows a color schematic of the surface stress contours.

In order to better evaluate the magnitude and location of the peak stresses and the stress gradient below the surface, a local model was constructed (shown in Figure 4-7) of the area of high stress found in the global model. This local model more accurately duplicated the geometry in the complex region where cracking was observed. Displacements from the global model results with various boundary conditions were used as boundary condition inputs to the local model. The principal stress peak in the local model was found at the radius between the vertical wall and the stud attachment boss and can be seen in Figure 4-9, which is a color schematic of the stress contours on the surface. The peak principal stress was found to be -92.2 ksi in that region at the surface. The local model was refined by adding 50% more elements and rerun under the same boundary condition. The peak stresses increased only slightly, indicating further mesh refinement was not necessary.

4.3 Crown/Skirt Interaction

The peak stresses calculated from the combined crown/skirt finite element models were presented and discussed in Section 4.2. The displacement behavior of the contact rings in these models is addressed in this section. The uniformity of the gap around the outer loading ring when the crown is pressurized, suggested by the experimental stress analysis, can be assessed from this information. The pressure at which the gap is predicted to close is also obtained from information on the vertical displacement of the contact rings of the crown and skirt.

Figures 4-10 and 4-11 show the calculated displacement on the inner and outer rings of the crown and skirt for a pressure of 1627 psig applied on top

of the crown. The data points correspond to nodal values of the displacement, and results are provided for the inner and outer edge of each of the contact rings. The lines drawn on the figures are for the average displacement of the ring as a function of angular position. The inequality of the displacements of the inner and outer edge is a result of "tipping" of the crown and skirt, i.e., the base of the crown on the inner contact ring does not remain horizontal.

The results of Figures 4-10 and 4-11 show significant angular variations of the ring displacements. Therefore, the boundary conditions on the top of the skirt do not correspond to a uniform vertical displacement, and the contact rings do not remain planar. However, Figures 4-10 and 4-11 show that the gap between the outer ring on the crown and skirt is virtually independent of the angular position. This is evident by the flatness of the dashed line in these figures, which is the difference between the vertical displacement on the outer ring of the crown and skirt ($\delta_{CO} - \delta_{SO}$). The uniformity of the gap around the circumference of the pressurized crown/skirt means that gap closure will occur uniformly around the circumference -- despite the fact that the contact rings do not remain planar. This observation is consistent with the deduction from the experimental results that the gap closes nearly simultaneously at all angular position on the outer contact ring.

The gap closure pressure for the two pistons at room temperature can be estimated from the results of Figures 4-10 and 4-11. Such estimates will be made in Section 6.2, where comparisons with experimental results will be presented.

4.4 Section 4 References

4-1 "Emergency Diesel Generator Crankshaft Failure Investigation, Shoreham Nuclear Power Station," Failure Analysis Associates' Report No. FaAA-83-10-2, Palo Alto, California, October 1983.

4-2 TDI Reported Values for Unit I, Division 2, of DSRV-16-4 Engine at Grand Gulf Nuclear Station.

4-3 E.L. Wilson, et al., "Incompatible Displacement Models," Numerical and Computer Methods in Structural Mechanics, Academic Press, New York, pages 43-57, 1973.

Table 4-1

PEAK SKIRT STRESSES FOR PRESSURIZED CROWN ON A SKIRT
(p = 1627 psig, all stresses in ksi)

	σ_{III}*	σ_e
AE global	-42.7	38.2
local	-68.1	61.3
AF global	-41.3	42.8
local	-92.2	79.9

* In all cases shown, the third (algebraic minimum) principal stress is maximum in absolute value.

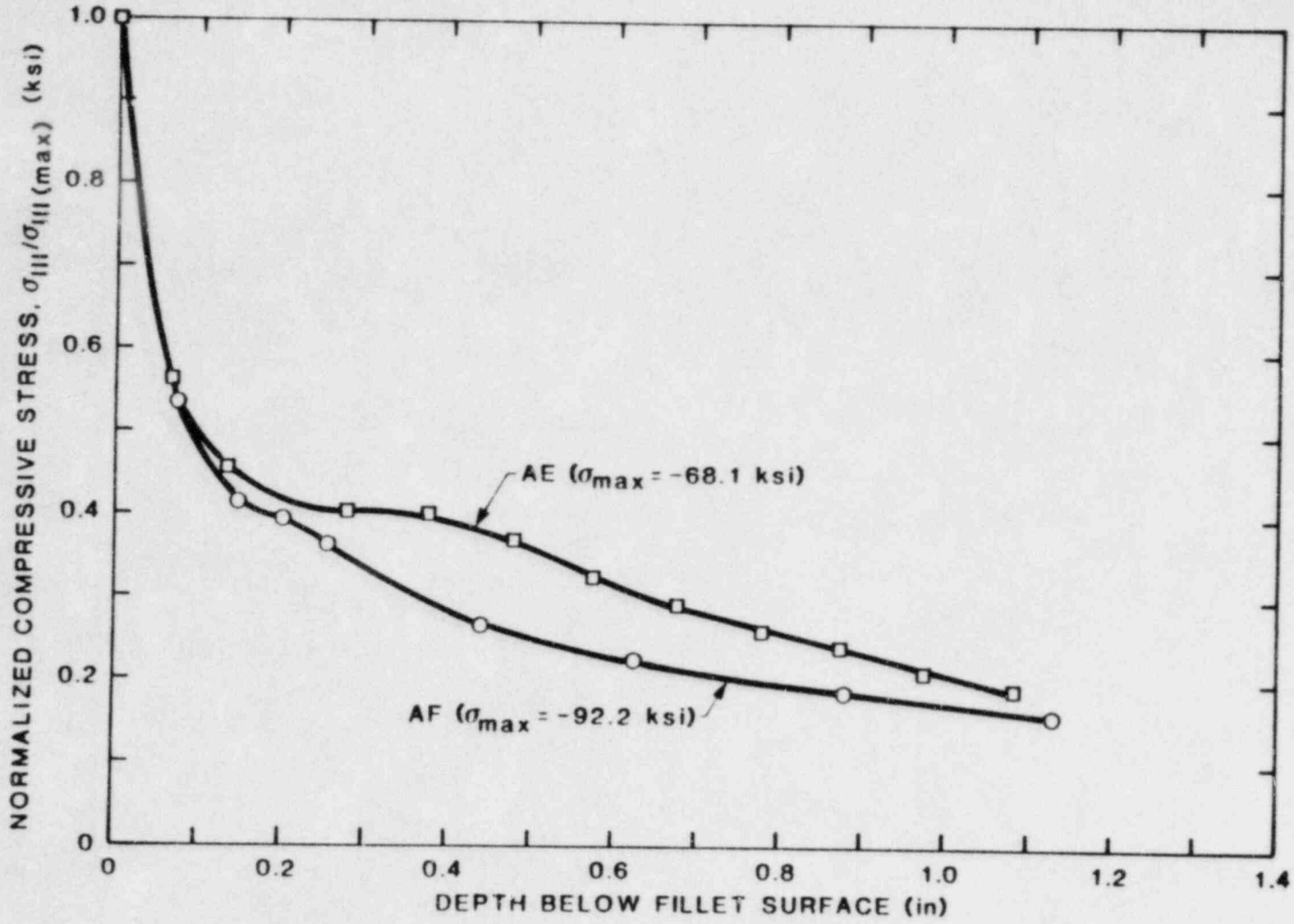

Figure 4-1. Normalized stress gradients in AE and AF local models.

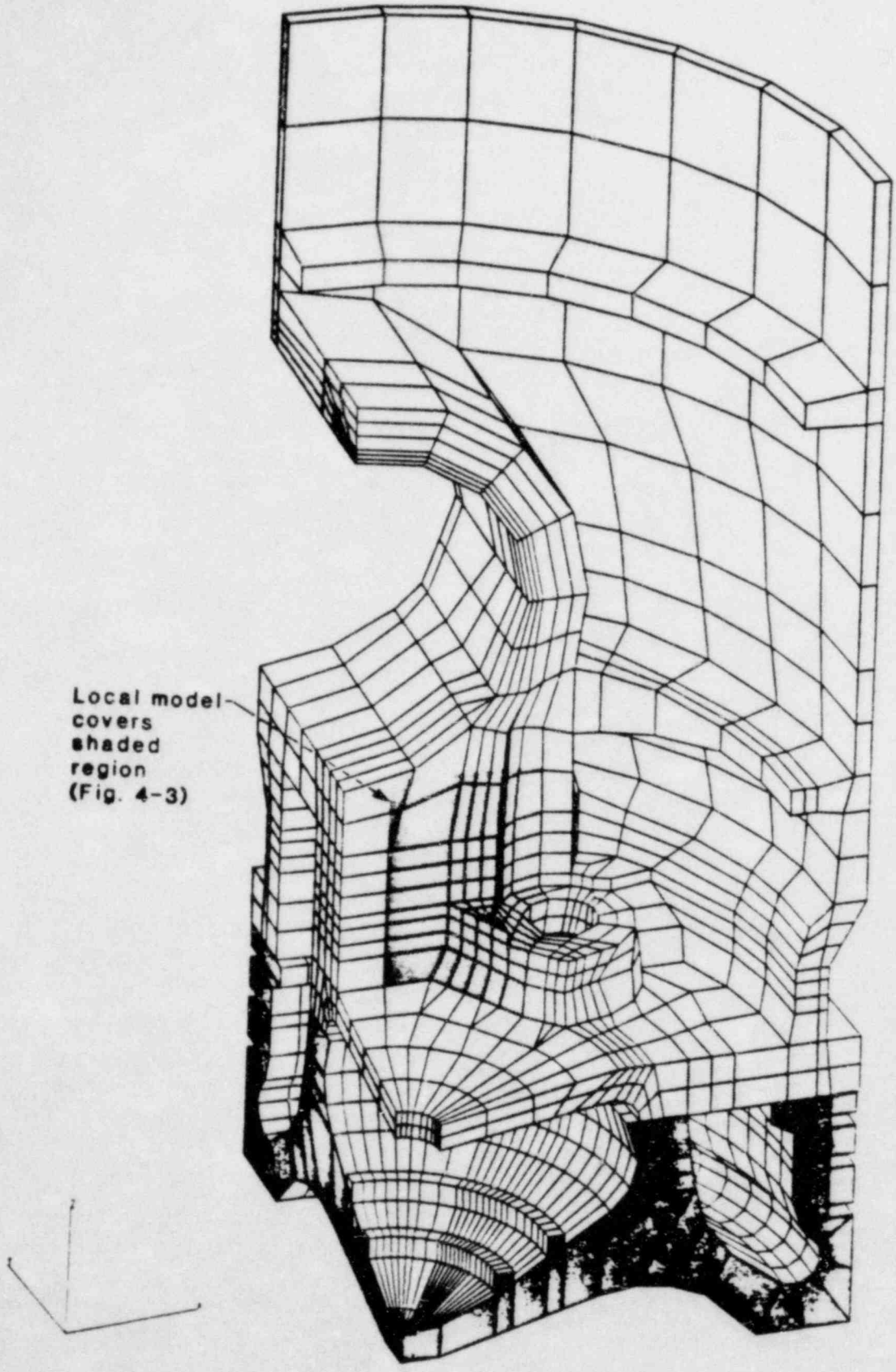

Figure 4-2. AE piston skirt global model with crown.

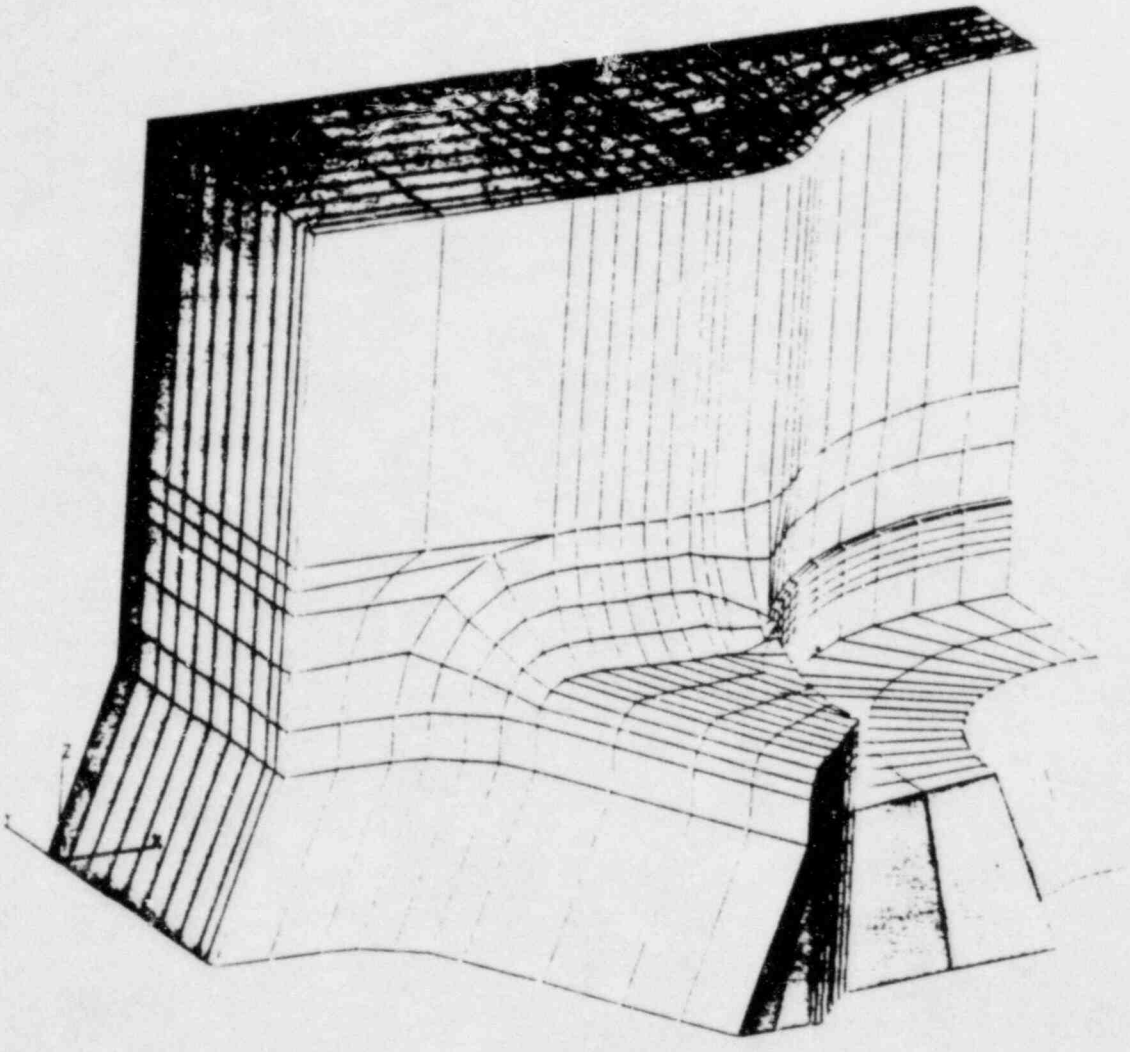

Figure 4-3. AE piston skirt local model.

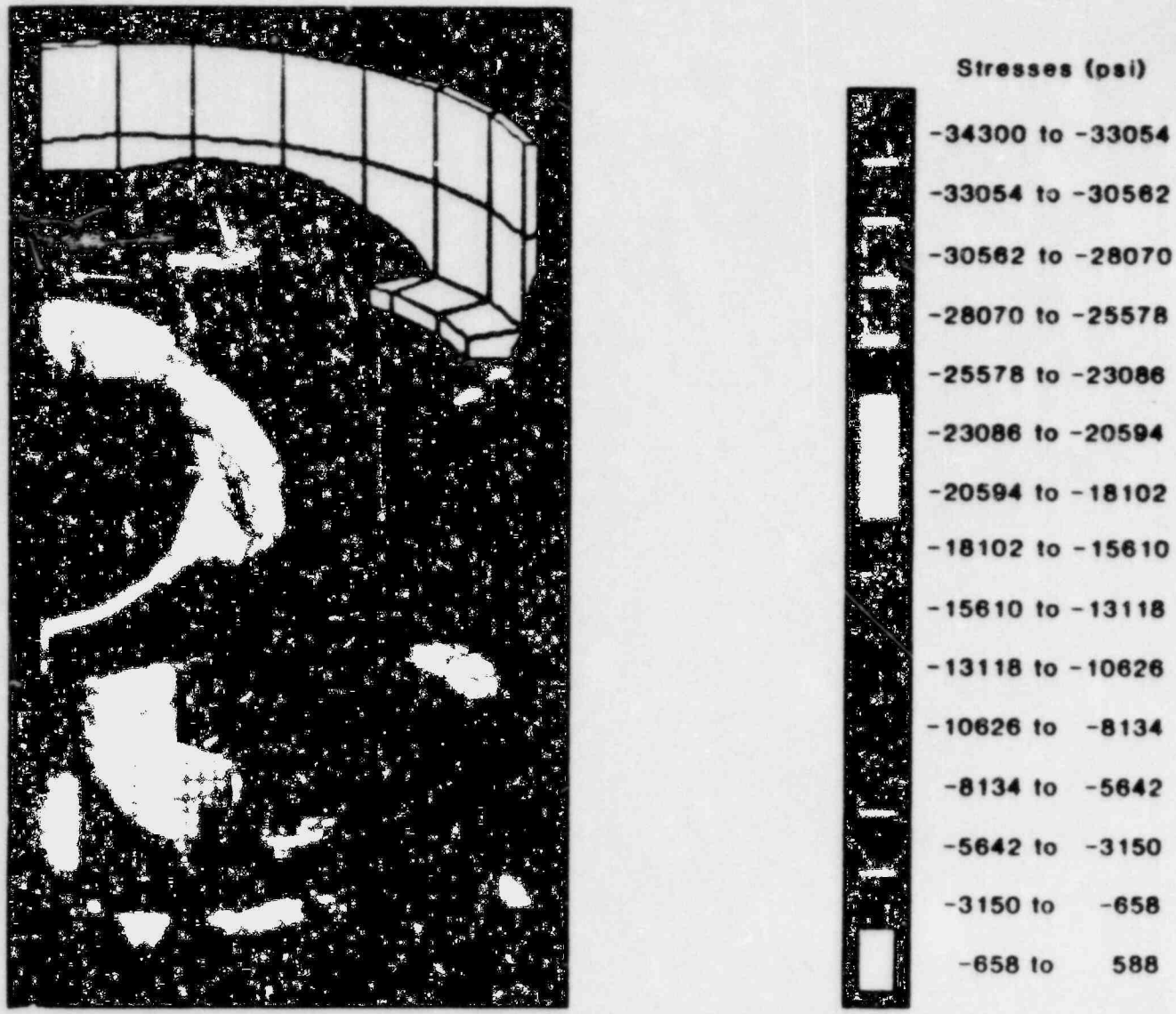

FaAA-84-2-14

Figure 4-1. Al piston skirt global model with stress contour of average element (σ_{111}) stresses for a skirt with a pressurized crown and no loading on the outer ring.

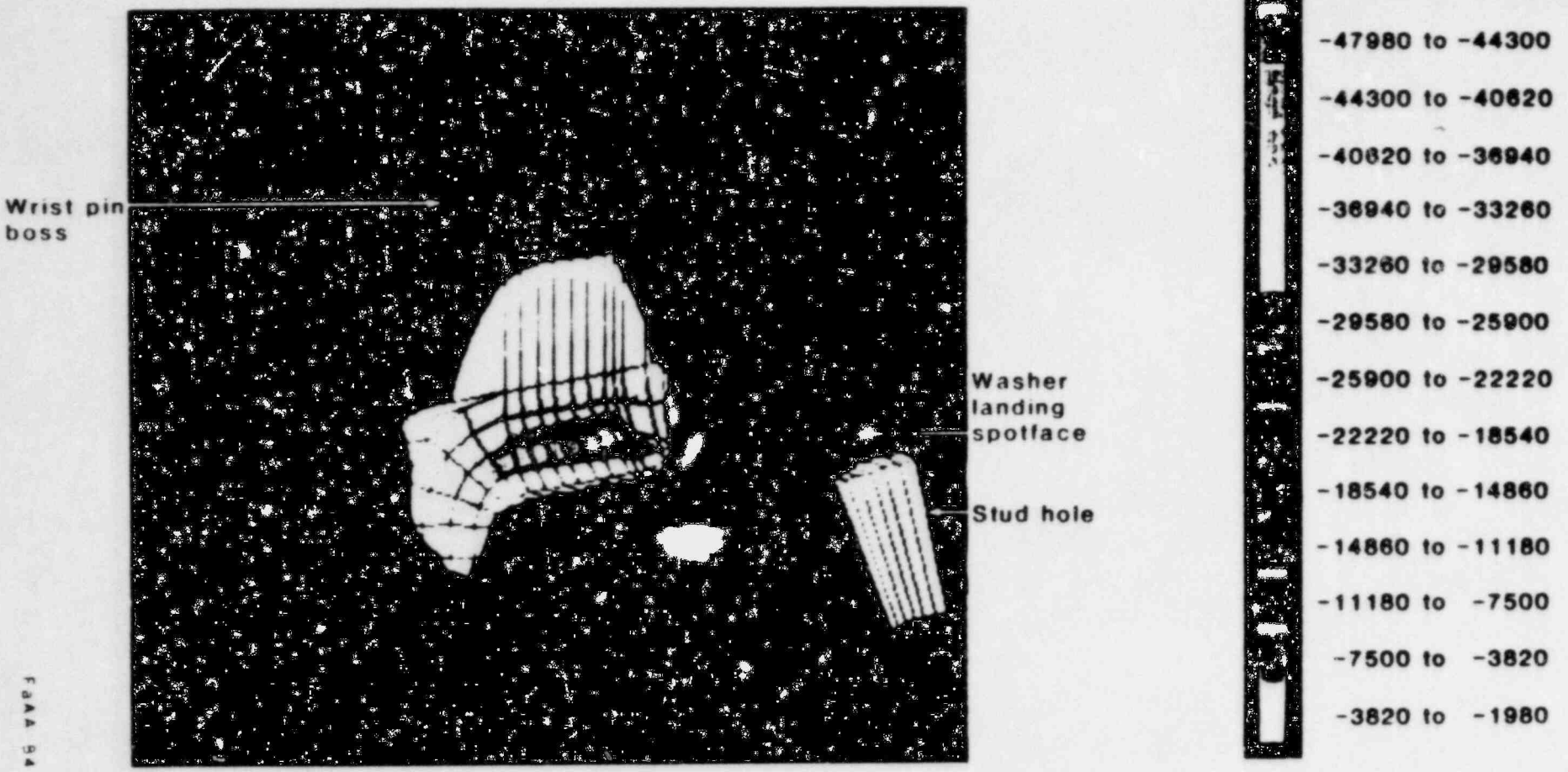

FAA 94 2 14

Figure 4-5. AE piston skirt local model with stress contour of average element (σ_{III}) stresses for a skirt with a pressurized crown and no loading on the outer ring.

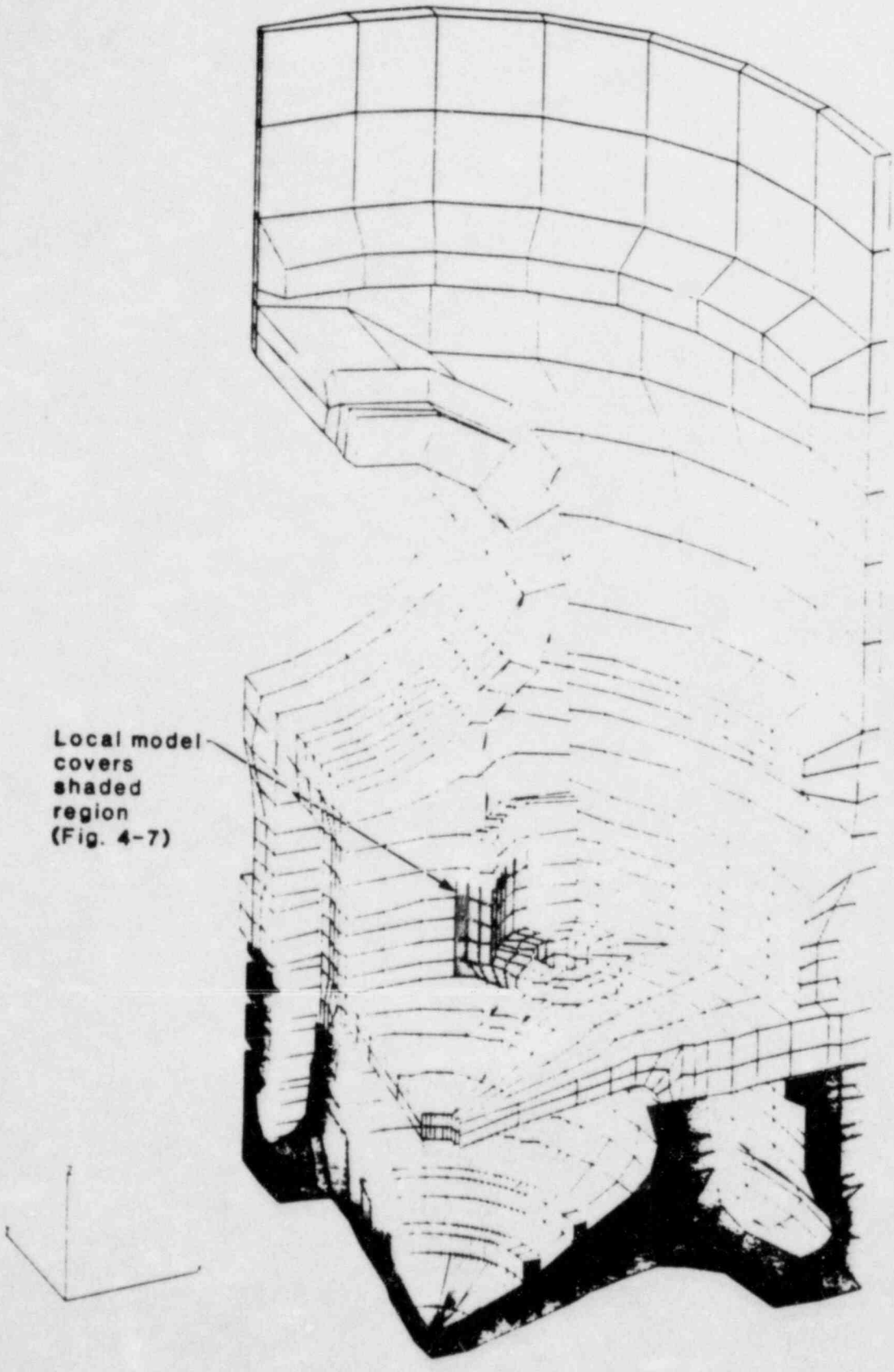

Figure 4-6. AF piston skirt global model with crown.

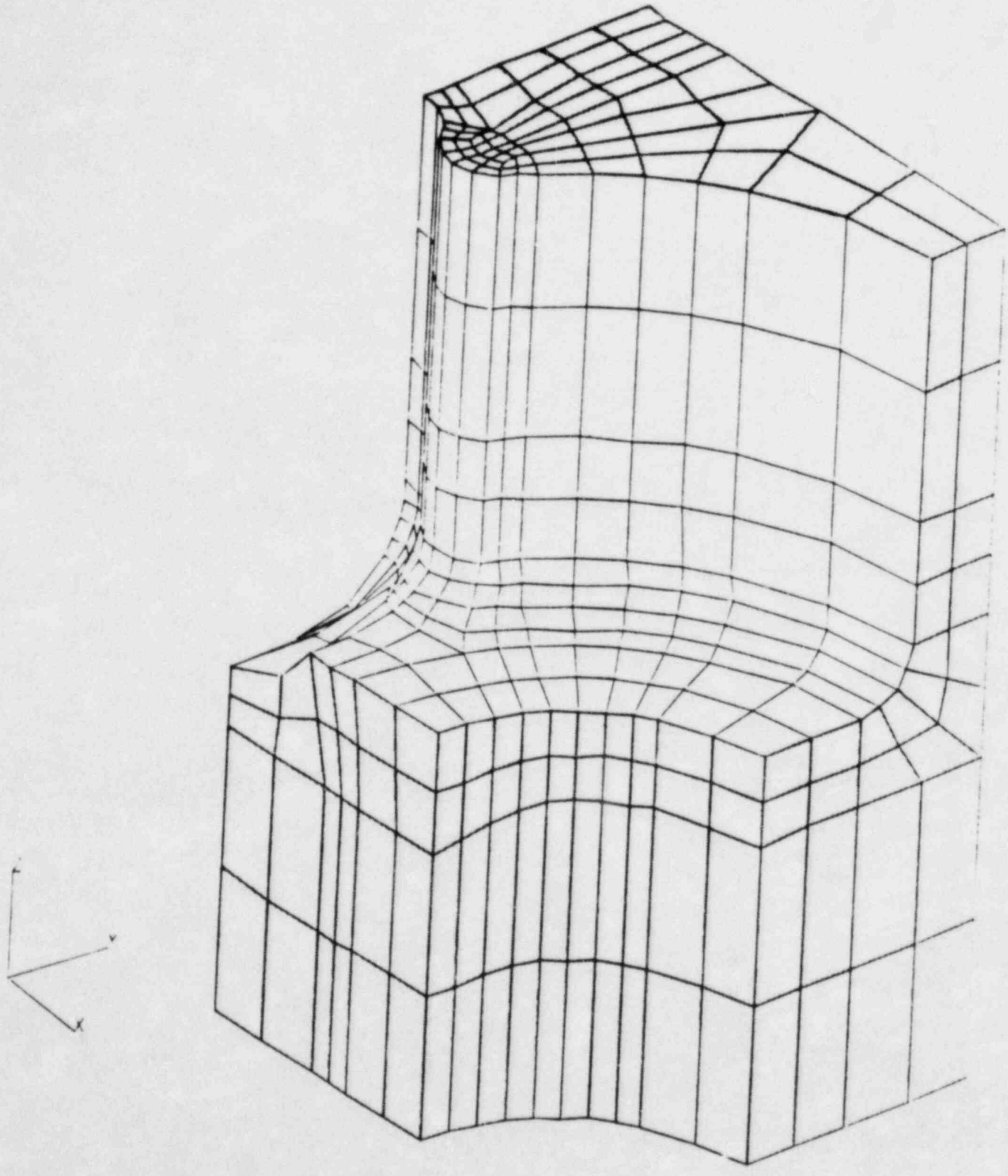

Figure 4-7. AF piston skirt stud-boss local model.

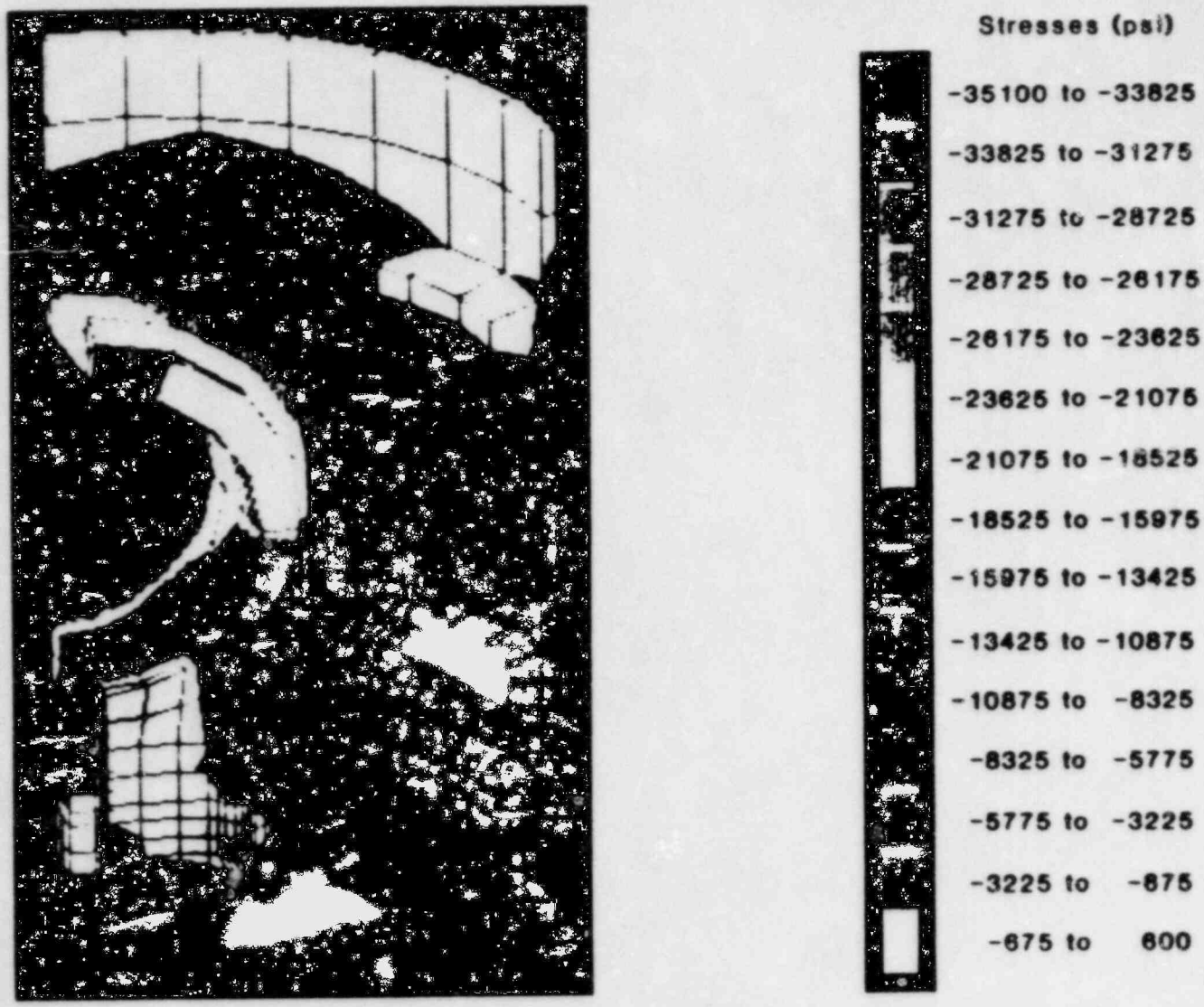

Figure 4-8. Al piston skirt global model with stress contour of average element (σ_{III}) stresses for a skirt with a pressurized crown and no loading on the outer ring.

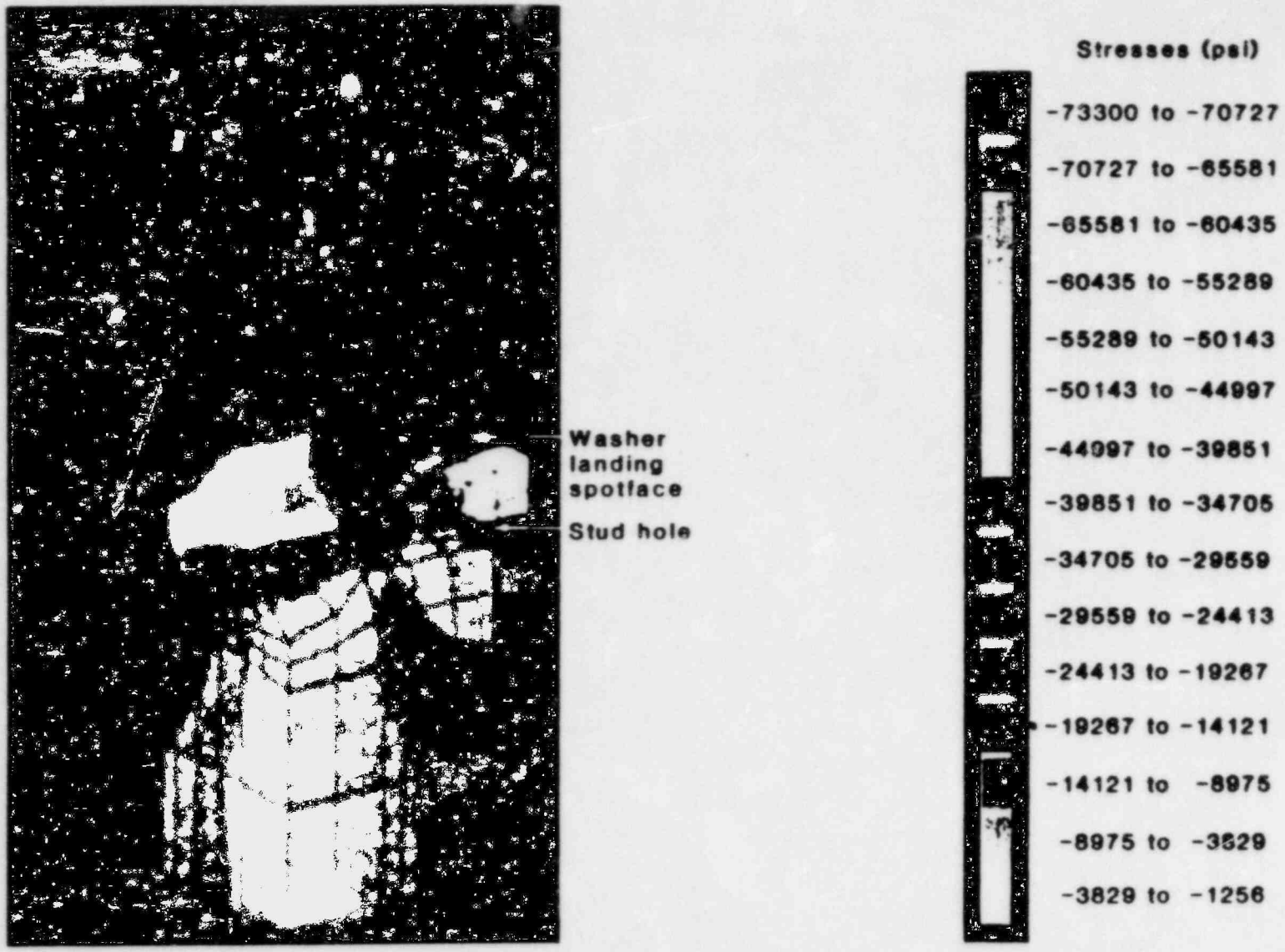

Figure 4-9. AF piston skirt local model with stress contour of average element (σ_{III}) stresses for a skirt with a pressurized crown and no loading on the outer ring.

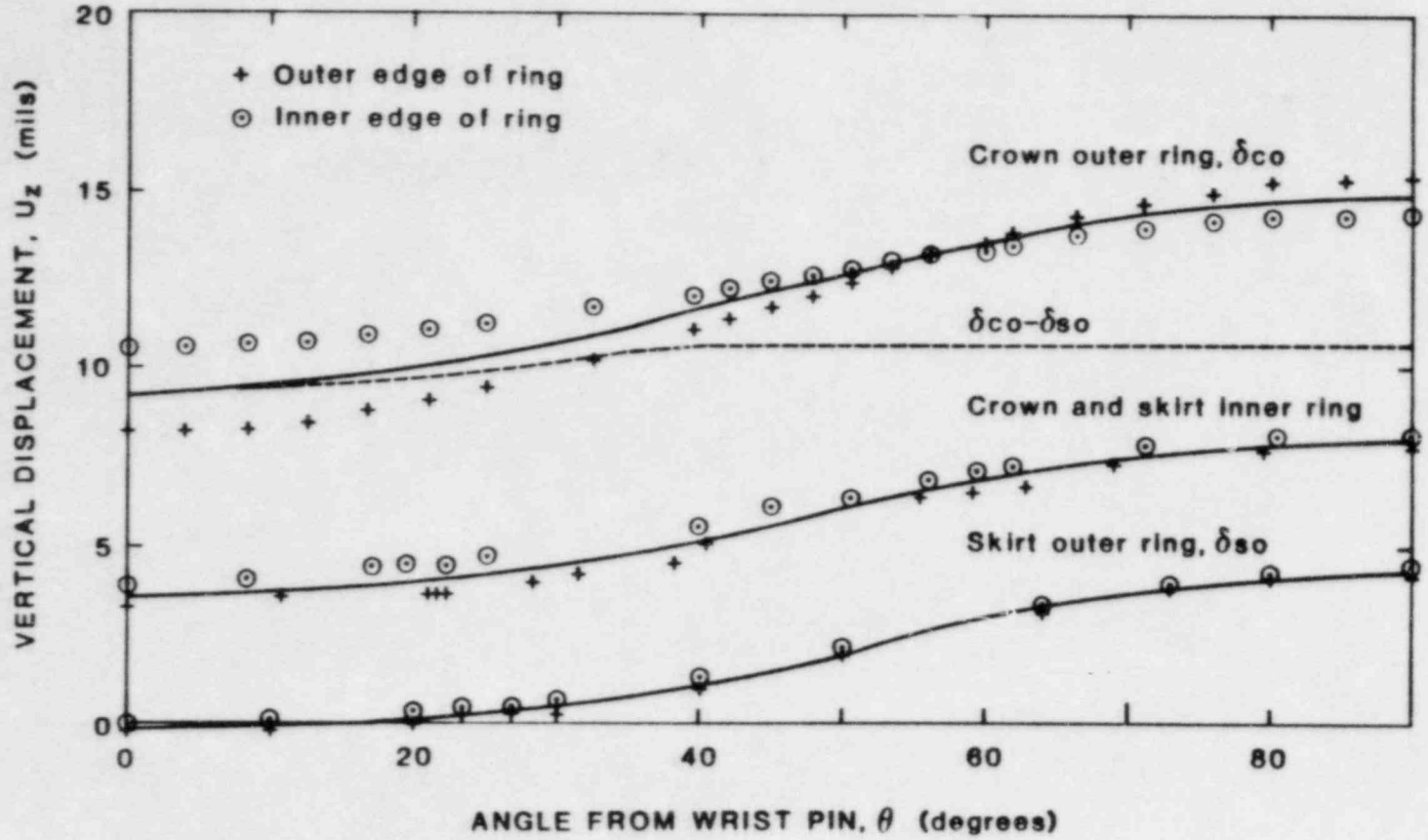

Figure 4-10. Computed crown and skirt vertical displacements on inner and outer rings as a function of angular position for an AE crown/skirt.

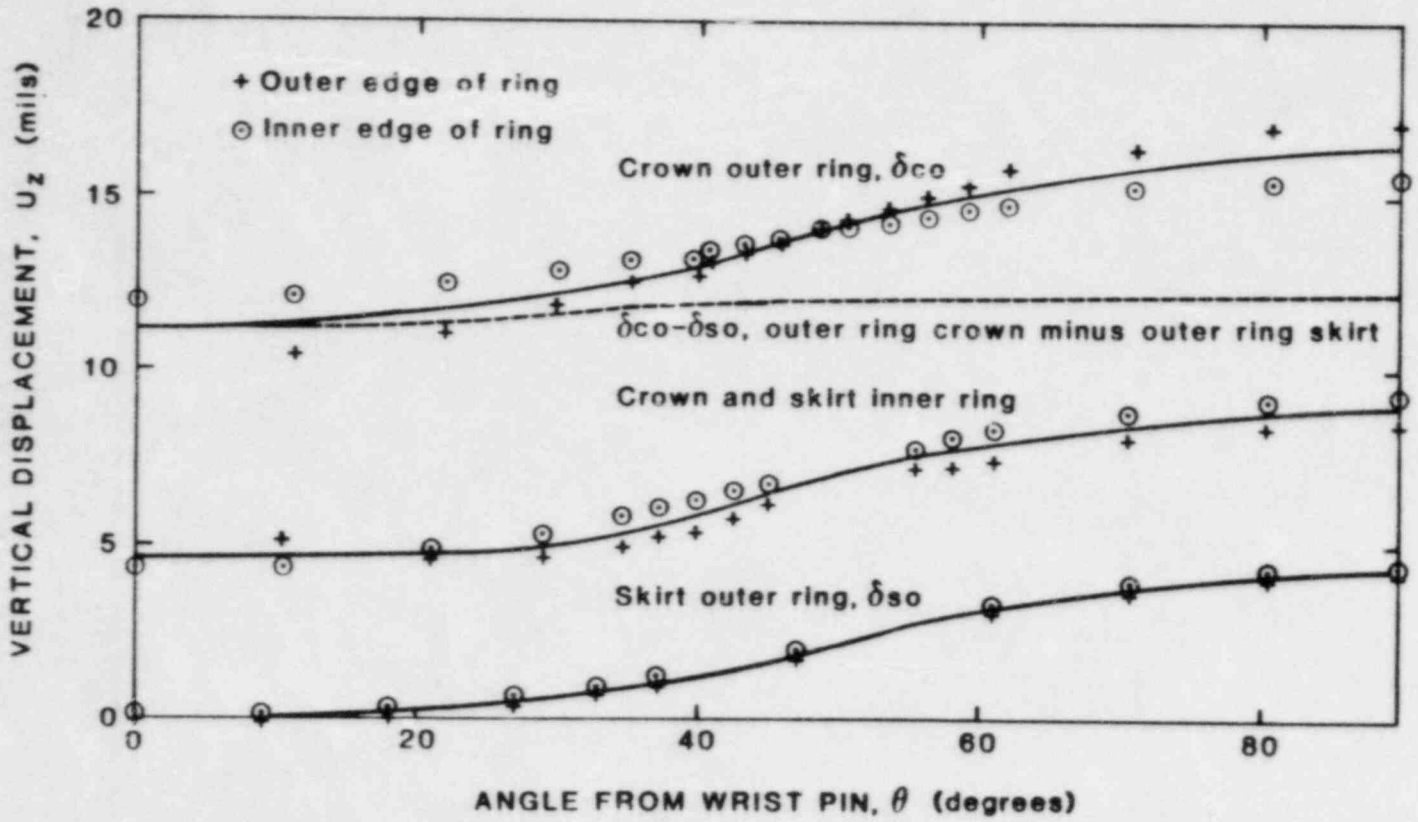

Figure 4-11. Computed crown and skirt vertical displacements on inner and outer rings as a function of angular position for an AF crown/skirt.

5.0 COMPARISON OF FINITE ELEMENT AND EXPERIMENTAL RESULTS

The finite element results presented in Section 4 will be compared with the experimental observations covered in Section 3. The comparisons include the maximum stress levels and gap closure pressures.

5.1 Stress Magnitudes

The peak stress magnitudes computed by finite element analysis for a skirt assembled to a crown are compared with the experimental results in Table 5-1. The finite element results for 1627 psig pressure loading are drawn directly from Table 4-1. These results are for no gap closure. Corresponding experimental results at 1627 psig are also presented in Table 5-1. The experimental results are drawn from Section 3 and, for comparison purposes, are compensated for gap closure, that was not represented in the finite element models, by linear extrapolation of stress values at pressures below the gap closure pressure. Experimental results are also adjusted for zero offset of the gages.

The results of Table 5-1 show good agreement between the experimental and finite element results. The AE finite element result is somewhat above the corresponding experimental values, with the average experimental value being 28% below the finite element value. The AF finite element result falls within the (wide) variation of the experimental values. The agreement between the experimental and finite element results is felt to be quite good. The large variation in the AF experimental results, which is discussed in detail in Section 3.4.2, precludes a precise comparison for this skirt. The 28% disagreement for the AE skirt is not large, and could be due to the assumption of a rigid wrist pin in the finite element model, neglecting friction between the skirt and crown and/or approximations in the finite element technique. Inaccuracies in the experimental results could also be a contributing factor. All of these possible sources of error taken together could easily account for a 28% disagreement.

5.2 Gap Closure Pressures

The pressure required to close the gap between the skirt and the crown at the outer load ring for a piston at room temperature was evaluated from the experimental results, as discussed in Section 3. Corresponding evaluations can be obtained from the finite element results presented in Section 4.3. Comparisons of these two sets of results are included in this section.

The gap closure pressure can be determined from the results of the finite element calculations of the crown and skirt displacements, such as summarized in Figures 4-10 and 4-11. These figures show that the movement of the outer ring of the crown relative to the outer ring of the skirt ($\delta_{co} - \delta_{so}$) is nearly independent of angular position. The values shown in Figures 4-10 and 4-11 are for a pressure of 1627 psig. The pressure, p*, to just close the gap, g_o, is given by

$$p^* = \frac{g_o}{\delta_{co} - \delta_{so}} 1627 \qquad (5\text{-}1)$$

Table 5-2 provides a comparison of the experimental and finite element results. This table shows that the experimental estimated gap closure pressures are invariably lower than the results derived from the finite element analysis, with the nominal experimental values being 18 to 29% below the corresponding nominal finite element values. This is felt to be acceptable agreement; the consistently higher finite element gap closure pressures result from higher crown and skirt stiffnesses; an inherent result of discretizing the real skirt/crown into a finite number of elements.

Table 5-1

COMPARISON OF PEAK STRESSES WITH NO GAP CLOSURE AS EXPERIMENTALLY MEASURED AND CALCULATED BY FINITE ELEMENTS
($-\sigma_{III}$, ksi)

	AE			AF	
Gage	Exp	F.E.	Gage	Exp	F.E.
B	54	68.1	B	107	92.2
C	48		D	63	
D	49		F	44	
E	49		H	45	
F	47				
G	52				
H	45				
I	44				
Average	49				

Table 5-2

COMPARISON OF EXPERIMENTAL AND FINITE ELEMENT RESULTS FOR GAP CLOSURE PRESSURES

	AE		AF	
	Exp	F.E.	Exp	F.E.
Nominal gap, mils	7.5	--	8.0	--
Range of gap, mils	7-8	--	7.5-9.5	--
Nominal $\delta_{co} - \delta_{so}$, mils	--	10.0(1)	--	11.6(2)
Range $\delta_{co} - \delta_{so}$, mils	--	9.2-10.6(1)	--	11.1-12.2(2)
Nominal p*, psig	1000(3)	1220(4)	800(3)	1120(4)
Range p*, psig	820-1050(3)	1074-1414(4)	700-1000(3)	1000-1390(4)

(1) From Figure 4-10.
(2) From Figure 4-11.
(3) From Table 3-7.
(4) From Equation 5-1.

6.0 FATIGUE AND FRACTURE ANALYSIS

The metallurgical evaluation of the AF piston skirt provided in Section 2 concluded that the observed cracks resulted from fatigue. The experimental and finite element stress analyses results, presented in the previous sections, are combined with the fatigue and fracture properties of the material to analyze the possibility of crack initiation in the piston skirts. The growth behavior of initiated cracks is also analyzed, and comparisons are made of the performance of AF and AE skirts.

The fatigue analysis predicted that cracks will initiate in the AF piston skirt for both the experimental and finite element cyclic stress levels. The initiated cracks can grow under certain conditions, but are predicted to arrest at depths of less than 0.15 inch. The AE piston skirt was predicted to not initiate cracks under cyclic stress levels obtained from the experiments, but cracks might initiate under conditions predicted from the finite element calculations. Initiated cracks were predicted to not grow in the AE piston under either the conditions predicted from the experimental or finite element results.

6.1 Material Properties

The fatigue and fracture properties of the piston skirt material are presented in this section.

6.1.1 Fatigue

The pistons experience 1.35×10^6 stress cycles every 100 hours of engine operation. Crack initiation under high cycle fatigue conditions is therefore of concern, in which case the endurance limit of the material is the property of interest. Reference 6-1, and references cited therein, indicate that a lower bound for the endurance limit of cast iron with the properties of the 100-70-03 material used in the skirt is 30 ksi.

The endurance limit of 30 ksi is applicable to fully reversed uniaxial loading, in which case the mean stress is zero, and the stress system is par-

ticularly simple. In order to perform the analysis on the piston skirt, two complications must be accounted for: non-zero mean stress and multiaxial stresses.

The case of non-zero mean stress can be treated in the standard manner by use of a Goodman diagram. Figure 6-1 shows the definition of terms for cyclic loads employed here. Figure 6-2, which closely follows Figure 15b of Reference 6-1, shows how the allowable cyclic stress for infinite life varies with the mean stress. This figure, which extends into the compressive range, is similar to that employed in Reference 6-2 for fatigue analysis of nodular cast iron piston skirts. The allowable stresses indicated in this figure are such that yielding in tension or compression is precluded, and at zero mean stress the value of σ_a is equal to the endurance limit, σ_n. The value of the yield strength of 60 ksi was used in the generation of Figure 6-2. This corresponds to a typical value measured at FaAA and reported in Section 2.7. The requirement that $\sigma_{max} \leq \sigma_{ys}$, $\sigma_{min} \geq -\sigma_{ys}$, combined with the definition of σ_a and σ_{mean}, along with the requirement that $\sigma_a = \sigma_n$ when $\sigma_{mean} = 0$ defines the lines in Figure 6-2.

The conditions outlined in Figure 6-2 are conveniently summarized in Figure 6-3, which directly plots the allowable cyclic stress for infinite life for a given mean stress. The representation in Figure 6-3 closely follows that included in References 6-2 and 6-3.

The results presented in Figures 6-2 and 6-3 are for uniaxial stress. Figure 6-3 can be generalized to multiaxial stress systems by procedures presented in References 6-3 and 6-4. However, the experimental results presented in Section 3.4.2 show that the stresses are nearly uniaxial in the highly stressed region of the stud mounting boss. Therefore, Figure 6-3 can be used directly in conjunction with the principal stress that has the largest cyclic amplitude (σ_{III} in this case).

6.1.2 Fracture Mechanics Properties

Analyses based on the previous section can be used to predict whether an initially uncracked component will have an infinite life. If a finite life

is predicted, then a crack will initiate. Once it has initiated, it may or may not grow, and its possible subsequent growth can be treated by fracture mechanics principles. The fracture mechanics properties of the material are required in this analysis and are summarized in this section.

Fracture Toughness. The fracture toughness of the material governs the point at which a crack grows catastrophically and is the critical value of the applied stress intensity factor [6-5]. Reference 6-1 and references cited therein provide information on the fracture toughness of nodular cast iron. The fracture toughness is influenced by temperature within the range of interest (room temperature to ~300°F) and increases with increasing temperature. Also, the toughness tends to decrease with increasing strength levels. Table 6-1 summarizes some relevant fracture toughness data from the literature. This table shows K_{Ic} of 40 ksi-in$^{1/2}$ to be a reasonable, but somewhat conservative, value of the fracture toughness. This was used as the nominal value of K_{Ic} in the fracture mechanics analysis. This value is especially conservative for use at the operating temperature of the piston skirt.

Fatigue Crack Growth Characteristics. For a given material and environment, the rate at which a fatigue crack grows is dependent mainly on the cyclic value of the stress intensity factor ($\Delta K = K_{max} - K_{min}$) [6-5]. Other factors, such as the mean value of K (measured as $R = K_{min}/K_{max}$) also have an influence. Information on the crack growth rate, da/dN, as a function of ΔK for nodular cast iron is included in References 6-1 and 6-7 through 6-10. Representative results of da/dN versus ΔK are included in Figure 6-4. A reasonable and somewhat conservative representation for the crack growth characteristics is given by the upper end of the shaded band in Figure 6-4. This result is conservative for all cases shown except R = 0.7, which corresponds to cyclic loading with large mean tensile stresses. The cyclic stresses in the piston skirt in the region of interest are primarily compressive and, therefore, do not have such a high positive R-ratio. The following equation, representing the upper end of the shaded band, provides the relationship between da/dN and ΔK that was used.

$$\frac{da}{dN} = 2.47 \times 10^{-12} (\Delta K)^{5.15} \qquad (6\text{-}1)$$

The constants in this equation are applicable when da/dN is in inches/cycle and ΔK is in ksi-$in^{1/2}$.

Equation 6-1 over-estimates crack growth rates when ΔK becomes small because there is a threshold below which cracks will not propagate. Reference 6-9 provides some information on fatigue thresholds for various R-values. The value of ΔK_{th} for R = 0.1 is indicated to be about 12 ksi-$in^{1/2}$. This value appears to be somewhat optimistic because Reference 6-11 suggests a value of 6.4 ksi-$in^{1/2}$ for a variety of steels for values of R close to zero. This value is stated in Reference 6-11 as being somewhat conservative and is used as the applicable value for the nodular iron considered here.

An approach to non-propagating fatigue cracks is provided by References 6-12 and 6-13, in which cases the influence of R-value on threshold conditions for crack propagation are treated. In this case, the Forman relation for crack growth is combined with the treatment of R-value from Reference 6-13 to provide a treatment of the influence of R on ΔK_{th}. Cracks are taken to not propagate for a given ΔK and R if $\Delta K < \Delta K_{th}(R)$. Reference 6-11 provides the details, and the procedures are included in the BIGIF code. This code is used for the fatigue crack growth calculations presented in Section 6.3 and is a widely used code for fracture mechanics analyses.

6.2 Cyclic Stress Levels

The cyclic stress values in the highly stressed region of the AE and AF skirts are required for the fatigue crack initiation and growth analysis. The experimental results of Section 3 showed that the stresses due to pressure are dependent on the initial gap size, g_o, because this parameter influences the gap closure pressure and load transfer between the inner and outer load rings. As shown in Figure 3-2, the initial gap can vary from 0.007 to 0.011 inch and still be within TDI specified tolerance. The finite element results reported in Section 4 are for no gap closure, and therefore do not consider the influence of outer ring loading in reducing the peak stresses.

The cyclic stress levels evaluated by finite elements for the AE and AF as a function of g_o under isothermal conditions can be estimated by use of the

experimental observations reported in Section 3, with the results shown in Table 6-2 being obtained. These results assume that no gap opens on the inner contact ring between the crown and skirt; such gap opening is not expected under the isothermal conditions considered in this report. The results of Table 6-2 show that the cyclic stresses are invariably larger in the AF skirt than the AE.

Cyclic stresses in the skirt can also be estimated directly from the strain gage results for the gap sizes present in the experiments. Table 6-3 summarizes such estimates. The cyclic stress levels in Tables 6-2 and 6-3 are used in the following section to see if crack initiation and growth can occur in the piston skirts.

6.3 Fatigue Crack Initiation Analysis

This section combines the cyclic stresses in Tables 6-2 and 6-3 with the crack initiation criteria from Section 6.1.1 to assess the possibility of cracks initiating under isothermal conditions in the AE and AF piston skirts. The results of Tables 6-2 and 6-3 are plotted on the allowable stress envelope for infinite life in Figures 6-5 and 6-6. The allowable stress envelope for each skirt type is constructed using both minimum and maximum yield strength levels for each skirt type from Table 2-2. An endurance limit of 30 ksi is used in all cases, and results for various gap sizes are shown for the finite element results.

The results of Figure 6-5 show that the finite element results predict that crack initiation will occur in the AF skirt regardless of the gap size and tensile properties used. The experimental results predict crack intiation if the largest stress value is used, but no initiation if the smallest stress value is used. This variance in predicted behavior is due to the large spread in the experimental peak stresses for the AF piston skirt.

The results of Figure 6-6 show that cracks are predicted to not initiate in the AE skirt under cyclic stresses corresponding to the experimental results. Use of the finite element results predicts that cracks might or might not initiate, depending on the tensile properties and gap size.

The finite element stresses for the AF piston skirt included in Table 6-2 are above the compressive yield strength of the material. Therefore, under these conditions localized plastic deformation is predicted to occur on at least the first few cycles of loading. This plastic deformation in compression will cause redistribution of the stresses in the highly stressed region, which shifts the mean stresses towards tension. Calculations of stress redistribution were performed for various conditions using the contained plasticity analysis included in BIGIF [6-12, 6-14]. This approach utilizes the Neuber approximation [6-15] for contained plastic deformation in conjunction with a Ramberg-Osgood representation of the material's stress-strain behavior in order to provide an estimate of the influence of plastic deformation on the stresses within a contained plastic zone. The redistributed stresses are used in the fatigue crack propagation analysis to be presented in Section 6.4.

Although the results in Table 6-2 predict that fatigue cracks can initiate under stress levels corresponding to the finite element stresses, these cracks will not necessarily propagate. This is because the initiated crack will be growing into a region of decreasing stresses, because of the steep stress gradient in the stud boss region.

In summary, the results of finite element calculations predict that cracks may initiate in both the AE and AF skirts. The experimental results predict that cracks will not initiate in the AE skirt, but may initiate in the AF skirt.

6.4 Fatigue Crack Growth Analysis

The concern raised by the discovery of cracks in the AF piston skirts is that the cracks may grow during operation and result in a failure of the pistons. This section analyzes whether the initiated cracks could grow in the pistons. The presence of a crack in the piston skirt does not necessarily lead to unsatisfactory performance of the piston, because the initiated cracks may not grow. Even if they do grow, they may arrest as they grow out of the localized region of high stress. The behavior of any cracks that do initiate can be analyzed by use of fracture mechanics principles. The fracture mech-

anics properties of the material that were summarized in Section 6.1.2 were used in this analysis, which was performed with the BIGIF fracture mechanics code [6-15].

The elastically calculated stresses from the finite element results are sufficient to cause yielding in the AF skirt and (depending on the initial gap) in the AE skirt. Residual tensile stresses are predicted in the localized region where the stresses exceed the yield strength. The contained-plasticity capability in BIGIF was used to obtain the elastic-plastic redistributed stress fields. Figure 6-7 presents the principal stress with the largest absolute value as a function of distance into the piston skirt for the AF piston subjected to pressure and inertia with all the loading on the inner ring. Also shown are the redistributed stresses which exist after yielding. This figure reveals the very steep stress gradients in the skirt in the localized highly stressed region near the stud boss and shows the substantial redistribution of stresses resulting from the plastic deformation. The elastic-plastic redistributed stresses show a substantial tensile component that can cause cracks to grow. These tensile components result from an upward shift in the mean stress due to yielding caused by the high compressive stresses under peak cylinder pressure.

The stress intensity factor range, ΔK, due to the plastically redistributed cyclic stresses was calculated using BIGIF. The crack was idealized as a plane strain crack in a strip of finite width. For the AF skirt, calculations were performed for two stress-strain curves: a "worst" curve, which corresponds to the lowest measured curve for the AF; and an "average" curve, which corresponds to the average of the measured curves. (See Section 2.7 and Table 2-2.) Values of ΔK, as calculated using BIGIF, are compared to the threshold value for crack growth, ΔK_{th}, to determine crack growth and arrest points. The BIGIF calculations account for the variation in ΔK_{th} with stress ratio, R. Crack growth is only possible when $\Delta K(R) > \Delta K_{th}(R)$.

The ΔK calculations showed that, under certain conditions, the cyclic stresses produced ΔK and R at crack depths greater than a_{th} which were sufficient to exceed threshold conditions. Therefore, a crack of this depth could grow. However, as the crack extends, ΔK passes through a peak and decreases

to the point where ΔK and R fall below the threshold conditions for fatigue crack growth. The fatigue crack is predicted to arrest at this depth, which is denoted as a_{ar}. Table 6-4 summarizes the results of such calculations for the isothermal AF skirt. This table shows that crack growth is not predicted in the AF skirt except for the case where no credit is taken for the stress reduction due to gap closure at peak firing pressure ($g_o = \infty$).* Under conditions in which crack growth can occur, the crack must be 0.031 inch deep before it exceeds threshold conditions. The arrested crack depths fall within the range of observed depths discussed in Section 2.

Corresponding fracture mechanics calculations for the AE piston skirt revealed that no crack depths provide ΔK and R values that exceed threshold conditions. Therefore, the cracks that may possibly initiate in the AE skirt are predicted never to grow under isothermal conditions.

The large gap size required in the AF skirt in order to predict crack growth, in combination with the consistent observation of cracking in the AF skirts at Shoreham, suggests that either (i) the finite element stresses are too low, (ii) small cracks can grow in this material under conditions in which fracture mechanics principles would predict no growth, or (iii) stress contributors other than those considered here are present during engine operation. Comparisons of the finite element and experimental results presented in Section 5 (see Table 5-1) suggest that the finite element results are not too low. It is not likely that the fracture mechanics procedures used here are underpredicting threshold conditions. Thermal effects that redistribute the stress are present during engine operation are not considered here. Non-uniform temperature distribution in the crown will produce thermal crown distortion which will alter the load distribution between the inner and outer load ring (load split). This may also result in opening a gap at the inner ring under inertia loading at top center of the exhaust stroke. Such lift-off

* From the discussion at the end of Section 3, gap closure would be predicted not to occur in the AF under isothermal conditions and peak firing pressure of 1670 psig (minus inertia force) if the gap is greater than 0.016 inch. Hence, an infinite gap is not required, but only one that is much larger than would meet TDI assembly tolerances (0.007 to 0.011 inch).

would alter the load path of the stud loads, which could increase σ_{max} substantially above the values used in this report (which assumed no lift-off). Such effects are beyond the scope of the current report, which considers only isothermal effects, and are the topic of a future report.

6.5 Section 6 References

6-1 Iron Castings Handbook, edited by C.F. Walton and T.J. Opar, Iron Casting Society, Inc., 1981.

6-2 R. Reipert, H. Moebus, and K. Schellmann, "Computer Design of a Steel-Nodular Cast Iron Piston Capable of Withstanding High Loads for Application in Medium Speed Diesel Engines," Paper No. 83-DGEP-8, American Society of Mechanical Engineers, New York, 1983.

6-3 H.O. Fuchs, "A Set of Fatigue Failure Criteria," Journal of Basic Engineering, pages 333-343, June 1965.

6-4 H.O. Fuchs and R.S. Stephens, Metal Fatigue in Engineering, John-Wiley and Sons, Inc., New York, 1980.

6-5 D. Broek, Elementary Engineering Fracture Mechanics, Sijthoff and Noordhoff, Alphen aan den Rijn, Netherlands, 1978.

6-6 R.K. Nanstad, F.J. Worzalz, and C.R. Loper, Jr., "Static and Dynamic Fracture Toughness of Ductile Cast Iron," AFS Transactions, Proceedings of 79th Annual Meeting, Vol. 83, pages 245-256, 1975.

6-7 B. Ostensson, "Fracture Toughness and Fatigue Crack Growth in Nodular Cast Iron," Scandinavian Journal of Metallurgy 2, Vol. 2, No. 4, pages 194-196, 1973.

6-8 D.G. Smith and K.P. Jen, "Fracture Properties of Nodular Iron Castings, Grade 80-55-06," Tennessee Technological University Department of Civil Engineering Report TTU-CE-82-1, Cookville, Tennessee, October 1982.

6-9 M. Castagna, P. Ferrero, R. Medana, and E. Natalu, "Fatigue Properties of 'In-Mold' Ductile Iron," AFS International Cast Metals Journal, Vol. 4, No. 4, pages 63-72, December 1979.

6-10 M.S. Starkey and P.E. Irving, "A Comparison of the Fatigue Properties of Machined and As-Cast Surfaces of SG Iron," International Journal of Fatigue, page 129-136, July 1982.

6-11 S.T. Rolfe and J.M. Barson, Fracture and Fatigue Control in Structures, Prentice-Hall, Inc., Englewood Cliffs, New Jersey, 1977.

6-12 P.M. Besuner et al., "BIGIF - Fracture Mechanics Code," EPRI Report NP-1830-CCM, Electric Power Research Institute, Palo Alto, California, 1981.

6-13 A. Yuen, S.W. Hopkins, G.R. Leverant, and C.A. Rau, "Calculations Between Fracture Surface Appearance and Fracture Mechanics Parameters for Stage II Fatigue Crack Propagation in Ti-6Al-4V," Metallurgical Transactions, Vol. 5, pages 1833-1842, August 1974.

6-14 P.M. Besuner and S.A. Rau, "Stress and Subcritical Crack Growth Analysis Under Contained Plastic Conditins," EPRI Report NP-81-8-LD, Electric Power Research Institute, Palo Alto, California, 1981.

6-15 H. Neuber, "Theory of Stress Concentration for Shear Strained Prismatical Bodies with Arbitrary Nonlinear Stress-Strain Law," Journal of Applied Mechanics, pages 544-550, December 1961.

Table 6-1

SUMMARY OF FRACTURE TOUGHNESS DATA FROM THE LITERATURE FOR NODULAR CAST IRON WITH STRENGTH LEVELS SIMILAR TO 100-70-03

K_{Ic} ksi-in$^{1/2}$	T, °F	σ_{ult}, ksi	σ_{ys}, ksi	Elong. %	Reference
41	70	133	80	3.6	6-6
36	70	85.3	76	1.6	6-6
48	220	116	90	--	6-7
40	70	116	90	--	6-7
~85	70	90	58	--	6-7
25	75	>80	>62	>3.0	6-1
47	75	--	104	--	6-1

Nominal value for calculations: 40 ksi-in$^{1/2}$.

Table 6-2

CYCLIC STRESS LOADS UNDER ISOTHERMAL CONDITIONS IN THE AE AND AF PISTON SKIRTS FOR VARIOUS GAP SIZES
(all stresses are in ksi)

	AE					AF				
g_o mils	load split	σ_{min}	σ_{max} (1)	σ_a	σ_m	load split	σ_{min}	σ_{max} (1)	σ_a	σ_m
7.5	88 (2)	-60.0	1.77	30.9	-29.1	--	--	--	--	--
8.0	--	--	--	--	--	80 (3)	-73.8	2.40	38.1	-35.7
8.5	<100	<-68.1	1.77	<34.9	<-33.2	81 (4)	-74.7	2.40	38.5	-36.2
11	<100	<-68.1	1.77	<34.9	<-33.2	86 (4)	-79.3	2.40	40.9	-38.4
∞	100	-68.1 (5)	1.77	34.9	-33.2	100	-92.2 (5)	2.40	47.3	-44.9

(1) $-0.026 \times (\sigma_{max}$ with no load split).
(2) From Figure 3-5.
(3) From Table 3-6
(4) Linear interpolation from Table 3-6 data for load split with and without shim.
(5) From Table 4-1.

Table 6-3

CYCLIC STRESS LEVELS UNDER ISOTHERMAL CONDITIONS IN THE AE AND AF PISTON SKIRTS FOR VARIOUS GAP SIZES AS ESTIMATED FROM EXPERIMENTAL RESULTS
(all stresses are in ksi)

	AE 88% load split		AF 80% load split	
	smallest value	largest value	smallest value	largest value
σ_{III} (1)	-44	-54	-44	-107
σ_{min} (2)	-38.7	-47.5	-35.2	-85.6
σ_{max} (3)	1.1	1.4	1.1	2.8
σ_a	19.9	24.5	18.2	44.2
σ_m	-18.8	-23.0	-17.0	-41.4

(1) From Table 5-1.
(2) (Load split) × (value from Table 5-1).
(3) -0.026 × (value from Table 5-1).

Table 6-4

VALUES OF CRACK DEPTH REQUIRED TO EXCEED THRESHOLD (a_{th}) AND CORRESPONDING ARRESTED CRACK DEPTH (a_{ar}) FOR VARIOUS CONDITIONS IN AN ISOTHERMAL AF PISTON SKIRT

	Nominal Tensile		Worst-Case Tensile	
g_o, mils	a_{th}, inch	a_{ar}, inch	a_{th}, inch	a_{ar}, inch
8	no crack growth		no crack growth	
8.5	no crack growth		no crack growth	
11	no crack growth		no crack growth	
∞	0.031	0.067	0.031	0.147

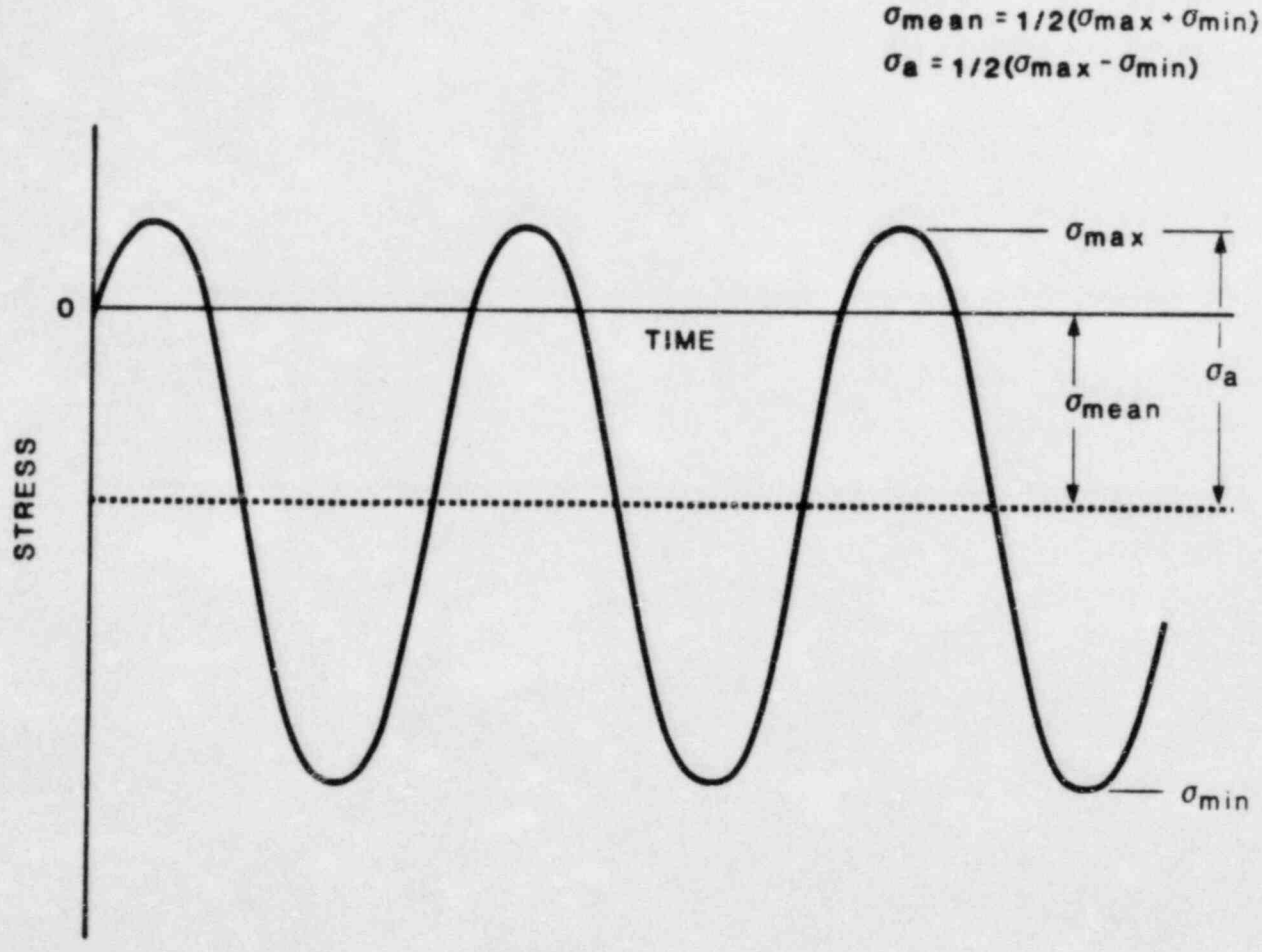

Figure 6-1. Definition of terms for cyclic applied forces.

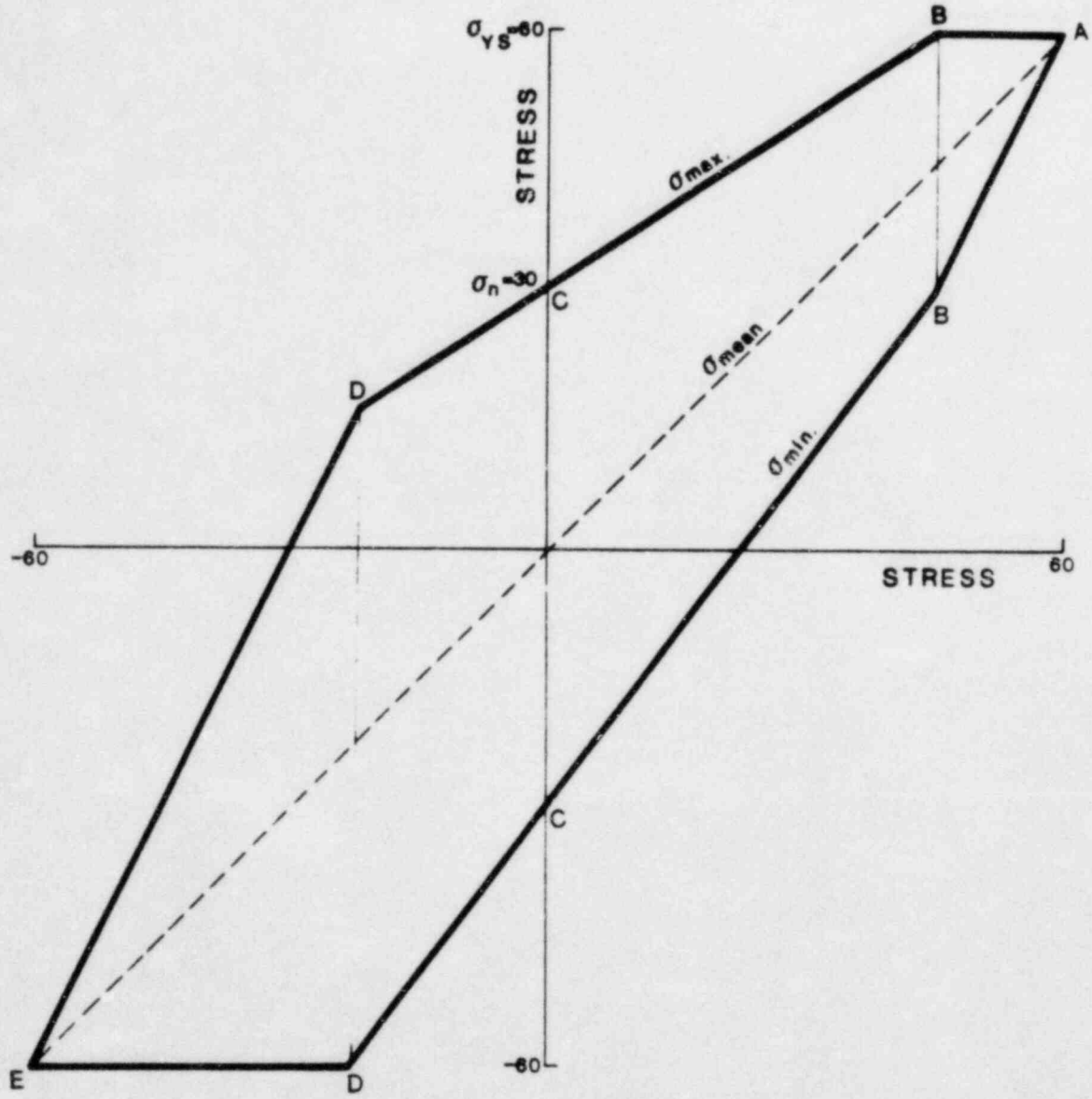

Figure 6-2. Mean and cyclic stresses for infinite fatigue life.

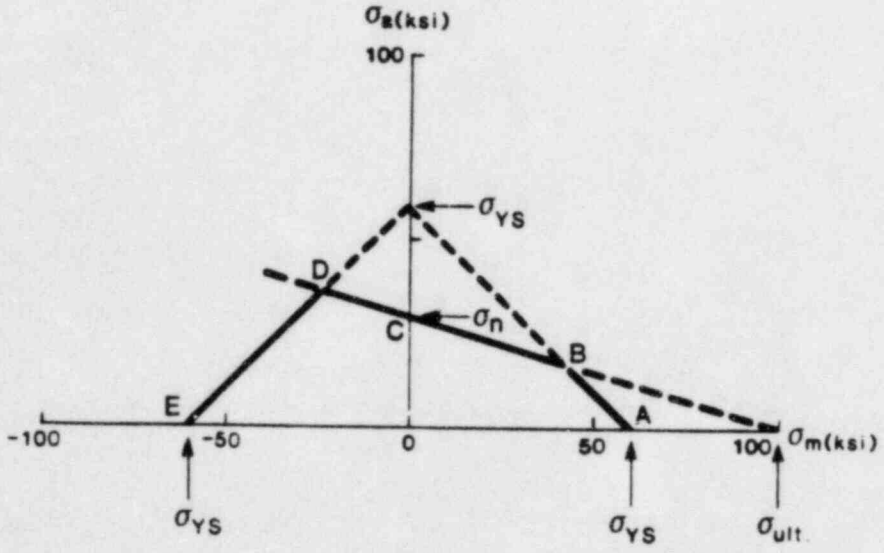

Figure 6-3. Mean and cyclic stresses for infinite fatigue life.

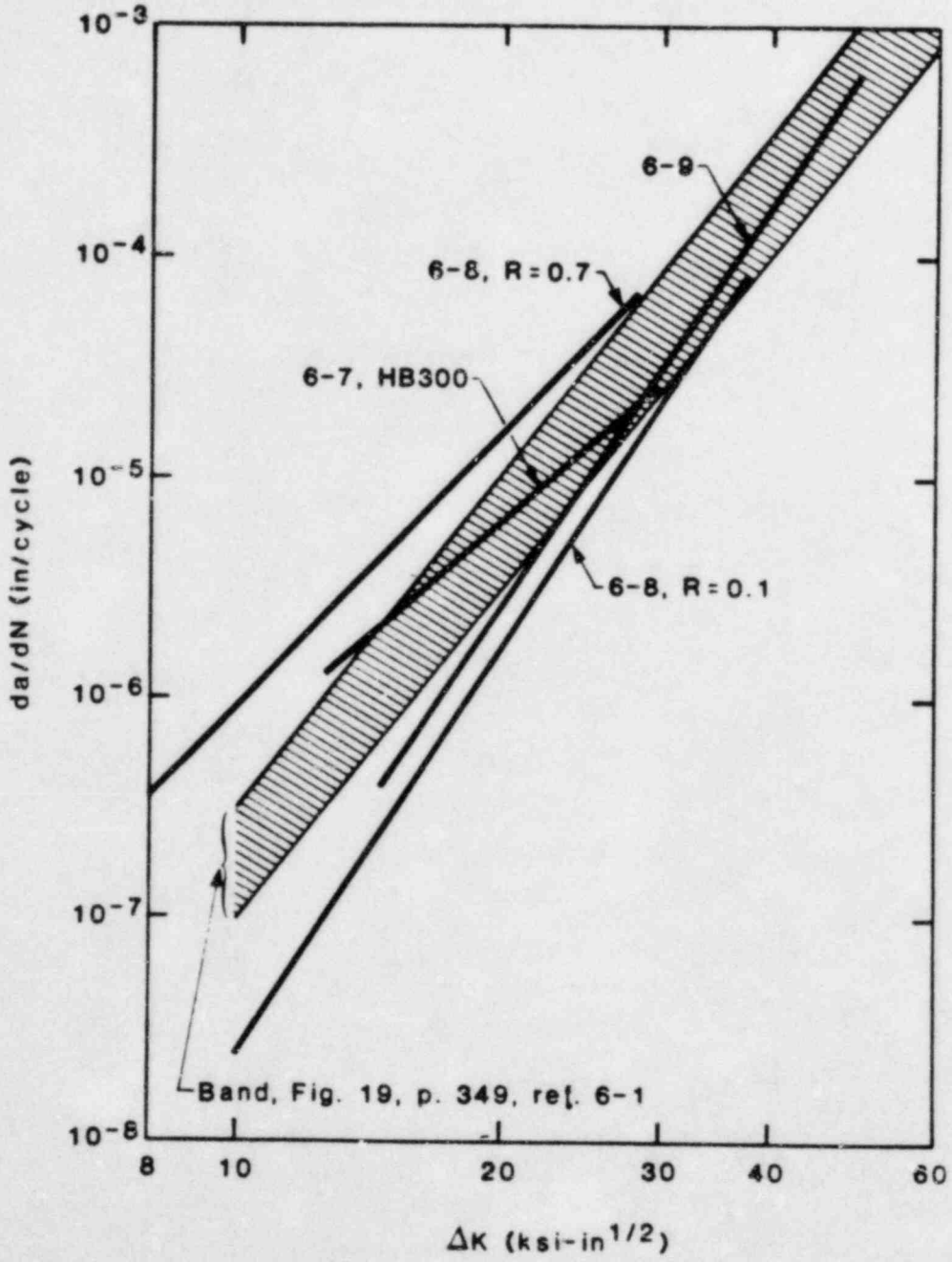

Figure 6-4. Representation of da/dN versus ΔK data for nodular condition.

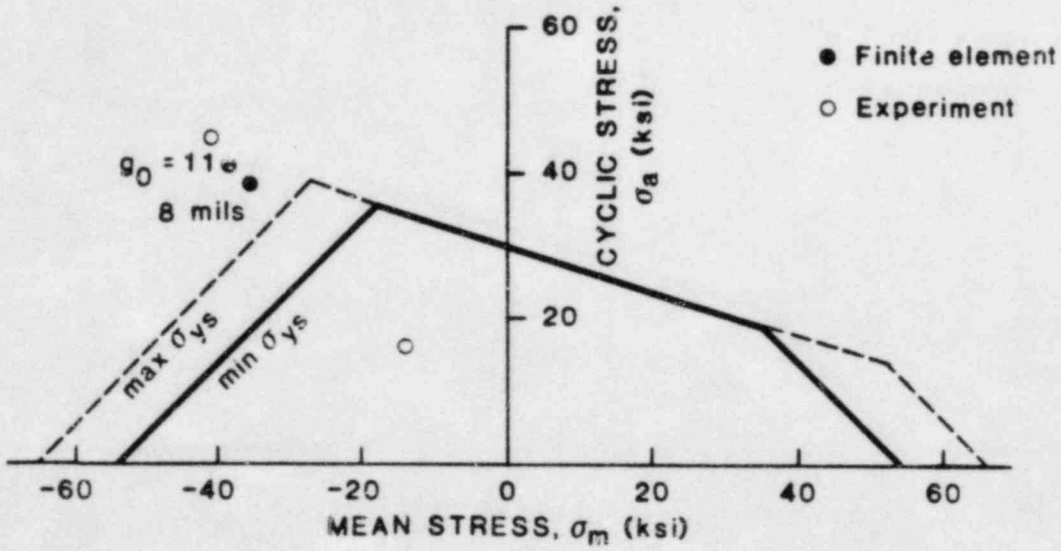

Figure 6-5. Stress states for isothermal AF piston skirt for various gap sizes plotted on graph of allowable stress amplitude as a function of mean stress.

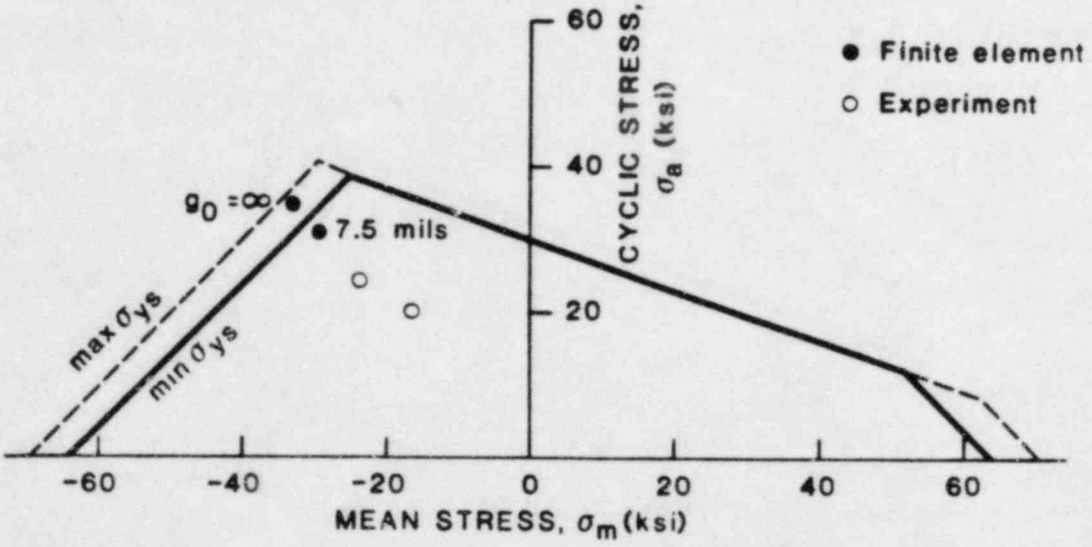

Figure 6-6. Stress states for isothermal AE piston skirt for various gap sizes plotted on graph of allowable stress amplitude as a function of mean stress.

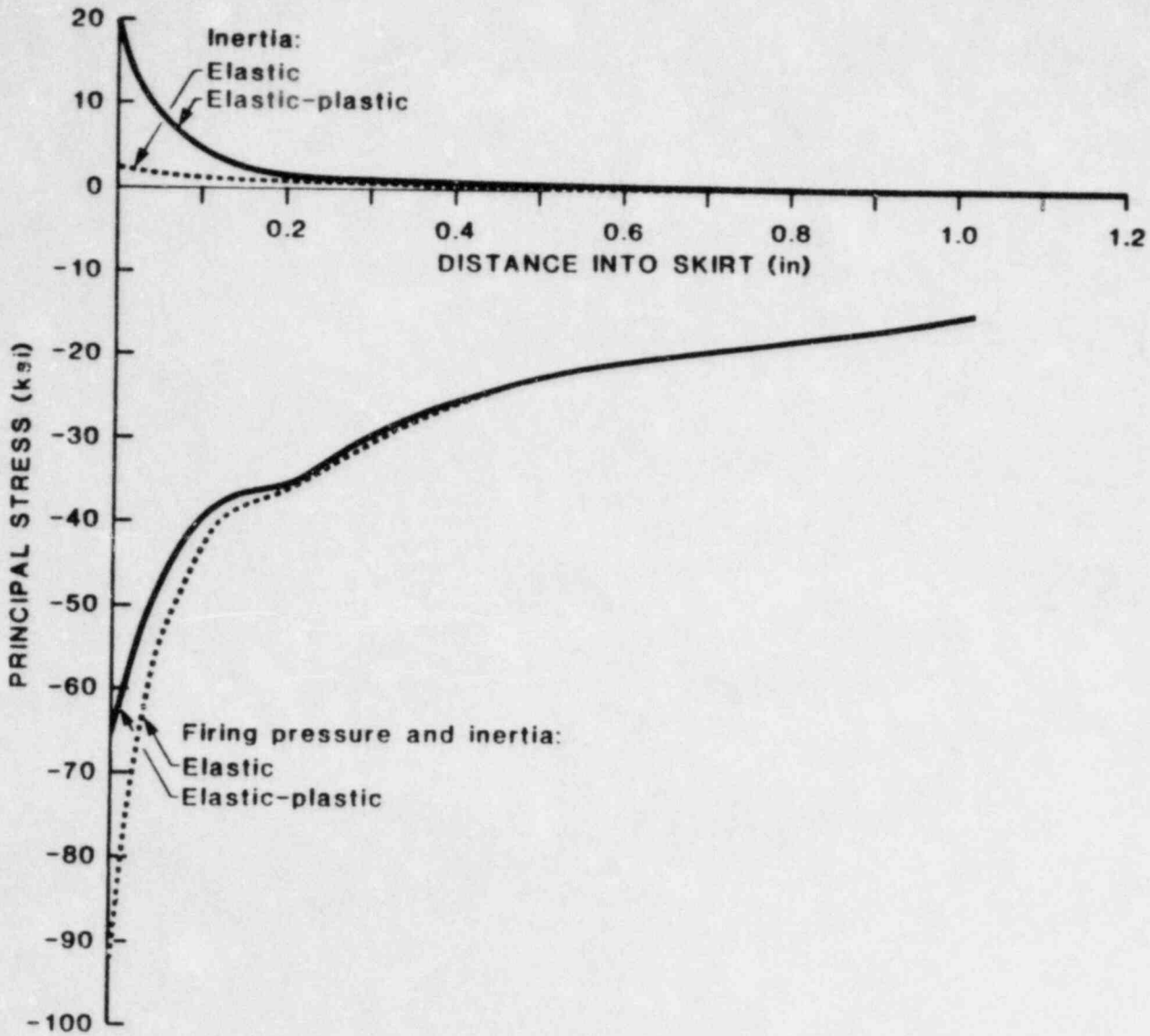

Figure 6-7. Elastic and steady-state elastic-plastic stresses as a function of distance into the skirt material for the AF piston.

FSAA-84-2-14

7.0 AE PISTON SKIRT INSPECTIONS

FaAA has conducted eddy-current inspections of engine-operated AE skirts. This high-resolution procedure, developed to differentiate between superficial dye-penetrant indications and fatigue cracks, is described fully in FaAA Procedure NDE 11.5.

Included in these inspections were four skirts each from the SNPS three engines, each of which had completed over 300 hours total operation, including 100 hours at 100% load. One SNPS engine had completed an additional 100 starts. No relevant indications were found in any of these pistons skirts.

One skirt was inspected from a RV-16-4 engine at the Kodiak Electric Association in Alaska. This engine had experienced over 6,000 hours of service with the AE skirts, at a peak firing pressure reported by the utility to be approximately 1,200 psi. Additionally, two skirts were inspected from the TDI R-5 development engine after operation at 2,000 psi or above for over 600 hours, according to TDI. These inspection reports are available from FaAA. None of the skirts disclosed any relevant indications.

8.0 CONCLUSIONS

1. Finite element and experimental stress analyses were conducted on modified Type AF and Type AE piston skirts with attached crowns under isothermal hydrostatic pressure loading. Fatigue and fracture mechanics analysis of the crown-to-skirt stud attachment bosses was carried out for both skirt types.

   The results of these tests and calculations showed the following:

   - Experimentally measured stresses are significantly lower in the stud attachment boss area in the AE skirts than in the modified AF skirts. Stresses in the stud attachment boss area calculated by finite element techniques are significantly lower in the AE skirts than in the modified AF skirts.

   - Based on experimentally measured stresses, fatigue cracks are predicted neither to initiate nor to propagate in the AE skirt.

   - Finite element stress analysis combined with fatigue analysis predicts that cracks may or may not initiate in the AE skirt depending on the initial value of the gap between the outer ring of the skirt and crown. Fracture mechanics analysis indicates that these cracks will not propagate if initiated.

   - Cracks are predicted to initiate and propagate in the modified AF skirt based on the larger of experimentally measured stresses or on finite element stress results. In no case are cracks predicted to propagate to a depth of more than 0.150 inch.

2. Based upon the results of inspections of engine-operated AE skirts and upon the results of stress analysis it is concluded that the AE skirts are adequate for unlimited life.

3. Based upon similar results for modified AF skirts, it is recommended that 100 percent inspection of stud boss attachments of AF skirts be conducted. Provided there are no relevent indications, these skirts are satisfactory for continued service with periodic inspections or for extended service at less than full rated load. Final recommendations

for inspection intervals and/or operation less than full rated load will be prepared on the basis of (i) evaluation of effects of thermal distortion and (ii) plant-specific engine operating conditions.